



UNIVERSITAT ROVIRA I VIRGIL

## DEVELOPMENT AND CALIBRATION OF AUTOMATIC REAL-TIME ENVIRONMENTAL RADIOACTIVITY MONITORS USING GAMMA-RAY SPECTROMETRY

Ramon Casanovas Alegre

Dipòsit Legal: T 960-2014

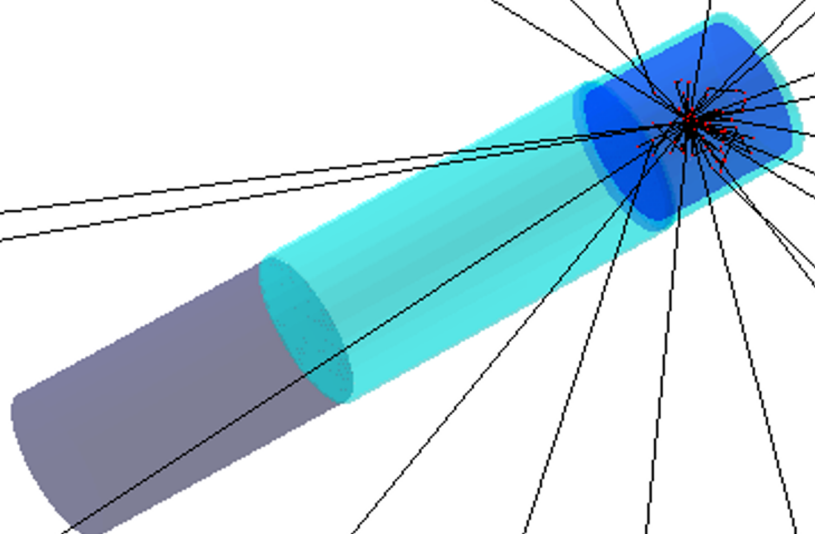
**ADVERTIMENT.** L'accés als continguts d'aquesta tesi doctoral i la seva utilització ha de respectar els drets de la persona autora. Pot ser utilitzada per a consulta o estudi personal, així com en activitats o materials d'investigació i docència en els termes establerts a l'art. 32 del Text Refós de la Llei de Propietat Intel·lectual (RDL 1/1996). Per altres utilitzacions es requereix l'autorització prèvia i expressa de la persona autora. En qualsevol cas, en la utilització dels seus continguts caldrà indicar de forma clara el nom i cognoms de la persona autora i el títol de la tesi doctoral. No s'autoritza la seva reproducció o altres formes d'explotació efectuades amb finalitats de lucre ni la seva comunicació pública des d'un lloc aliè al servei TDX. Tampoc s'autoritza la presentació del seu contingut en una finestra o marc aliè a TDX (framing). Aquesta reserva de drets afecta tant als continguts de la tesi com als seus resums i índexs.

**ADVERTENCIA.** El acceso a los contenidos de esta tesis doctoral y su utilización debe respetar los derechos de la persona autora. Puede ser utilizada para consulta o estudio personal, así como en actividades o materiales de investigación y docencia en los términos establecidos en el art. 32 del Texto Refundido de la Ley de Propiedad Intelectual (RDL 1/1996). Para otros usos se requiere la autorización previa y expresa de la persona autora. En cualquier caso, en la utilización de sus contenidos se deberá indicar de forma clara el nombre y apellidos de la persona autora y el título de la tesis doctoral. No se autoriza su reproducción u otras formas de explotación efectuadas con fines lucrativos ni su comunicación pública desde un sitio ajeno al servicio TDR. Tampoco se autoriza la presentación de su contenido en una ventana o marco ajeno a TDR (framing). Esta reserva de derechos afecta tanto al contenido de la tesis como a sus resúmenes e índices.

**WARNING.** Access to the contents of this doctoral thesis and its use must respect the rights of the author. It can be used for reference or private study, as well as research and learning activities or materials in the terms established by the 32nd article of the Spanish Consolidated Copyright Act (RDL 1/1996). Express and previous authorization of the author is required for any other uses. In any case, when using its content, full name of the author and title of the thesis must be clearly indicated. Reproduction or other forms of for profit use or public communication from outside TDX service is not allowed. Presentation of its content in a window or frame external to TDX (framing) is not authorized either. These rights affect both the content of the thesis and its abstracts and indexes.

DEVELOPMENT AND CALIBRATION OF AUTOMATIC  
REAL-TIME ENVIRONMENTAL RADIOACTIVITY MONITORS  
USING GAMMA-RAY SPECTROMETRY

*PhD Thesis*



RAMON CASANOVAS ALEGRE

*Universitat Rovira i Virgili*



Development and calibration of automatic real-time  
environmental radioactivity monitors using gamma-ray  
spectrometry

PhD Thesis

**Ramon Casanovas Alegre**

Supervised by: PhD Marçal Salvadó Artells

Unitat de Física Mèdica, Departament de Ciències Mèdiques Bàsiques



UNIVERSITAT ROVIRA I VIRGILI

Reus

February 2014





I STATE that the present study, entitled "**Development and calibration of automatic real-time environmental radioactivity monitors using gamma-ray spectrometry**", presented by Ramon Casanovas Alegre for the award of the degree of Doctor, has been carried out under my supervision at the Medical Physics Unit of the Department of Basic Medical Science of this university, and that it fulfils all the requirements to be eligible for the European Doctorate Award.

Reus, 5<sup>th</sup> February 2014

Doctoral Thesis Supervisor

A blue ink signature of 'Marçal Salvadó Artells'.

PhD. Marçal Salvadó Artells



# Resum executiu (in Catalan)

## Introducció

A Espanya, hi ha set reactors nuclears en operació, allotjats en cinc centrals nuclears que produueixen, actualment, aproximadament el 20% de l'electricitat consumida<sup>1</sup>. Tres dels reactors, estan situats a Catalunya, un a Vandellòs (anomenat Vandellòs-II) i els altres dos a Ascó (Ascó-I i Ascó-II).

El Tractat Euratom confereix importants poders a la Comissió Europea en relació amb el seguiment i l'avaluació dels nivells de radioactivitat al medi ambient i a les descàrregues d'efluents [1]. En particular, l'Article 35 del Tractat Euratom estableix que cada Estat membre ha de disposar de les instal·lacions necessàries per dur a terme un seguiment continu dels nivells de radioactivitat a l'aire, aigua i sòl, així com garantir el compliment d'unes normes bàsiques [2].

Des del punt de vista de la salut, en funcionament normal, les instal·lacions nuclears no produueixen alliberaments significatius de radioactivitat. Per tant, la preocupació pel control de la radioactivitat ambiental no és estrictament un tema relacionat amb la protecció de la salut. No obstant, el control de la radioactivitat ambiental segueix sent una tasca important als Estats Membres en quant a proporcionar informació a la població, i així, ajudar a preservar la transparència i la minuciositat de la vigilància radiològica ambiental a Europa [3].

El Consell de Seguretat Nuclear (CSN) és l'organisme competent a Espanya en matèria de protecció contra les radiacions ionitzants. Per tal de garantir que els nivells de radioactivitat es mantenen inferiors als límits legals, el CSN disposa d'una xarxa de vigilància anomenada REVIRA (Red de Vigilancia Radiológica Ambiental). Aquesta està constituïda per dues subxarxes [4], [5]: la REA (Red de Estaciones Automáticas) i la REM (Red de Estaciones de Muestreo). La REA implica diversos tipus de mesura automàtica, remota i in-situ, mentre que la REM implica prendre mostres (aire, aigua, aliments, terra i sediments) i analitzar-les en un laboratori. A Catalunya, les competències de gestió de

---

<sup>1</sup>Fins al 6 de Juliol del 2013, hi havia vuit reactors nuclears en operació, allotjats en sis centrals nuclears, però la central nuclear de Santa María de Garoña (que disposava d'un reactor nuclear) va ser tancada per problemes econòmics.

la REVIRA estan transferides al Servei de Coordinació d'Activitats Radioactives (SCAR) de la Generalitat de Catalunya i integrades amb la seva pròpia xarxa de vigilància en temps real.

Des del 2006 fins a l'actualitat, diverses tasques relacionades amb la xarxa de vigilància radiològica ambiental i en temps real de Catalunya han estat encarregades a la Unitat de Física Mèdica de la Universitat Rovira i Virgili. Algunes d'elles han estat la gestió, control, manteniment tècnic, calibratge, incorporació de millores, recerca i anàlisi de dades. Com a conseqüència del desenvolupament d'aquestes tasques, el nostre grup de recerca ha acumulat una àmplia experiència en el camp de la mesura de la radioactivitat ambiental en temps real.

## Motivació

Aquesta experiència amb la xarxa catalana ens ha permès contribuir a implementar-hi diverses millores per tal d'obtenir una millor qualitat i quantitat de dades. A més, per poder donar una resposta ràpida davant de problemes amb els equips de mesura o davant un possible incident radiològic, en un estudi previ (Article [I]) vam desenvolupar una metodologia d'anàlisi de dades basada en criteris estadístics fàcils d'implementar. En aquest mateix estudi es va realitzar un anàlisi de les capacitats de la xarxa catalana que va posar de manifest la necessitat de disposar de més informació radiològica en temps real. Atenent aquest fet, es suggeria la implementació d'equips de mesura que efectuessin espectrometria gamma in-situ i en temps real. Aquesta millora dotaria a la xarxa de millors capacitats d'anàlisi i permetria efectuar una resposta més eficient en front d'un possible increment radiològic.

A partir d'aquest moment, l'SCAR va recolzar la idea i va decidir disposar d'equips de mesura de la radioactivitat ambiental mitjançant espectrometria gamma en temps real. En conseqüència, es van signar diversos contractes entre la Universitat Rovira i Virgili i la Generalitat de Catalunya per tal de desenvolupar equips propis amb aquestes característiques. El tipus de detectors de radiació que es van escollir per als desenvolupaments van ser detectors d'escintillació de  $\text{LaBr}_3(\text{Ce})$  de  $2'' \times 2''$ . No obstant, també es van utilitzar detectors de  $\text{NaI}(\text{Tl})$  de  $2'' \times 2''$  pel seu cost inferior i per poder-los comparar amb els de  $\text{LaBr}_3(\text{Ce})$ . La Universitat Politècnica de Catalunya i Raditel Serveis i Subministraments Tecnològics S.L. també van participar en el projecte.

## Metodologies de calibratge i d'estabilització d'espectres

Per tal de donar significat físic a les dades obtingudes pels detectors d'espectrometria, va ser necessari desenvolupar una metodologia de calibratge completa per a ambdós tipus de detectors de  $\text{NaI}(\text{Tl})$  i  $\text{LaBr}_3(\text{Ce})$ . Aquesta metodologia, que va ser publicada a l'Article [II], comprèn els calibratges en energia, resolució i eficiència.

Pels dos primers calibratges, vam estudiar diferents tipus de funcions matemàtiques trobades a la literatura, mitjançant l'ús de fonts radioactives de  $^{241}\text{Am}$ ,  $^{133}\text{Ba}$ ,  $^{137}\text{Cs}$ ,  $^{60}\text{Co}$  i  $^{152}\text{Eu}$ . En l'estudi, es va trobar que tant per establir la relació energia-canal com per establir la relació entre l'amplada dels pics i l'energia la millor funció a utilitzar és un polinomi de grau 2. D'altra banda, pel calibratge en eficiència, es va programar un codi d'usuari amb diverses implementacions importants pel sistema EGS5 que permet realitzar simulacions de Monte Carlo. El codi conté tota la informació del terme font de radiació (tipus de partícules, energia i probabilitats d'emissió, posició i geometria, direcció d'emissió, etc.) i de la geometria del detector (components, mides, materials, etc.). A més, conté tots els càlculs relacionats amb les quantitats a obtenir, que són bàsicament l'espectre de raigs gamma (amb o sense eixamplament de pics) i els càlculs d'eficiència, ambdós amb les seves incerteses estadístiques associades. Aquest codi va ser validat mitjançant la comparació dels seus resultats amb d'altres obtinguts experimentalment.

La metodologia de calibratge desenvolupada garanteix un correcte funcionament dels detectors de NaI(Tl) i LaBr<sub>3</sub>(Ce) en condicions de laboratori. No obstant, quan els detectors s'utilitzen al medi ambient, i per tant operen en condicions de temperatura variables, es poden produir inestabilitats en el guany dels detectors que desemboquen en un desplaçament dels pics de l'espectre durant les mesures. I en conseqüència, el calibratge en energia queda invalidat. Per tal de solucionar aquest problema, es va realitzar un estudi (Article [III]) on es proposaven dues metodologies per estabilitzar els espectres mitjançant algoritmes programables.

La primera de les metodologies d'estabilització utilitza una funció matemàtica que relaciona la posició de cadascun dels canals amb la temperatura ambient. No obstant, requereix d'una caracterització prèvia del detector al laboratori en condicions de temperatura controlades. D'altra banda, el segon mètode no requereix mesures prèvies al laboratori, però és necessari que a tots els espectres hi hagi algun pic coneget, que pot no sempre estar disponible o identifiable, especialment pels detectors de NaI(Tl). Pels detectors de LaBr<sub>3</sub>(Ce), el pic causat per la contaminació interna del  $^{138}\text{La}$ , junt amb la millor resolució energètica del detector, faciliten l'aplicació del mètode.

## Desenvolupament i calibratge

El desenvolupament d'equips de mesura automàtics de la radioactivitat ambiental per la Generalitat de Catalunya es va dur a terme en paral·lel amb el desenvolupament de les metodologies anteriors de calibratge i d'estabilització d'espectres. De fet, el desenvolupament d'aquestes metodologies va estar motivat per les futures necessitats que tindrien els monitors desenvolupats.

Així, es van desenvolupar tres tipus de monitors de radioactivitat mitjançant l'ús d'espectrometria gamma: un per mesurar els nivells de radioactivitat en aigua i dos que permeten mesurar els nivells de radioactivitat en aire de dues formes diferents.

El primer tipus de monitor, el monitor d'aigua, va ser una millora dels dos monitors d'aigua ja existents a la xarxa catalana. Els sistemes de mesura estan situats al Riu Ebre, abans i després del seu pas per la central nuclear d'Ascó, perquè la central utilitza l'aigua del riu per tal de refrigerar els dos reactors. Els monitors capten l'aigua del riu a través d'una bomba d'aspiració i aquesta és analitzada dins d'una cubeta blindada amb Pb.

La millora va consistir en la implementació d'espectrometria gamma mitjançant detectors de NaI(Tl), que es va fer mitjançant la instal·lació d'un mòdul paral·lel d'espectrometria gamma al disseny original del monitor. Abans de la millora, aquests monitors només eren capaços de proporcionar mesures de la concentració d'activitat total gamma en aigua. Després de la implementació, els monitors permeten la identificació i quantificació en temps real del contingut isotòpic de l'aigua del riu.

Els monitors van ser calibrats (veure Article [IV]) mitjançant les metodologies anomenades prèviament. Pel calibratge en eficiència, que es va realitzar mitjançant simulacions pel mètode de Monte Carlo, es va adaptar el codi d'usuari desenvolupat per tal d'incloure un model realista del monitor i de la geometria de mesura. Per tal de ressaltar els avantatges de la nova implementació, es va estudiar un increment radiològic durant un episodi de pluja, on es va constatar que els isòtops involucrats en l'increment eren d'origen natural. Finalment, es va realitzar un estudi de les capacitats de mesura dels monitors mitjançant l'avaluació de les concentracions d'activitat mínimes detectables de  $^{131}\text{I}$ ,  $^{137}\text{Cs}$  i  $^{40}\text{K}$  per diferents temps d'integració. En comparació amb d'altres sistemes que mesuren directament dins l'aigua, aquestes van ser més baixes, demostrant que la identificació i quantificació dels isòtops radioactius és més eficaç pels monitors desenvolupats.

El segon tipus de monitor desenvolupat va ser un monitor de mesura en temps real de la radioactivitat a l'aire mitjançant espectrometria gamma sobre filtre de partícules, anomenat RARM-F per les seves sigles en anglès. El RARM-F col·lecta un flux constant d'aire i el fa circular a través d'un filtre de partícules que reté els aerosols presents a l'aire. El filtre està encarat a un detector d'escintil·lació de NaI(Tl) o LaBr<sub>3</sub>(Ce) que s'utilitza per fer espectrometria gamma. Tant el detector com la part activa del filtre estan dins d'un blindatge de Pb que permet reduir el fons radiològic de la mesura. Aquest desenvolupament es va protegir amb una sol·licitud de patent (veure Patent [i]).

En un estudi previ (Article [V]) es van discutir els detalls del desenvolupament i calibratge de dos monitors tipus RARM-F, un que utilitza un detector NaI(Tl) i l'altre que n'utilitza un de LaBr<sub>3</sub>(Ce). El calibratge es va efectuar seguint les metodologies anteriors. Pel calibratge en eficiència, es van realitzar simulacions de Monte Carlo utilitzant un model que reproduïa el monitor i la seva geometria de mesura. En aquest estudi també es van estudiar les capacitats de mesura d'ambdós monitors mitjançant el càlcul de la concentració d'activitat mínima detectable de  $^{137}\text{Cs}$ . Els resultats van mostrar unes capacitats de mesura més elevades que d'altres monitors de radioactivitat ambiental, especialment quan s'utilitza el detector de LaBr<sub>3</sub>(Ce).

El tercer tipus de monitor que es va desenvolupar va ser també un detector de radioactivitat en aire, però en aquest cas les mesures es realitzen directament al medi ambient (és a dir sense la necessitat de concentrar els isòtops en un filtre). El monitor s'anomena RARM-D2, que correspon a les sigles angleses de monitor de mesura en temps real de la radioactivitat a l'aire mitjançant espectrometria gamma amb dos detectors mesurant directament. El RARM-D2 està format bàsicament per dos detectors d'escintilació, un orientat cap amunt i l'altre cap avall, i que estan blindats amb Pb per mesurar únicament en el semiplà d'interès. Aquesta disposició geomètrica, juntament amb els blindatges, fa possible la discriminació entre els isòtops continguts en un núvol radioactiu i aquells dipositats o emergint del terra, que pot ser d'interès després d'un accident nuclear per tal de caracteritzar el terme font de radioactivitat. Els resultats d'aquest desenvolupament també van ser protegits mitjançant una sol·licitud de patent (veure Patent [ii]).

El RARM-D2 va ser completament calibrat utilitzant les metodologies desenvolupades anteriorment i per totes les combinacions de detectors de NaI(Tl) i LaBr<sub>3</sub>(Ce) (veure Article [VI]). Pel calibratge en eficiència, es va adaptar el codi de Monte Carlo desenvolupat a les condicions de mesura d'aquest monitor. Abans però, es va estudiar l'efecte que tenia la mida d'un terme font de radioactivitat de <sup>137</sup>Cs en els càlculs d'eficiència, tant pels detectors que apunten amunt com per als que apunten avall. Es va trobar que una bona aproximació de font homogènia i infinita és un cilindre de radi 250 m i alçada 250 m pel detector que apunta amunt i un disc de radi 250 m pel detector que apunta avall. Finalment, per aquesta geometria, es van avaluar les capacitats de mesura del monitor per detectar <sup>131</sup>I i <sup>137</sup>Cs en diferents temps d'integració. Aquesta avaluació es va fer per totes les configuracions (amunt i avall) i per detectors tant de NaI(Tl) com de LaBr<sub>3</sub>(Ce).

Finalment, com a conclusió general de les aportacions d'aquesta tesi, es pot dir que la xarxa automàtica de vigilància radiològica en temps real de Catalunya ofereix nova i millor informació radiològica. Això s'ha assolit gràcies al desenvolupament i calibratge de tres tipus de monitors de radioactivitat mitjançant espectrometria gamma en temps real, que permeten la identificació i quantificació del contingut d'isòtops radioactius en aigua i aire. Així, mentre que la identificació dels isòtops involucrats en possibles increments radiològics permet distingir si aquests són d'origen natural o artificial, la seva quantificació fa possible una comparació de les dades obtingudes amb els límits legals establerts per les concentracions d'activitat, que alhora facilita l'establiment de nivells d'alarma que permeten una actuació ràpida en cas d'increment radiològic.



# Resumen ejecutivo (in Spanish)

## Introducción

En España, hay siete reactores nucleares en operación, alojados en cinco centrales nucleares que producen, actualmente, aproximadamente el 20% de la electricidad consumida<sup>2</sup>. Tres de los reactores, están situados en Catalunya, uno en Vandellòs (llamado Vandellòs-II) y los otros dos en Ascó (Ascó-I y Ascó-II).

El Tratado Euratom confiere importantes poderes a la Comisión Europea con relación al seguimiento y evaluación de los niveles de radiactividad en el medio ambiente y a las descargas de efluentes[1]. En particular, el Artículo 35 del Tratado Euratom establece que cada Estado miembro debe disponer de las instalaciones necesarias para llevar a cabo un seguimiento continuo de los niveles de radiactividad en aire, agua y suelo, así como garantizar el cumplimiento de unas normas básicas [2].

Des del punto de vista de la salud, en funcionamiento normal, las instalaciones nucleares no producen liberaciones significativas de radiactividad. Por tanto, la preocupación por el control de la radiactividad ambiental no es estrictamente un tema relacionado con la protección de la salud. No obstante, el control de la radiactividad ambiental sigue siendo una tarea importante en los Estados Miembros en cuanto a proporcionar información a la población, y así, ayudar a preservar la transparencia y la minuciosidad de la vigilancia radiológica ambiental en Europa [3].

El Consejo de Seguridad Nuclear (CSN) es el organismo competente en España en materia de protección contra las radiaciones ionizantes. Para garantizar que los niveles de radiactividad se mantienen inferiores a los límites legales, el CSN dispone de una red de vigilancia llamada REVIRA (Red de Vigilancia Radiológica Ambiental). Esta está constituida por dos subredes [4], [5]: la REA (Red de Estaciones Automáticas) y la REM (Red de Estaciones de Muestreo). La REA implica varios tipos de medida automática, remota e in-situ, mientras que la REM implica tomar medidas (aire, agua, alimentos, tierra y sedimentos) y analizarlas en un laboratorio. En Catalunya, las competencias

---

<sup>2</sup>Hasta el 6 de Julio de 2013, había ocho reactores en operación, alojados en seis centrales nucleares, pero la central nuclear de Santa María de Garoña (que disponía de un reactor nuclear) fue cerrada por problemas económicos.

de gestión de la REVIRA están transferidas al Servicio de Coordinación de Actividades Radiactivas (SCAR) de la Generalitat de Catalunya e integradas con su propia red de vigilancia en tiempo real.

Des de 2006 hasta la actualidad, varias tareas relacionadas con la red de vigilancia radiológica ambiental y en tiempo real de Catalunya han sido encargadas a la Unidad de Física Médica de la Universidad Rovira i Virgili. Algunas de ella han sido la gestión, control, mantenimiento técnico, calibración, incorporación de mejoras, investigación y análisis de datos. Como consecuencia del desarrollo de estas tareas, nuestro grupo de investigación ha acumulado una amplia experiencia en el campo de la medida de la radiactividad ambiental en tiempo real.

## **Motivación**

Esta experiencia con la red catalana nos ha permitido contribuir a implementarle varias mejoras para obtener una mejor calidad y cantidad de datos. Además, para poder dar una respuesta rápida frente a problemas con los equipos de medida o frente a un posible incidente radiológico, en un estudio previo (Artículo [I]) se desarrolló una metodología de análisis de datos basada en criterios estadísticos fáciles de implementar. En este mismo estudio se realizó un análisis de las capacidades de medida de la red catalana que puso de manifiesto la necesidad de disponer de más información radiológica en tiempo real. Atendiendo este hecho, se sugería la implementación de equipos de medida que efectuasen espectrometría gamma -situ y en tiempo real. Esta mejora dotaría a la red de mejores capacidades de análisis y permitiría efectuar una respuesta más eficiente frente a un posible incremento radiológico.

Desde este momento, el SCAR respaldó la idea y decidió disponer de equipos de medida de la radiactividad ambiental mediante espectrometría gamma en tiempo real. En consecuencia, se firmaron diversos contratos entre la Universidad Rovira i Virgili y la Generalitat de Catalunya para desarrollar equipos propios con estas características. El tipo de detectores que se escogieron para los desarrollos fueron detectores de centelleo de LaBr<sub>3</sub>(Ce) de 2"×2". No obstante, también se utilizaron detectores de NaI(Tl) de 2"×2" por su coste inferior y para poderlos comparar con los de LaBr<sub>3</sub>(Ce). La Universidad Politécnica de Catalunya y Raditel Serveis i Subministraments Tecnològics S.L. también participaron en el proyecto.

## **Metodologías de calibración y de estabilización de espectros**

Para dotar de significado físico a los datos obtenidos por los detectores de espectrometría, fue necesario desarrollar una metodología de calibración completa para ambos tipos de detectores de NaI(Tl) y LaBr<sub>3</sub>(Ce). Esta metodología, que fue publicada en el Artículo [II], comprende las calibraciones en energía, resolución y eficiencia.

Para las dos primeras calibraciones, se estudiaron diferentes tipos de funciones matemáticas halladas en la literatura, mediante el uso de fuentes radiactivas de  $^{241}\text{Am}$ ,  $^{133}\text{Ba}$ ,  $^{137}\text{Cs}$ ,  $^{60}\text{Co}$  y  $^{152}\text{Eu}$ . En el estudio, se encontró que tanto para establecer la relación energía-canal como para establecer la relación entre la anchura de los picos y la energía la mejor función a utilizar es un polinomio de grado 2. Por otro lado, para la calibración en eficiencia, se programó un código de usuario con diversas implementaciones importantes para el sistema EGS5 que permite realizar simulaciones de Monte Carlo. El código contiene toda la información del término fuente de radiación (tipo de partículas, energía y probabilidades de emisión, posición y geometría, dirección de emisión, etc.) y de la geometría del detector (componentes, medidas, materiales, etc.). Además, contiene todos los cálculos relacionados con las cantidades a obtener, que son básicamente el espectro de rayos gamma (con o sin ensanchamiento de picos) y los cálculos de eficiencia, ambos con sus respectivas incertidumbres estadísticas asociadas. Este código fue validado mediante la comparación de sus resultados con otros obtenidos experimentalmente.

La metodología de calibración desarrollada permite un correcto funcionamiento de los detectores de NaI(Tl) y LaBr<sub>3</sub>(Ce) en condiciones de laboratorio. No obstante, cuando los detectores se utilizan en el medio ambiente, y por tanto operan en condiciones de temperatura variables, se pueden producir inestabilidades en la ganancia de los detectores que desemboquen en un desplazamiento de los picos del espectro durante las medidas. Y en consecuencia, la calibración en energía queda invalidada. Para solucionar este problema, se desarrolló un estudio (Artículo [III]) dónde se proponían dos metodologías para estabilizar los espectros mediante algoritmos programables.

La primera de las metodologías de estabilización utiliza una función matemática que relaciona la posición de cada uno de los canales con la temperatura ambiente. No obstante, requiere de una caracterización previa del detector en el laboratorio en condiciones de temperatura controladas. Por otro lado, el segundo método no requiere medidas previas en laboratorio pero es necesario que en todos los espectros haya un pico conocido, que puede no siempre estar disponible o identificable, especialmente para los detectores de NaI(Tl). Para los detectores de LaBr<sub>3</sub>(Ce), el pico causado por la contaminación interna de  $^{138}\text{La}$ , junto con la mejor resolución energética del detector, facilitan la aplicación del método.

## Desarrollo y calibración

El desarrollo de equipos de medida automáticos de la radiactividad ambiental para la Generalitat de Catalunya se llevó a cabo en paralelo con el desarrollo de las metodologías anteriores de calibración y estabilización de espectros. De hecho, el desarrollo de estas metodologías estuvo motivado por las futuras necesidades que tendrían los monitores desarrollados.

Así, se desarrollaron tres tipos de monitores de radiactividad mediante el uso de es-

pectrometría gamma: uno para medir los niveles de radiactividad en agua y dos que permiten medir los niveles de radiactividad en aire de dos formas distintas.

El primer tipo de monitor, el monitor de agua, fue una mejora de los dos monitores de agua ya existentes en la red catalana. Los sistemas de medida están situados en el Río Ebro, antes y después de su paso por la central nuclear de Ascó, debido a que la central utiliza el agua del río para refrigerar los dos reactores. Los monitores captan agua del río a través de una bomba de aspiración y ésta es analizada en una vasija blindada con Pb.

La mejora consistió en la implementación de espectrometría gamma mediante detectores de NaI(Tl), que se efectuó mediante la instalación de un módulo paralelo de espectrometría gamma en el diseño original del monitor. Antes de la mejora, estos monitores solo eran capaces de proporcionar medidas de la concentración de actividad total gamma en agua. Después de la implementación, los monitores permiten la identificación y cuantificación en tiempo real del contenido isotópico del agua del río.

Los monitores fueron calibrados (ver Artículo [IV]) mediante las metodologías descritas previamente. Para la calibración en eficiencia, que se realizó mediante simulaciones por el método de Monte Carlo, se adaptó el código de usuario desarrollado para incluir un modelo realista del monitor y de la geometría de medida. Para resaltar las ventajas de la nueva implementación, se estudió un incremento radiológico durante un episodio de lluvia, donde se constató que los isótopos involucrados en el incremento eran de origen natural. Finalmente, se realizó un estudio de las capacidades de medida de los monitores mediante la evaluación de las concentraciones de actividad mínimas detectables de  $^{131}\text{I}$ ,  $^{137}\text{Cs}$  y  $^{40}\text{K}$  para distintos tiempos de integración. En comparación con otros sistemas que miden directamente dentro del agua, estas fueron más bajas, demostrando que la identificación y cuantificación de los isótopos radiactivos es más eficaz para los monitores desarrollados.

El segundo tipo de monitor desarrollado fue un monitor de medida en tiempo real de la radiactividad en aire mediante espectrometría gamma sobre filtro de partículas, llamado RARM-F por sus siglas en inglés. El RARM-F colecta un flujo constante de aire y lo hace circular a través de un filtro de partículas que retiene los aerosoles presentes en el aire. El filtro está enfrentado a un detector de centelleo de NaI(Tl) o LaBr<sub>3</sub>(Ce) que se utiliza para hacer espectrometría gamma. Tanto el detector como la parte activa del filtro se encuentran dentro de un blindaje de Pb que permite reducir el fondo radiológico de la medida. Este desarrollo se protegió con una solicitud de patente (ver Patente [i]).

En un estudio previo (Artículo [V]) se discutieron los detalles del desarrollo y calibración de dos monitores RARM-F, uno que utiliza un detector de NaI(Tl) y el otro que utiliza uno de LaBr<sub>3</sub>(Ce). La calibración se efectuó según las metodologías anteriores. Para la calibración en eficiencia, se realizaron simulaciones de Monte Carlo utilizando un modelo que reproducía el monitor y su geometría de medida. En este estudio también

se estudiaron las capacidades de medida de ambos monitores mediante el cálculo de la concentración de actividad mínima detectable de  $^{137}\text{Cs}$ . Los resultados mostraron unas capacidades de medida más elevados con respecto a otros monitores de radiactividad ambiental, especialmente cuando se utiliza el detector de  $\text{LaBr}_3(\text{Ce})$ .

El tercer tipo de monitor que se desarrolló fue también un detector de radiactividad en aire, pero en este caso las medidas se realizan directamente en el medio ambiente (es decir sin necesidad de concentrar los isótopos en un filtro). El monitor se llama RARM-D2, que corresponde a las siglas inglesas de monitor de medida en tiempo real de la radiactividad en aire mediante espectrometría gamma con dos detectores midiendo directamente. El RARM-D2 está formado básicamente por dos detectores de centelleo, uno orientado hacia arriba y el otro hacia abajo, y que están blindados con Pb para medir únicamente en el semiplano de interés. Esta disposición geométrica, junto con los blindajes, hace posible la discriminación entre los isótopos contenidos en una nube radiactiva y aquellos depositados o emergiendo del suelo, que puede ser de interés después de un accidente nuclear para caracterizar el término fuente de radiactividad. Los resultados de este desarrollo también fueron protegidos mediante una solicitud de patente (ver Patente [ii]).

El RARM-D2 fue completamente calibrado utilizando las metodologías desarrolladas anteriormente y para todas las combinaciones de detectores de  $\text{NaI}(\text{Tl})$  y  $\text{LaBr}_3(\text{Ce})$  (ver Artículo [VI]). Para la calibración en eficiencia, se adaptó el código de Monte Carlo desarrollado a las condiciones de medida de este monitor. Antes pero, se estudió el efecto que tenía el tamaño de un término fuente de radiactividad de  $^{137}\text{Cs}$  en los cálculos de eficiencia, tanto para los detectores que apuntan hacia arriba como para los que apuntan hacia abajo. Se encontró que una buena aproximación de fuente homogénea e infinita es un cilindro de radio 250 m y altura 250 m para el detector que apunta hacia arriba y un disco de radio 250 m para el detector que apunta hacia abajo. Finalmente, para esta geometría, se evaluaron las capacidades de medida del monitor para detectar  $^{131}\text{I}$  y  $^{137}\text{Cs}$  en diferentes tiempos de integración. Esta evaluación se hizo para todas las configuraciones (arriba y abajo) y para detectores tanto de  $\text{NaI}(\text{Tl})$  como de  $\text{LaBr}_3(\text{Ce})$ .

Finalmente, como conclusión general de las aportaciones de esta tesis, se puede decir que la red automática de vigilancia radiológica en tiempo real de Catalunya ofrece nueva y mejor información radiológica. Esto se ha logrado gracias al desarrollo y calibración de tres tipos de monitores de radiactividad mediante espectrometría gamma, que permiten la identificación y cuantificación del contenido de isótopos radiactivos en agua y aire. Así, mientras que la identificación de los isótopos involucrados en posibles incrementos radiológicos permite distinguir si estos son de origen natural o artificial, su cuantificación hace posible una comparación de los datos obtenidos con los límites legales establecidos para las concentraciones de actividad, que a su vez facilita el establecimiento de niveles de alarma que permiten una actuación rápida en caso de incremento radiológico.



# Acknowledgments

I would like to express my sincere appreciation to everyone who have helped me, directly or indirectly, during the completion of this thesis. Your advices have helped me to grow not only professionally but also personally.

First, I would like to offer my special thanks to my supervisor Dr. Marçal Salvadó, head of the Medical Physics Unit of the Universitat Rovira i Virgili, for his support, guidance and encouragement throughout the thesis. I would also like to thank you for being so pleasant, listening my opinions and providing all the resources that I have needed.

I would like to express my gratitude to Miguel López, the founder of the Medical Physics Unit and the Radiation Protection Service of the Universitat Rovira i Virgili, for giving me the opportunity of being part of them. I have learnt a lot from your way of addressing the problems, your ability to relate to the people and your vision for the future.

I wish to acknowledge the support and trust provided by Juan José Morant, the head of the Radiation Protection Service of the Universitat Rovira i Virgili. You have transmitted me your courage to face new challenges and your practical way to do the things.

I want to show my appreciation to my office mate and friend Maria Cros for our long conversations and her unconditional support. I also want to thank Elena Prieto for her incorporation into the project and for her future contributions on it, and to my colleague Irene Hernández for offering her help. To all of you, thank you for contributing to a nice work environment.

I am particularly grateful to Diego Molina for understanding our needs so quickly and attending them immediately. The customized software that you have programmed and your ability to anticipate our necessities has saved us an incalculable amount of time.

I would like to express the deepest appreciation to Enric Batalla, the head of the SCAR (Radioactive Activities Coordination Service) of the Generalitat de Catalunya, for his energy and enthusiasm. Without your passion for research, your decisive support and your continuous contributions, this project would not have had any sense.

I would also like to thank the people from Raditel Seveis i Subministraments Tecnògics S.L. for their technical assistance, specially at the beginning of the project. In particular, I would like to thank Juan Toral for his indispensable contributions to the developments presented in this thesis.

I wish to be grateful to the members of the Section of Nuclear Engineering of the Universitat Politècnica de Catalunya, with special emphasis to Alfredo de Blas, for their interest in the project and subsequent incorporation and support.

My special gratitude goes also to Dr. Harri Toivonen, the head of the Laboratory for Security Technology of STUK (Radiation and Nuclear Safety Authority in Finland), for giving me the opportunity to do a research stay under his supervision. I would also like to thank all the STUK staff who helped me during my stay there and that were so warm despite of the Finnish winter. Specially, I would like to thank my new friends Sakari Ihantola and Philip Holm for helping me to deeply discover the Finnish culture.

I would like to thank AGAUR (Agència de Gestió d'Ajuts Universitaris i de Recerca) of Generalitat de Catalunya for the grant BE-DGR 2011 in the framework of Grants for Research Stays abroad, which financed my research stay in STUK (Finland).

I would like to acknowledge CSUC (Consorci de Serveis Universitaris de Catalunya) for the cession of their supercomputers, previously available from CESCA (Centre de Supercomputació de Catalunya), to perform all the Monte Carlo simulations. My special acknowledgment to its staff for the technical support provided.

Finally, I would especially like to thank all the people that have not been directly involved with my thesis, but without their support it would have been more difficult. First, I want to thank my innumerable friends, with special mention to those who have been also involved with a doctorate and know what this really means. Second, I would also like to give special thanks to all my family. In particular, words cannot express how grateful I am to my father Ramon, my mother Anna Maria and my brother Albert for all the affection provided. Besides, I wish to show my appreciation to my father-in-law Miguel and my mother-in-law Tomi for receiving me as a son. At the end, I would like to express my infinite appreciation to my beloved nearly-wife Natalia who has been always at my side and has brought brightness to my life.

# List of contributions

## Thesis papers

This thesis is based on the following peer-reviewed publications, which will be referred to in the text by their capital Roman numerals:

- [I] R. Casanovas, J.J. Morant, M. López, I. Hernández-Girón, E. Batalla, M. Salvadó. *Performance of data acceptance criteria over 50 months from an automatic real-time environmental radiation surveillance network.* Journal of Environmental Radioactivity 102 (2011) 742-748.
- [II] R. Casanovas, J.J. Morant, M. Salvadó. *Energy and resolution calibration of NaI(Tl) and LaBr<sub>3</sub>(Ce) scintillators and validation of an EGS5 Monte Carlo user code for efficiency calculations.* Nuclear Instruments and Methods in Physics Research A 675 (2012) 78-83.
- [III] R. Casanovas, J.J. Morant, M. Salvadó. *Temperature peak-shift correction methods for NaI(Tl) and LaBr<sub>3</sub>(Ce) gamma-ray spectrum stabilisation.* Radiation Measurements 47 (2012) 588-595.
- [IV] R. Casanovas, J.J. Morant, M. Salvadó. *Implementation of gamma-ray spectrometry in two real-time water monitors using NaI(Tl) scintillation detectors.* Applied Radiation and Isotopes 80 (2013) 49-55.
- [V] R. Casanovas, J.J. Morant, M. Salvadó. *Development and calibration of a real-time airborne radioactivity monitor using gamma-ray spectrometry on a particulate filter.* IEEE Transactions on Nuclear Science 61 (2014) 727-731.
- [VI] R. Casanovas, J.J. Morant, M. Salvadó. *Development and calibration of a real-time airborne radioactivity monitor using direct gamma-ray spectrometry with two scintillation detectors.* Applied Radiation and Isotopes 89 (2014) 102-108.

## Patent applications

In the context of this thesis, two patent applications have been made. They correspond, respectively, to the developments described in papers [V] and [VI]. They will be referred to in the text by their Roman numerals:

- [i] R. Casanovas, M. Salvadó, M. López, C. Tapia, A. de Blas. *Estación de identificación y medida en tiempo real de la radiactividad ambiental gamma mediante espectrometría sobre filtro de papel* (in Spanish). ES Patent Application P201230408, 16th March 2012. Available: [http://www.oepm.es/pdf/ES/0000/000/02/42/58/ES-2425801\\_A1.pdf](http://www.oepm.es/pdf/ES/0000/000/02/42/58/ES-2425801_A1.pdf)
- [ii] R. Casanovas, M. Salvadó, M. López. *Estación de identificación y medida en tiempo real de la radiactividad ambiental gamma, mediante espectrometría con dos cristales de centelleo* (in Spanish). ES Patent Application P201230236, 15th February 2012. Available: [http://www.oepm.es/pdf/ES/0000/000/02/42/32/ES-2423236\\_A1.pdf](http://www.oepm.es/pdf/ES/0000/000/02/42/32/ES-2423236_A1.pdf)

## Preliminary reports

Preliminary reports based on the contents of this thesis have been given at:

- R. Casanovas, E. Prieto, M. Salvadó. *Calibración y estudio de las capacidades de medida de los equipos de espectrometría gamma en tiempo real desarrollados para la renovación de la red de estaciones automáticas de vigilancia radiológica ambiental de la Generalitat de Catalunya*. 39 Reunión Anual de la Sociedad Nuclear Española. Reus, 2013.
- E. Prieto, R. Casanovas, M. Salvadó. *Estudio comparativo entre las medidas radiológicas adquiridas mediante espectrometría gamma con cristales de NaI(Tl) y LaBr<sub>3</sub>(Ce) y aquellas obtenidas con detectores Geiger*. 39 Reunión Anual de la Sociedad Nuclear Española. Reus, 2013.
- R. Casanovas, J.J. Morant, M. Salvadó. *Desarrollo y calibración de equipos automáticos de medida en tiempo real de la radiactividad ambiental mediante espectrometría gamma*. III Congreso Conjunto de las Sociedades Españolas de Física Médica y Protección Radiológica. Cáceres, 2013.
- E. Prieto, M. Salvadó, R. Casanovas. *Método para analizar espectros y establecer alertas tempranas en medidas de espectrometría gamma ambiental en tiempo real*. III Congreso Conjunto de las Sociedades Españolas de Física Médica y Protección Radiológica. Cáceres, 2013.
- R. Casanovas. *Utilización de detectores de LaBr<sub>3</sub>(Ce) para espectrometría gamma en tiempo real*. VII Jornadas sobre Calidad en el Control de la Radiactividad Ambiental. Tarragona, 2012.

- R. Casanovas, J.J. Morant, M Salvadó. *Development and calibration of a real-time airborne radioactivity monitor using gamma-ray spectrometry on a particulate filter.* Real Time Conference (RT)18th IEEE-NPSS, 1-4. Berkeley (California), 2012.
- R. Casanovas. *Desarrollo de un equipo de medida de la radiactividad en aerosoles, captados en un filtro de papel, con capacidad de análisis mediante espectrometría gamma utilizando un cristal de NaI(Tl). Resultados preliminares.* VI Jornadas sobre Calidad en el Control de la Radiactividad Ambiental. Cáceres, 2010.
- R. Casanovas, A. de Blas, M. Salvadó, X. Serra, J. Toral, J. Sánchez, E. Batalla, M. López, C. Tapia. *Desarrollo e implantación de un sistema de monitorización de la medida de concentración de actividad gamma en agua de río e identificación espectrométrica de emisores gamma basado en centelleadores de NaI(Tl). Resultados preliminares.* 35 Reunión Anual de la Sociedad Nuclear Española. Sevilla, 2009.

## Other scientific results

The following scientific results were produced during a research stay in STUK (Radiation and Nuclear Safety Authority, Helsinki, Finland), in the Laboratory for Security Technology (Head of Laboratory: Harri Toivonen). Period: From November 2011 to February 2012.

- R. Casanovas. *Calibration of a 1.5"×1.5" LaBr<sub>3</sub> scintillation detector for its use in Vasilika detection system.* Developed in STUK (Radiation and Nuclear Safety Authority of Finland). Helsinki, 2012.
- R. Casanovas. *Peak-efficiency calibration of a 5"×4" NaI scintillation detector (Pikkumusta detector).* Developed in STUK (Radiation and Nuclear Safety Authority of Finland). Helsinki, 2012.

## Other peer-reviewed publications

Other contributions in peer-reviewed journals that are not related to this thesis:

- J.J. Morant, M. Salvadó, R. Casanovas, I. Hernández-Girón, E. Velasco, A. Calzado. *Validation of a Monte Carlo based code for dose assessment in dental cone beam CT examinations.* Physica Medica: European Journal of Medical Physics 28 (2011) 200-209.
- J.J. Morant, M. Salvadó, I. Hernández-Girón, R. Casanovas, R. Ortega, A. Calzado. *Dosimetry of a cone beam computed tomography device for oral and maxillofacial radiology using Monte Carlo techniques and ICRP adult reference computational phantoms.* Dentomaxillofacial Radiology 42 (2013) 92555893.

## Book chapters

During this thesis, the following book chapters were written:

- J.J. Morant, R. Casanovas. *Interacción de la radiación con la materia (II)*. M. Alcaraz, E. Velasco (eds.). *Bases físicas y biológicas del radiodiagnóstico medico. Curso de capacitación para dirigir y operar equipos de radiodiagnóstico medico y dental*. Servicio de publicaciones de la Universidad de Múrcia. 3a Edición, pp. 26-30. 2013, ISBN: 978-84-15463-57-3.
- J.J. Morant, R. Casanovas. *Sistemas de imagen*. M. Alcaraz, E. Velasco (eds.). *Bases físicas y biológicas del radiodiagnóstico medico. Curso de capacitación para dirigir y operar equipos de radiodiagnóstico medico y dental*. Servicio de publicaciones de la Universidad de Múrcia. 3a Edición, pp. 62-74. 2013, ISBN: 978-84-15463-57-3.
- J.J. Morant, R. Casanovas, M. Alcaraz, M. Cros. *Física de las radiaciones*. J.J. Morant, M. Alcaraz, E. Velasco (eds.). *Formación básica en protección radiológica. Curso de protección radiológica dirigido al personal técnico de las empresas de venta y asistencia técnica de equipos de rayos X dentales*. Servicio de publicaciones de la Universidad de Múrcia. 1a Edición, pp. 11-68. 2013, ISBN: 978-84-15463-89-4.
- J.J. Morant, R. Casanovas, F. Velasco, P. Martínez. *Pruebas de aceptación y calibración de monitores de visualización*. J.J. Morant, M. Alcaraz, E. Velasco (eds.). *Formación básica en protección radiológica. Curso de protección radiológica dirigido al personal técnico de las empresas de venta y asistencia técnica de equipos de rayos X dentales*. Servicio de publicaciones de la Universidad de Múrcia. 1a Edición, pp. 319-334. 2013, ISBN: 978-84-15463-89-4.

## Book editions

- M. López, F. Borrull, M. Salvadó, C. Aguilar, R. Casanovas, M. Cros, I. Hernández, J.J. Morant, A. Nieto, S. Peñalver. Edition of the proceedings of the conference *VII Jornadas sobre calidad en el control de la radiactividad ambiental*, Tarragona (Spain), 2012. Available: [http://www.csn.es/images/stories/publicaciones/otras\\_publicaciones/coediciones/vii\\_jornades\\_de\\_calidad\\_web.pdf](http://www.csn.es/images/stories/publicaciones/otras_publicaciones/coediciones/vii_jornades_de_calidad_web.pdf).

# Contents

<b>Resum executiu (in Catalan)</b>	<b>vii</b>
<b>Resumen ejecutivo (in Spanish)</b>	<b>xiii</b>
<b>Acknowledgments</b>	<b>xix</b>
<b>List of contributions</b>	<b>xxi</b>
<b>Contents</b>	<b>xxv</b>
<b>1 Introduction</b>	<b>1</b>
1.1 Motivation, hypothesis and objectives . . . . .	1
1.2 Detector choice . . . . .	2
1.3 Calibration methods and spectrum stabilisation . . . . .	6
1.3.1 Energy, resolution and efficiency calibration methods . . . . .	6
1.3.2 Spectrum stabilisation methods . . . . .	7
1.4 Development and calibration . . . . .	7
1.4.1 Gamma-ray spectrometry in two water monitors . . . . .	7
1.4.2 Gamma-ray spectrometry on a particulate filter . . . . .	8
1.4.3 Direct gamma-ray spectrometry with two detectors . . . . .	8
1.5 Thesis outline . . . . .	9
<b>2 Motivation, hypothesis and objectives</b>	<b>11</b>
2.1 Performance of data acceptance criteria . . . . .	11
<b>3 Calibration methods and spectra stabilisation</b>	<b>19</b>
3.1 Energy, resolution and efficiency calibration methods . . . . .	19
3.2 Spectrum stabilisation methods . . . . .	26
<b>4 Development and calibration</b>	<b>35</b>
4.1 Gamma-ray spectrometry in two water monitors . . . . .	35
4.2 Gamma-ray spectrometry on a particulate filter . . . . .	43
4.3 Direct gamma-ray spectrometry with two detectors . . . . .	49

<b>5 Discussion</b>	<b>57</b>
5.1 Results discussion . . . . .	57
<b>6 Conclusions</b>	<b>61</b>
6.1 Main conclusions . . . . .	61
6.2 Future work . . . . .	64
<b>7 Bibliography</b>	<b>65</b>
<b>A Patent applications</b>	<b>67</b>
A.1 Patent application 1 . . . . .	67
A.1.1 Summary (in Spanish) . . . . .	67
A.1.2 Summary (in English) . . . . .	67
A.2 Patent application 2 . . . . .	75
A.2.1 Summary (in Spanish) . . . . .	75
A.2.2 Summary (in English) . . . . .	75

# Chapter 1

## Introduction

### 1.1 Motivation, hypothesis and objectives

In Spain, there are seven nuclear reactors in operation, housed in five nuclear power plants that produce, at present, approximately 20% of the electricity consumed<sup>1</sup>. Three of them are located in Catalonia (ES-E, Spain-East), about 150 km from Barcelona and are named Vandellòs-II, Ascó-I and Ascó-II.

The Euratom Treaty confers important powers to the European Commission with regard to monitoring and assessment of levels of radioactivity in the environment and discharges with effluents [1]. In particular, the Article 35 of the Euratom Treaty requires each Member State to establish the necessary facilities to carry out continuous monitoring of the level of radioactivity in air, water and soil and to ensure compliance with the basic standards [2].

From a health point of view, nuclear installations do not produce significant releases of radioactivity in normal operation. Thus, environmental radioactivity control is no longer primarily concerned with health protection. However, the environmental radioactivity control is still an important task in Member States in terms of providing information to the population, and thus, preserving the transparency and comprehensiveness of environmental radioactivity monitoring in Europe [3].

The *Consejo de Seguridad Nuclear* (CSN, Nuclear Safety Council) is the national organism responsible for protection from ionizing radiation in Spain. In order to ensure that the radioactivity levels are in agreement with legal limits, the CSN holds a surveillance network called *Red de Vigilancia Radiológica Ambiental* (REVIRA, Environmental Radiological Surveillance Network). It consists of two subnetworks [4], [5]: the *Red de Estaciones Automáticas* (REA, Automatic Stations Network) and the Red de Estaciones de Muestreo

---

<sup>1</sup>Until 6<sup>th</sup> July of 2013, there were eight nuclear reactors in operation, housed in six nuclear power plants, but the only reactor housed in the nuclear power plant of Santa María de Garoña was closed due to economic issues.

(REM, Sampling Stations Network). The REA involves several types of remote, real-time and in-situ radiation measurements, whereas the REM involves sampling (air, water, food, ground and sediments) followed by laboratory analysis. In Catalonia, the management of REVIRA is transferred to the *Servei de Coordinació d'Activitats Radioactives* (SCAR, Radioactive Activities Coordination Service) of the *Generalitat de Catalunya* (Catalan government) and integrated with its own real-time surveillance network.

From 2006 to present, several tasks concerning the Catalan real-time radiation surveillance network have been commissioned to the *Unitat de Física Mèdica* (Medical Physics Unit) of the *Universitat Rovira i Virgili* (Rovira i Virgili University). Some of them have been management, control, technical maintenance, calibration, improvement, research and data analysis. As a consequence of the development of these tasks, our research group has gained a broad experience on real-time environmental radiation monitoring.

This experience with the Catalan network has permitted us to make several improvements in it to get better quality and quantity of data. Then, to give a quick response to equipment failures or possible radiological incidents, an easily implementable data analysis methodology was set. All this, was fully described in the first paper that conforms this thesis, Paper [I]. In the paper, we also made an exhaustive inspection of the Catalan network capabilities. In particular, we studied the network capabilities during the incident occurred in Ascó on December 2007, which was classified as Level 2 [6] in the International Nuclear and Radiological Event Scale (INES) [7]. The main conclusion of the inspection was the need of having better radiological information in real-time. To overcome this limitation, the implementation of in-situ real-time gamma-ray spectrometry was suggested as a solution. This improvement should provide the network with better analysis capabilities and should make it possible a more efficient response in case of increment of the radiation levels.

After the conclusions of Paper [I], the SCAR supported our suggestion and decided to go for real-time gamma-ray spectrometry. Thus, several agreements were signed between the *Universitat Rovira i Virgili* and the *Generalitat de Catalunya* to start the development of automatic real-time environmental radioactivity monitors using gamma-ray spectrometry. Other participants in the project were *Universitat Politècnica de Catalunya* and *Raditel Serveis i Subministraments Tecnològics S.L.*

## 1.2 Detector choice

To implement gamma-ray spectrometry in the Catalan network, several options concerning the type of detectors were available. The properties of an ideal detector for gamma-ray spectrometry are well summarized in [8]:

- output proportional to gamma-ray energy

## 1.2. DETECTOR CHOICE

3

- good efficiency (high absorption coefficient, high atomic number)
- easy mechanism for collecting the detector signal
- good energy resolution
- good stability over time, temperature and operating parameters
- reasonable cost
- reasonable size

However, there is no ideal detector fulfilling all these criteria and the choice of a detector is always a compromise among these factors.

In the measurement of gamma-ray energies above several hundred keV, there are, at present, only two detector categories of major importance [9]: inorganic scintillators and germanium semiconductor detectors. When used for gamma-ray spectrometry, the most relevant difference between them, which is clearly observed in the obtained spectra, is the energy resolution. In routine use, the semiconductor detectors have better energy resolution than scintillation detectors.

Since the discovery of NaI(Tl) as a scintillation material in 1948, significant effort has been put into the research and development of new scintillators for detection of nuclear radiation. A summary of the progress in the development of scintillation detectors for gamma-ray spectrometry can be found in the literature [10, 11]. A history of this progress is represented in Figure 1.1.

The first germanium detectors were the Ge(Li) ones and became commercially available in the early 1960s. Then, in the early 1980s, the widespread availability of high-purity germanium (HPGe) provided an alternative to them. In general, the important performance characteristics such as detection efficiency and energy resolution are essentially identical for Ge(Li) and HPGe detectors of the same size. Thus, the main difference between them is that whereas Ge(Li) detectors must be continuously maintained at low temperature, HPGe detectors can be allowed to warm to room temperature between uses, which gives them much greater operational convenience [9]. However, this is still a limitation in comparison with scintillation detectors, which can be operated at room temperature.

The mentioned limitation is the main motivation for this statement from [8]: “Until the commercial advent of the semiconductor detector, scintillation detectors, in the main based on sodium iodide, were standard for gamma-ray spectrometry. Indeed, even now their influence on gamma spectrometry is apparent in the fact that we still relate semiconductor detector efficiency to sodium iodide. There is a general feeling abroad that scintillation detectors are a thing of the past. [...] Nevertheless, scintillation spectrometry still has a number of valuable roles to play in gamma-ray measurement and, with recent developments in lanthanum halide detectors, this scope may broaden.”

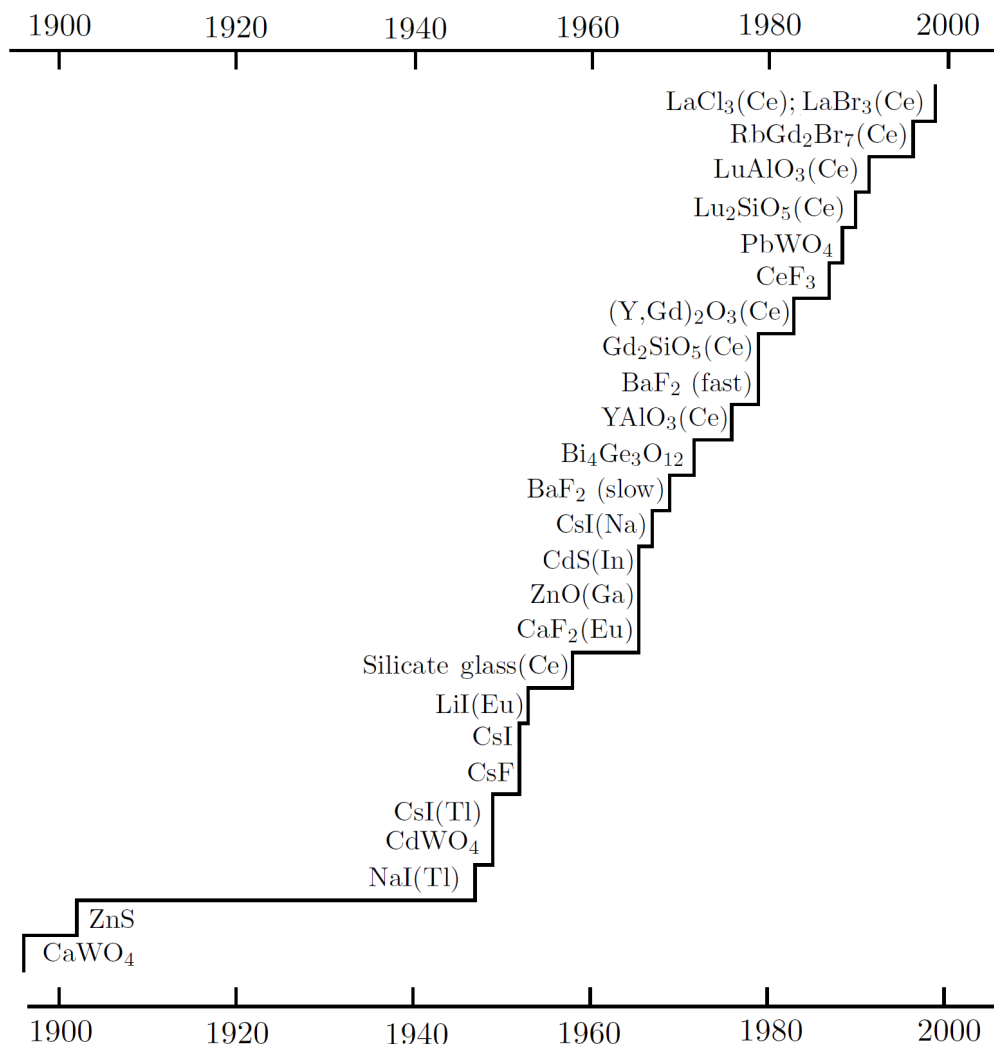


Figure 1.1: History of the discovery of major inorganic scintillation materials. Adapted from [11].

## 1.2. DETECTOR CHOICE

5

There are circumstances where space limitations or a hostile environment preclude the use of semiconductor detectors”.

Thus, considering the previous characteristics and basically to avoid the dependence on cooling systems of detectors that could be placed hundreds of kilometers away from the control base, the best choice for real-time gamma-ray spectrometry are scintillation detectors.

From all the scintillation materials, the choice must be based in the desired properties that they should have [8]:

- reasonable number of electron-hole pairs produced per unit of gamma-ray energy
- high stopping power for gamma radiation (high density and atomic number)
- the response must be proportional to energy
- transparent to the emitted light
- the decay time of the excited state must be short to allow high count rates
- it should be available in optical quality in reasonable amounts at reasonable cost
- its refractive index should be near to that of glass ( $\sim 1.5$ ) to permit efficient coupling to photomultipliers

Following the previous properties, the materials that have found particular application for gamma-ray measurements are [8]: sodium iodide (NaI), caesium iodide (CsI), calcium fluoride (CaF<sub>2</sub>), bismuth germanate (Bi<sub>4</sub>Ge<sub>3</sub>O<sub>12</sub>, commonly abbreviated as BGO) and recently, lanthanum halides (LaCl<sub>3</sub> and LaBr<sub>3</sub>). Table 1.1 provides a comparison of their properties for gamma-ray detection.

From Table 1.1, all materials (except CaF<sub>2</sub>(Eu)) have larger densities than NaI(Tl). However, when used with normal bialkali photomultiplier tubes (PMT), only lanthanum halides have larger conversion efficiencies. The conversion efficiency is related with the light output of the crystals, which in turn is related to its energy resolution. Thus, only lanthanum halides provide better performance than NaI(Tl) in gamma-ray spectrometry. Even so, these detectors have an inherent radioactive impurity content of <sup>138</sup>La and <sup>227</sup>Ac that may be necessary to remove [12].

In particular, LaBr<sub>3</sub>(Ce) is the only that has larger conversion efficiency and significantly larger density than NaI(Tl). Nevertheless, its current cost is not proportional to the advantages that it offers, but this is expected to change with time. Even so, as stated in [13]: “one should keep in mind that a LaBr<sub>3</sub>(Ce) detector costs less than HPGe having the same efficiency for <sup>60</sup>Co”.

Considering all these arguments, the implementation of gamma-ray spectrometry in the Catalan network was planned with LaBr<sub>3</sub>(Ce) detectors. Still, NaI(Tl) detectors

Table 1.1: Properties of scintillator materials for gamma-ray detection (data from [8])

Scintillator	Density (g/cm <sup>3</sup> )	WL <sup>a</sup> (nm)	DCT <sup>b</sup> (ns)	RI <sup>c</sup>	RCE <sup>d</sup> (%)
NaI(Tl)	3.67	415	230	1.85	100
CsI(Tl)	4.51	550	1000	1.79	45
CsI(Na)	4.51	420	630	1.84	85
CsI	4.51	315	16	1.95	4-6
CaF <sub>2</sub> (Eu)	3.18	435	940	1.47	50
BGO	7.13	480	300+60	2.15	15-20
LaCl <sub>3</sub> (Ce)	3.79	350	28	~1.9	130
LaBr <sub>3</sub> (Ce)	5.29	380	16	~1.9	160

<sup>a</sup> Wavelength at maximum emission.

<sup>b</sup> Decay time.

<sup>c</sup> Refractive index.

<sup>d</sup> Relative conversion efficiency (relative to NaI(Tl)), i.e. net detector output using a bialkali photomultiplier tube (PMT).

were also used, not only for their low cost but also for having the possibility to compare them with LaBr<sub>3</sub>(Ce) detectors. For both type of scintillators, the chosen size was 2" × 2", which was a compromise between the smallest and the largest LaBr<sub>3</sub>(Ce) size that was commercially available.

## 1.3 Calibration methods and spectrum stabilisation

### 1.3.1 Energy, resolution and efficiency calibration methods

After choosing the type of detectors, it was necessary to give physical significance to the measured data. For this, we set a full calibration methodology for both NaI(Tl) and LaBr<sub>3</sub>(Ce) detectors, which was fully described in Paper [II]. The full calibration comprised energy, resolution and efficiency calibrations.

For the two former calibrations, we made a review of the different functions that were used by different authors. We tested them with our own experimental data from our NaI(Tl) and LaBr<sub>3</sub>(Ce) detectors by using radioactive sources of <sup>241</sup>Am, <sup>133</sup>Ba, <sup>137</sup>Cs, <sup>60</sup>Co and <sup>152</sup>Eu. Otherwise, for the efficiency calibration, we developed a Monte Carlo user code for the EGS5 code system. The user code was prepared to contain all of the information of the radiation source (type of particles, energy and probabilities of emission, position and geometry, direction of emission, etc.) and the detector geometry (components, sizes, materials, etc.). Besides, it contained all the calculations related to the quantities to be obtained, which were basically the obtention of the gamma-ray

## 1.4. DEVELOPMENT AND CALIBRATION

7

energy spectra (with or without peak broadening) and the efficiency calculations, both with their associated statistical uncertainties. The code was validated by comparing its results with experimental measurements.

### 1.3.2 Spectrum stabilisation methods

Although the calibration methodology described in Paper [II] is enough to warrant a correct performance of the detectors in laboratory conditions, it is not when detectors are used in an open environment. In an open environment, the detectors operate under unstable temperature conditions that may lead to gain instabilities and result in a peak shift and spectral distortion during measurements. And thus, the energy calibration can not be used. To solve this issue, two methodologies for spectra stabilisation using software algorithms were presented in Paper [III]. These methodologies are of special interest for detectors with analogue gain control, which not make it possible to adjust it automatically.

The methods proposed in Paper [III] were validated in the laboratory under controlled temperature conditions for both NaI(Tl) and LaBr<sub>3</sub>(Ce) detectors. Although they were initially designed for detectors with analogue gain control, they could also be used in detectors with digital gain control when their correction systems are not able to perform the stabilisation.

## 1.4 Development and calibration

The development of automatic real-time environmental radioactivity monitors for the *Generalitat de Catalunya* was carried out in parallel with development of the previous calibration methodologies and methods for spectra stabilisation. In fact, the development of these methodologies was motivated for the future needs of the developed monitors.

Thus, three types of radioactivity monitors using gamma-ray spectrometry were developed: one to measure radioactivity levels in water and the other two to measure the airborne radioactivity (i.e. the radioactive content in the air) using two different approaches.

### 1.4.1 Gamma-ray spectrometry in two water monitors

The first type of monitor, the water monitor, was an improvement of two existing water monitors of the Catalan network. These detection systems are located in the Ebre River, before and after passing by the nuclear plant at Ascó, because the plant uses the river water to cool its two reactors. The monitors collect the water from the river through a pump and it is analyzed in a vessel, which is shielded with Pb.

The improvement consisted in the implementation of gamma-ray spectrometry using

NaI(Tl) detectors, which was conducted through the installation of a parallel spectrometric module in the initial design of the monitor. Before the improvement, these monitors had only been providing the total gamma activity concentration in water. After the implementation, the monitor enabled the real-time identification and quantification of radioactive isotope content in the river water. The details of the implementation are fully described in Paper [IV]. In the paper, the full calibration of the monitor is discussed and an example of a radiological increment during rain is used to show the advantages of gamma-ray spectrometry. Besides, the minimum detectable activity concentrations (MDACs) for  $^{131}\text{I}$ ,  $^{137}\text{Cs}$  and  $^{40}\text{K}$  are presented for different integration times, which give an idea of the capabilities of the monitor.

#### 1.4.2 Gamma-ray spectrometry on a particulate filter

The second developed monitor was a Real-time Airborne Radioactivity Monitor using gamma-ray spectrometry on a particulate Filter (RARM-F). The RARM-F collects a constant flow of air that passes across a particulate filter, where airborne aerosols are collected. Then, the filter is faced toward a NaI(Tl) or LaBr<sub>3</sub>(Ce) scintillation detector that is used for gamma-ray spectrometry. Both the detector and the active part of the filter are inside a Pb shielding, which is used to reduce the surrounding background radiation.

This development lead to Patent Application [i]. Besides, a comprehensive description of the development and calibration of RARM-F can be found in Paper [V]. In the paper, the performance of two different RARM-Fs (with different crystals) was discussed and their measurement capabilities were evaluated with some values of the MDACs for  $^{137}\text{Cs}$ . The results showed better performance for these monitors in comparison with other measuring directly in the environment.

#### 1.4.3 Direct gamma-ray spectrometry with two detectors

The third type of developed monitor was also an airborne radioactivity monitor, but in this case the measurements are made directly in the environment (i.e. without needing to concentrate the isotopes in a fiber or charcoal filter). The monitor is called Real-time Airborne Radioactivity Monitor using direct gamma-ray spectrometry with two scintillation detectors (RARM-D2). The RARM-D2 is basically formed by two scintillation detectors, one pointing up and the other pointing down, which are shielded with Pb. This geometrical disposition together with the shielding permits the discrimination between the isotopes contained in a radioactive cloud from those deposited or emerging from the ground, which can be of interest after a nuclear accident to characterize the radiation source term.

Paper [VI] describes the main aspects of the development and calibration of the RARM-D2, either using NaI(Tl) or LaBr<sub>3</sub>(Ce) detectors, with particular emphasis on the efficiency

## 1.5. THESIS OUTLINE

9

calibration. Besides, some typical spectra were shown and the measurement capabilities of this monitor were studied for  $^{131}\text{I}$  and  $^{137}\text{Cs}$  with different integration times and for both type of detectors. The results of this development have also been protected by Patent Application [ii].

### 1.5 Thesis outline

This thesis presents a collection of six papers, which have been published in peer-reviewed scientific journals, in the field of real-time environmental radioactivity detection. After a general introduction in Chapter 1, the papers are presented in chronological order of development and publication. They are grouped in three main categories that name, respectively, Chapters 2 to 4: “Motivation, hypothesis and objectives”, “Calibration methods and spectra stabilisation” and “Development and calibration”.

Chapter 2, which is formed by Paper [I], presents an overview of the automatic real-time environmental radiation surveillance network of Catalonia before the contributions of this thesis. The paper presented some improvements that have permitted the obtention of better quality and quantity of data. Besides, a data analysis methodology was set and tested in a broad range of situations that produce radiological increments. The main conclusion of the paper was the need of having better radiological information in real-time. To overcome this limitation, the implementation of in-situ real-time gamma-ray spectrometry was suggested as a solution.

Chapter 3 deals with general methodologies to ensure the optimal performance of gamma-ray spectrometry systems that use scintillation detectors. This chapter includes Paper [II] and Paper [III]. In the former, the calibration methodology for NaI(Tl) and LaBr<sub>3</sub>(Ce) detectors is discussed. In the second, two methods to stabilise gamma-ray spectra are presented and validated.

In Chapter 4, the three different developments motivated by the conclusions of Chapter 2 are presented. To ensure their optimal performance, the calibration methodologies described in Chapter 3 are adapted and applied to each of them. The details are presented in three papers (one for each monitor) that correspond to Papers [IV], [V] and [VI].

Finally, in Chapters 5 and 6, the discussion of the results and the main conclusions of the thesis are presented. Besides, future work related with the project is also stated.



## Chapter 2

# Motivation, hypothesis and objectives

## 2.1 Performance of data acceptance criteria over 50 months from an automatic real-time environmental radiation surveillance network

### Abstract

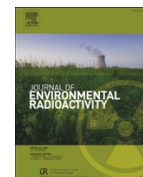
The automatic real-time environmental radiation surveillance network of Catalonia (Spain) comprises two subnetworks; one with 9 aerosol monitors and the other with 8 Geiger monitors together with 2 water monitors located in the Ebre river. Since September 2006, several improvements were implemented in order to get better quality and quantity of data, allowing a more accurate data analysis. However, several causes (natural causes, equipment failure, artificial external causes and incidents in nuclear power plants) may produce radiological measured values mismatched with the own station background, whether spurious without significance or true radiological values. Thus, data analysis for a 50-month period was made and allowed to establish an easily implementable statistical criterion to find those values that require special attention. This criterion proved a very useful tool for creating a properly debugged database and to give a quick response to equipment failures or possible radiological incidents. This paper presents the results obtained from the criterion application, including the figures for the expected, raw and debugged data, percentages of missing data grouped by causes and radiological measurements from the networks. Finally, based on the discussed information, recommendations for the improvement of the network are identified to obtain better radiological information and analysis capabilities.



Contents lists available at ScienceDirect

## Journal of Environmental Radioactivity

journal homepage: [www.elsevier.com/locate/jenvrad](http://www.elsevier.com/locate/jenvrad)



# Performance of data acceptance criteria over 50 months from an automatic real-time environmental radiation surveillance network

R. Casanovas <sup>a,\*</sup>, J.J. Morant <sup>b</sup>, M. López <sup>a,b</sup>, I. Hernández-Girón <sup>a</sup>, E. Batalla <sup>c</sup>, M. Salvadó <sup>a</sup>

<sup>a</sup> Unitat de Física Mèdica, Facultat de Medicina i Ciències de la Salut, Universitat Rovira i Virgili, ES-43201 Reus (Tarragona), Spain

<sup>b</sup> Servei de Protecció Radiològica, Facultat de Medicina i Ciències de la Salut, Universitat Rovira i Virgili, ES-43201 Reus (Tarragona), Spain

<sup>c</sup> Servei de Coordinació d'Activitats Radioactives, Departament d'Economia i Finances, Generalitat de Catalunya, ES-08018 Barcelona, Spain

### ARTICLE INFO

**Article history:**

Received 22 October 2010

Received in revised form

21 February 2011

Accepted 1 April 2011

Available online 12 May 2011

**Keywords:**

Environmental radiation surveillance network

Aerosol monitors

Geiger detectors

Data analysis

### ABSTRACT

The automatic real-time environmental radiation surveillance network of Catalonia (Spain) comprises two subnetworks; one with 9 aerosol monitors and the other with 8 Geiger monitors together with 2 water monitors located in the Ebre river. Since September 2006, several improvements were implemented in order to get better quality and quantity of data, allowing a more accurate data analysis. However, several causes (natural causes, equipment failure, artificial external causes and incidents in nuclear power plants) may produce radiological measured values mismatched with the own station background, whether spurious without significance or true radiological values. Thus, data analysis for a 50-month period was made and allowed to establish an easily implementable statistical criterion to find those values that require special attention. This criterion proved a very useful tool for creating a properly debugged database and to give a quick response to equipment failures or possible radiological incidents. This paper presents the results obtained from the criterion application, including the figures for the expected, raw and debugged data, percentages of missing data grouped by causes and radiological measurements from the networks. Finally, based on the discussed information, recommendations for the improvement of the network are identified to obtain better radiological information and analysis capabilities.

© 2011 Elsevier Ltd. All rights reserved.

## 1. Introduction

In Spain, there are eight nuclear reactors in operation, housed in six nuclear power plants that produce, at present, approximately 20% of the electrical capacity of the country. Three of them are located in Catalonia (ES-E, Spain-East), about 150 km from Barcelona and are named Vandellòs-II, Ascó-I and Ascó-II.

The Euratom Treaty requires each Member State to establish the necessary facilities to carry out real-time monitoring of the level of radioactivity in air, water and soil and to ensure compliance with the basic standards (2000/473/Euratom, 2000). Following these requirements, there is a surveillance network in Spain, as in all Member States, such as Belgium (Sombré and Lambotte, 2004), France (Abida et al., 2008), Italy (De Felice, 2001), Portugal (Madruga, 2008), Slovenia (Štuhec et al., 2006), Sweden (Wallberg and Moberg, 2002) or the United Kingdom (Jackson, 1993).

The Consejo de Seguridad Nuclear (CSN, Nuclear Safety Council) is the national organism responsible for protection from ionizing

radiation in Spain. In order to ensure that the radioactivity levels are in agreement with legal limits, the CSN holds a surveillance network called *Red de Vigilancia Radiológica Ambiental* (REVIRA, Environmental Radiological Surveillance Network). It consists of two subnetworks (CSN 23.2009, 2009), (CSN 22.2009, 2009): the *Red de Estaciones Automáticas* (REA, Automatic Stations Network) and the *Red de Estaciones de Muestreo* (REM, Sampling Stations Network). The REA involves several types of remote, real-time and in-situ radiation measurements, whereas the REM involves sampling (air, water, food, ground and sediments) followed by laboratory analysis. In Catalonia, the management of REVIRA is transferred to the *Servei de Coordinació d'Activitats Radioactives* (Radioactive Activities Coordination Service) of the *Generalitat de Catalunya* (Catalan government) and integrated with its own real-time surveillance network which is commissioned to the *Universitat Rovira i Virgili* (Rovira i Virgili University).

The main objective of an automatic real-time surveillance network is to detect as quickly as possible anomalous levels of radioactivity in the environment, especially those from the nuclear power plants. The correct network performance requires a permanent checking of the monitors and communication systems. Data

\* Corresponding author. Tel.: +34 977759382; fax: +34 977759322.  
E-mail address: [ramon.casanovas@urv.cat](mailto:ramon.casanovas@urv.cat) (R. Casanovas).

## 2.1. PERFORMANCE OF DATA ACCEPTANCE CRITERIA

13

R. Casanovas et al. / Journal of Environmental Radioactivity 102 (2011) 742–748

743

must be constantly analyzed to determine abnormalities as soon as possible. In this paper, we present how several incidences affect radiological data and a simple statistical criterion useful to early detect these incidences. This analysis methodology was implemented in the Catalan network and tested during a period of 50 months, from September 2006 to October 2010.

### 2. Materials and methods

The Catalan automatic radiation surveillance network is formed by two subnetworks, called the General Network and the Vigilance Network.

#### 2.1. Location of the measurement stations

The General Network comprises nine automatic measurement stations around the perimeter of Catalonia and near the nuclear power plants (see Fig. 1) that monitor the concentration of activity of airborne radioactivity.

The Vigilance Network comprises ten measurement stations. Eight of them monitor the ambient dose equivalent rate  $H^*$  (10) and are situated around the nuclear power plants (no further than 5 km); four around Vandellòs-II and four around Ascó-I, II. These stations ensure the continuous measurement of external ambient gamma dose rate, allowing the assessment of the external exposure of the population, as required by law (2000/473/Euratom, 2000). The other two stations are located at the Ebre river (see Fig. 2). They monitor the concentration of activity in the water before and after the river passes by both nuclear reactors at Ascó, as it is used for human consumption and crop watering.

#### 2.2. Measurement devices

##### 2.2.1. The General Network measurement devices

All of the General Network stations are equipped with a Berthold BAI-9850 (Berthold Technologies GmbH & Co.KG, Germany) measuring device. At each station, a flow of  $5 \text{ m}^3/\text{h}$  of air is collected through a moving glass-fiber filter tape that passes continuously under a ZnS(Ag) detector. It can detect alpha and beta particles and pseudocoincidences (alpha particles detected after beta particles within 200  $\mu\text{s}$ ). The pseudocoincidences are attributed to the



**Fig. 1.** Location of major cities (circles), nuclear power plants (radioactive symbol) and airborne radioactivity stations of the General Network (squares). The stations are named according to the city where they are: 1-Barcelona, 2-Roses, 3-Girona, 4-Puigcerdà, 5-Tarragona, 6-Lleida, 7-Ascó, 8-Vandellòs and 9-Viella.

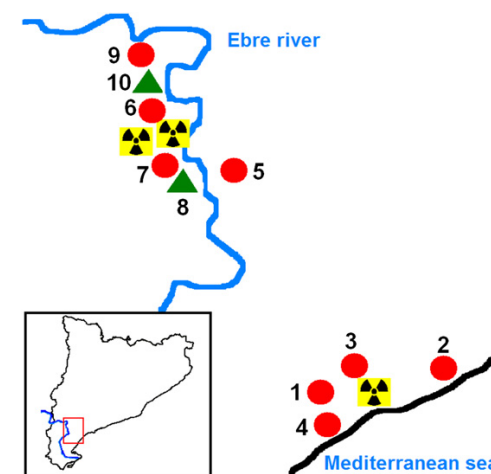


**Fig. 2.** Location of nuclear power plants (radioactive symbol) and the Vigilance Network stations (circles for dose rate monitors and triangles for in-water concentration of activity monitors). There are four stations around the nuclear power plant at Vandellòs-II (1, 2, 3, 4), four around the nuclear power plant at Ascó (5, 6, 7, 9) and two at the Ebre river before (10) and after (8) it passes by the nuclear reactors at Ascó-I, II.

natural radon decay chain ( $^{214}\text{Bi}-^{214}\text{Po}$  decays) that is the major contribution to the natural alpha and beta emissions. Thus, if the natural contributions (background and radon products) are removed from the total alpha and beta measurements, the artificial alpha and beta activity concentrations ( $\text{Bq}/\text{m}^3$ ) can be estimated. In addition, the radon activity concentration can be deduced from the pseudocoincidences (Vargas et al., 2008). After passing the filter, the air flow crosses a carbon filter and the gamma concentration of activity (due mainly to the retained iodine isotopes) is measured with a NaI(Tl) detector. Measurements are made in real-time and integrated every hour.

##### 2.2.2. The Vigilance Network measurement devices

Each Vigilance Network station giving the ambient dose equivalent rate contains two Berthold LB-6500 Geiger counters (Berthold Technologies GmbH & Co.KG, Germany), one for low doses (down to  $2 \text{ mSv}/\text{h}$ ) and the other for higher doses (up to  $10 \text{ Sv}/\text{h}$ ). Besides, both river monitors are equipped with a Berthold LB/BAI 9110 (Berthold Technologies GmbH & Co.KG, Germany) including a 25 L sample recipient with a NaI(Tl) detector to determine the total concentration of gamma activity ( $\text{Bq L}^{-1}$ ) in water. All data obtained in the Vigilance Network are measured in real-time and integrated every 10 min.

##### 2.2.3. Meteorological data

In 2008, as an important improvement, a Davis Vantage Pro2-Weather Station (Davis Instruments Corp., California, USA) was installed at each station of both networks. Before this, only the two monitors nearest to the nuclear power plants had a meteorological station. The available data from these stations are: wind speed and direction, temperature, humidity, barometric pressure, rainfall and solar radiation. Measurements are integrated every 10 min and data are transmitted via ADSL connection.

### 2.3. Data transmission and communications

Since 2008, all the General Network stations transmit via TCP/IP protocol (ADSL) except one (situated above 1400 m, at the Pyrenees) that transmitted via radio frequency (GSM) due to the

difficulty of the access until November 2010. An optical fibre line is used for the transmissions since that date. The Vigilance Network stations transmit via radio frequency signals (TETRA) but a TCP/IP (ADSL) connection is also possible if the TETRA system fails. All data (radiological and meteorological) are stored in an SQL database located in a central server. In order to grant a remote and real-time access to all data, a software in Delphi (a computer programming environment, based on Pascal language) was designed, programmed and tested specifically for this purpose.

#### 2.4. Data analysis

The raw data of all the stations are accessed and analyzed everyday by trained analysts. After the analysis, they generate another database (a debugged database) excluding the spurious values that do not correspond to valid radiological measurements and can be generated in a broad variety of situations. The database analysis is mainly focussed on the study of two items: the values that differ significantly from the mean values (called suspicious values) and the missing data.

##### 2.4.1. Suspicious values

In order to make the data analysis more straightforward, a simple discrimination criterion was established to find the suspicious values. Thus, each  $x_i$  value obtained from any monitor of the networks is checked to be in the interval described by (1):

$$\bar{x} - k\sigma \leq x_i \leq \bar{x} + k\sigma \quad (1)$$

where  $\bar{x}$  is the mean value in a long time period (e.g. 1 year),  $\sigma$  the standard deviation in the same period and  $k$  a confidence factor.

If the value fails the criterion described in (1) it is assumed to be a suspicious value and a detailed examination is made, especially if it is above the interval. Otherwise it is assumed to be normal. Once the suspicious values have been analyzed, those that do not correspond to valid radiological measurements are eliminated.

There can be many causes which can produce differences between the measured and mean data values. They can be grouped into 4 broad categories: natural, equipment failure, external (artificial non-nuclear causes) and incidents at the nuclear power plants.

It is known that several natural causes affect the radiological measurements (Mercier et al., 2009; Smetsers and Blaauwboer, 1997; Blaauwboer and Smetsers, 1997; Gómez et al., 1996; Smetsers and Blaauwboer, 1994). Some of these are rainfall, wind, temperature, humidity, air pressure and variations in the cosmic radiation intensity. In order to learn if the data are affected by natural causes, some correlations with meteorological data are checked. If these exist, the suspicious values are considered true radiological data and they are stored in the debugged database.

An important cause of suspicious values that are actually anomalous is equipment failure and therefore, communication between the technical staff and the analysts is indispensable. Spurious values generated during equipment failure are not included in the debugged database because they are not radiologically significant.

When a radiological increment is observed, it is important to consider other possible non-natural radiation sources different from nuclear power plants emissions. For example, some sources of radiological data exceeding the criterion of suspicious values can be gammagraphies (such as gamma-source welding inspection equipment) or other emissions from non-nuclear industries in the vicinity of the monitors. Hence, if there is no previous notification, an investigation about the activities performed around the monitors becomes necessary.

Finally, when evidence of natural causes, equipment failure or external causes are not found, radioactive increments may be

related to incidents in the nuclear plants. In these cases, it is essential to compare the information given by the automatic network with other sources of environmental radioactivity measurement, such as the REM network (sampling and high flow filters analyzed with germanium detectors). Regarding this, for the water monitors located in the Ebre river, when the concentration of activity is above  $3 \text{ Bq L}^{-1}$  there is an automatic system that fills two recipients of 15 L each as a way of sampling for later analysis.

##### 2.4.2. Missing data

When there are missing data, the affected monitor does not work in real-time and the previous methodology analysis cannot be applied. Generally, the most common reasons for the lack of data are electricity supply failure, communication problems, technical interventions (calibrations, cleaning, tests, etc.) and equipment failure (computer locks, mechanical problems, etc.). In order to reduce the missing data periods and the number of visits to the stations, remotely-controlled (through an IP address) switches and circuit breakers were installed. When communication is recovered, data saved in the local hard disks are recovered into the main database (SQL server) and data analysis is performed.

#### 2.5. Data calculations

The calculations and graphic representations of data are carried out with an analysis program in a Delphi environment which was designed, programmed and tested by our research group. The program works with the values taken directly from the SQL database and allows several calculations to be made using the raw and the debugged databases. The program calculations include means, standard deviations, number of obtained and lost data, number of data inside or outside the interval  $\bar{x} \pm k\sigma$  and the corresponding percentages, and maximum and minimum values. Moreover, its graphic interface allows the representation and visualization of the radiological and meteorological data, either separately or together.

The obtained data are used to perform daily, monthly and annual reports that are submitted to the competent organism. Besides, the system can randomly generate spurious data (virtual values) in order to test the procedures in case of radiological increments.

### 3. Results

#### 3.1. Data analysis

The criterion described by equation (1), which is simple to implement, was tested and proved from September 2006 to October 2010. This criterion proved to be useful for the automatic detection of the anomalous values produced by several causes taking  $k = 3$  for the General Network and  $k = 2$  for the Vigilance Network. One year is a period long enough to calculate the mean and the standard deviation since shorter periods would not properly account for the small seasonal variations observed in the measurements (see Fig. 3).

As an illustration of the former criterion, some examples are given and classified as in the 4 categories explained in section 2.4.1.

Rainfall is the main natural cause producing values above the defined interval in the dose rate (see Fig. 4). During rain episodes, the radon flushes from the subsoil to the atmosphere and some aerosols are deposited, increasing the equivalent dose rate. During the data analysis, when correlations with rain and suspicious radiological values are found, data are considered valid and stored in the debugged database.

Another easily observed effect is the accumulation of sediments and algae in the pump and the vessel of the river monitors. This

## 2.1. PERFORMANCE OF DATA ACCEPTANCE CRITERIA

15

R. Casanovas et al. / Journal of Environmental Radioactivity 102 (2011) 742–748

745

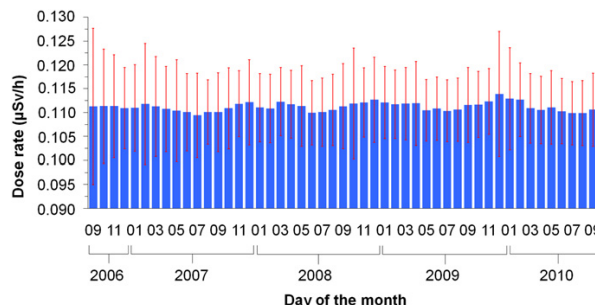


**Fig. 3.** Monthly averages of the ambient dose equivalent rate (bars) and representation of  $2\sigma$  (intervals) during the period September 2006–October 2010. The seasonal variations are clearly observed.

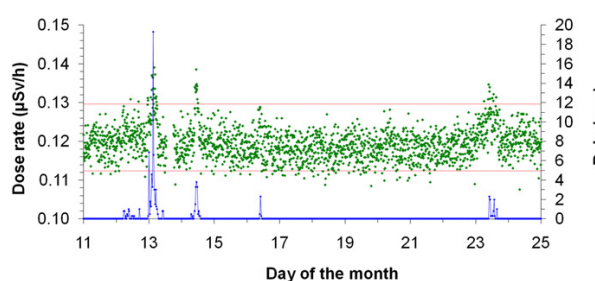


**Fig. 4.** Representation of the dose rate (dots), the  $2\sigma$  criterion calculated over one year (dotted lines) and instant rainfall (solid lines). Correlations between radiological increments and rain are clear, and hence, the values are not considered spurious.

accumulation depends on many external parameters such as rainfall (implying a rise of the sediments), weather (affecting the reproductive cycle of the algae), river flow (critical when dragging sediments or algae) or the maintenance cleaning operations. The observed effect is a progressive increase in the radiological values (see Fig. 5) that disappears once the maintenance cleaning operations are carried out. Although the cleanup is planned every month, extra cleaning operations are performed when significant increments are observed, mainly due to rainfall. Sometimes, this unpredictable behaviour makes it difficult to apply the criterion to the river monitors because it produces a non-constant mean and a large standard deviation. Even so, the criterion is useful to notice when cleaning operations are necessary.

In most cases, anomalous radiological values are produced by equipment failure. The most common problem occurs with the particulate monitors and it is due to a glass-fiber filter rupture or jam (see Fig. 6 for an example). Regarding this, each measurement

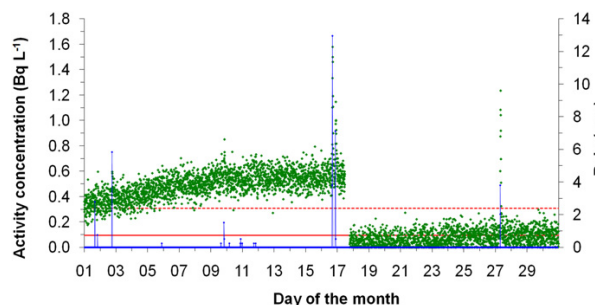


**Fig. 5.** Representation of activity concentration in a river monitor (dots), annual activity concentration average (horizontal solid line), annual  $2\sigma$  upper interval (dotted line) and instant rainfall (vertical solid lines). The variation of the activity concentration due to the vessel and pump cleaning on 17th day is clearly shown.

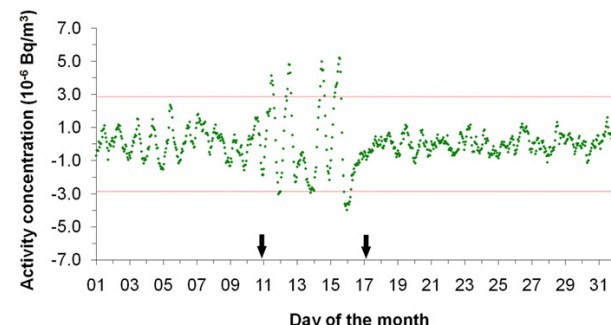


**Fig. 6.** Representation of the gamma activity concentration for an aerosol monitor (dots) and the  $3\sigma$  criterion (dotted lines). The arrows indicate when a filter rupture was produced and when it was repaired in order to appreciate its effect in the gamma concentration of activity.

station has a webcam connected by ADSL that permits to see the status of the filter (in addition to grant the installation security). Other general problems affecting the values may be a loss of the calibration parameters, an alteration of air or water flow, a computer block and a broad variety of mechanical and electronic problems. See Fig. 7 for an example of anomalous values appearing in the gamma channel after a particulate monitor restart.

Due to their simplicity, Geiger monitors do not show such a range of problems. However, they may also be affected by electronic problems (see Fig. 8 for an example that shows the effect on the dose rate of a broken fluorescent lamp near a Geiger monitor). In these cases, the data debugging criteria vary depending on the case, but usually, only isolated measurements exceeding the interval are individually eliminated.

The river monitors rarely present any operational problems. However, an alteration of the water flow or the loss of calibration parameters could cause anomalous values.

Sometimes, radiological increases appear with no evidence of any correlations with natural causes or equipment failure and that may not be related to nuclear plants operation. Fig. 9 shows an example of the effect of industrial gammographies in the vicinity of a nuclear power plant. In this case, all the gammagraphy interventions were previously notified, documented and authorized and the peaks were observed at the same time that the provided interventions.

In December 2007, there was an incident (Level 2 on the INES scale of the IAEA) in the nuclear power plant at Ascó and some radioactive particles were found inside and outside the nuclear

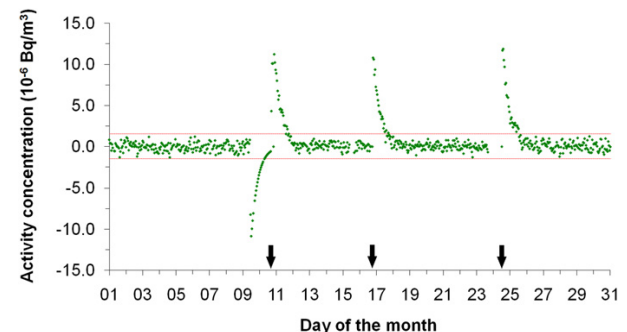


**Fig. 7.** Representation of the gamma activity concentration for an aerosol monitor (dots) and the  $3\sigma$  criterion (dotted lines). The arrows indicate when equipment restarts happened. The first set of anomalous values below the lower dotted line is due to a filter rupture.

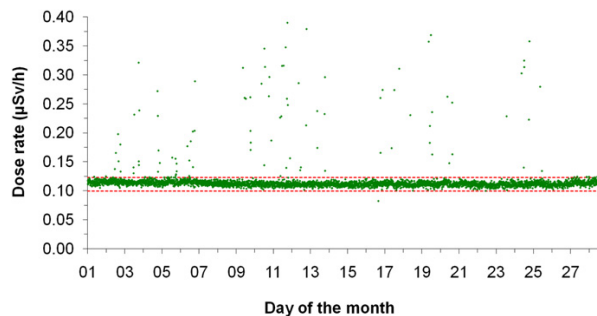


**Fig. 8.** Representation of the dose rate (dots) and the  $2\sigma$  criterion calculated over one year (dotted lines). No rainfall was present on these days. The values outside the interval were considered spurious because they were caused by the effect of the electronic interferences of a broken fluorescent lamp near the Geiger counter.

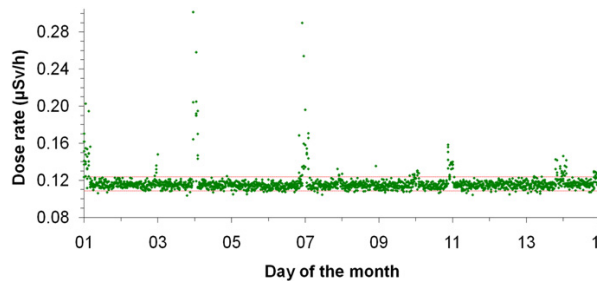


**Fig. 9.** Representation of the dose rate (dots) and the  $2\sigma$  criterion calculated over one year (dotted lines). No rainfall was present on these days. The values above the interval were produced by the performance of industrial gammographies in the vicinity of the Geiger monitor.

power plant perimeter (CSN, 2008). The incident was detected at the nearest monitor to the power plant. Fig. 10 shows the ambient dose equivalent rate evolution together with the rainfall intensity (which was not correlated to the increase). When the radiological values were studied, it was found that natural, equipment or other causes of suspicious values could be discarded, and thus, the probability of an incident at a nuclear power plant was high. Later, more detailed studies confirmed these suspicions.

During the incident, the mean of the radiological measurements increased by  $0.023 \mu\text{Sv/h}$  with respect to the annual mean value of the station. The monthly mean of this station increased significantly along with the standard deviation during the incident (see Fig. 11).

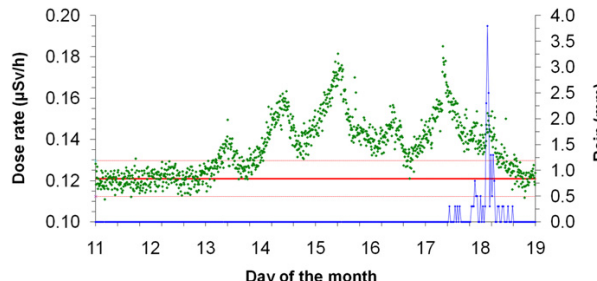


**Fig. 10.** Representation of the dose rate (dots), the annual dose rate average (solid horizontal line), the  $2\sigma$  criterion calculated over one year (dotted lines) and the rain (vertical solid lines). It can be clearly seen that no rain was presented before the 17th day. The values above the interval were produced by the referred incident in the nuclear power plant of Ascó.

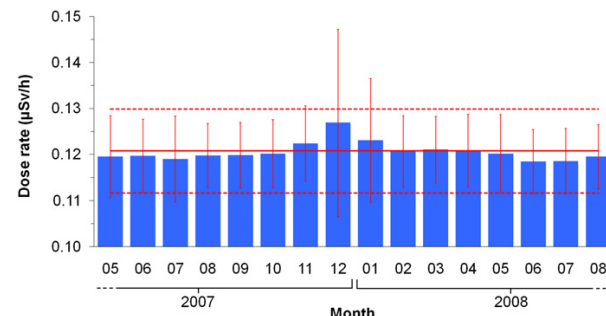


**Fig. 11.** Monthly (bars) and annual (solid line) averages of the ambient dose equivalent rate together with the representation of the  $2\sigma$  monthly average (intervals) and annual  $2\sigma$  (dotted lines) during the incident occurred in December 2007.

### 3.2. Number of valid data

During the period of analysis (September 2006–October 2010), a total of 1,315,008 radiological values were expected for the General Network and 2,191,680 values for the Vigilance Network. Table 1 shows the number of expected data together with the received data (raw data) and the stored data after the data analysis (debugged data).

The difference between the number of raw and debugged data is due to several incidences. During the analysis period, the General Network registered 631 incidences whereas 540 incidences are attributable to the Vigilance Network. The mean percentages of the different causes attributed to the lack of data in both networks are represented in Table 2.

### 3.3. Radiological measurements

After the data analysis, the means ( $\bar{x}$ ) and the standard deviations ( $\sigma$ ) of the values obtained in all the stations of both networks (General Network and Vigilance Network) were calculated using the debugged database. Tables 3 and 4 show the means and the corresponding standard deviations obtained during the period of study in the General Network and the Vigilance Network, respectively.

For the aerosol monitors, calculations over 12, 18, 25 and 36 months were compared to those performed over the whole period (50 months) giving, in some cases, discrepancies higher than 2200% for the means and below 38% for standard deviations. The

**Table 1**

Number of expected, not debugged and debugged data (September 2006–October 2010). The values in brackets are the percentages calculated relative to expected data.

	General Network	Vigilance Network
Expected data	1,315,008	2,191,680
Raw data	1,284,661 (97.7%)	2,140,335 (97.7%)
Debugged data	1,243,311 (94.5%)	2,125,344 (97.0%)

**Table 2**

Mean percentages of missing data due to different causes in both networks (September 2006–October 2010). The values in brackets are the ranges (minimum and maximum) obtained at the individual stations.

	General Network (%)	Vigilance Network (%)
Electricity supply	0.7 (0.1–2.0)	0.4 (0.0–1.5)
Communications	0.4 (0.0–1.1)	0.9 (0.4–2.7)
Technical interventions	0.9 (0.6–1.8)	0.5 (0.1–2.2)
Equipment failure	3.1 (0.3–5.5)	0.8 (0.0–2.4)
Mean for all causes	5.2 (2.7–7.6)	2.6 (1.0–6.5)

## 2.1. PERFORMANCE OF DATA ACCEPTANCE CRITERIA

17

R. Casanovas et al. / Journal of Environmental Radioactivity 102 (2011) 742–748

747

**Table 3**

Mean and standard deviation of the concentration of activity ( $\text{Bq}/\text{m}^3$ ) of artificial alpha and beta emitters, radon and gamma for the General Network. Period September 2006–October 2010.

Measurement Station	Alpha		Beta		Radon		Gamma	
	$\bar{x}$	$\sigma$	$\bar{x}$	$\sigma$	$\bar{x}$	$\sigma$	$\bar{x}$	$\sigma$
1 Barcelona	0.002	0.068	-0.011	0.093	5.32	5.67	$3.2 \cdot 10^{-9}$	$5.3 \cdot 10^{-7}$
2 Roses	0.001	0.036	0.003	0.077	5.03	4.00	$-9.8 \cdot 10^{-9}$	$6.2 \cdot 10^{-7}$
3 Girona	0.015	0.052	0.020	0.118	10.69	9.46	$1.3 \cdot 10^{-8}$	$1.4 \cdot 10^{-6}$
4 Puigcerdà	0.003	0.045	-0.018	0.122	9.97	8.62	$9.9 \cdot 10^{-9}$	$1.4 \cdot 10^{-6}$
5 Tarragona	0.013	0.055	0.032	0.095	5.29	4.00	$1.9 \cdot 10^{-8}$	$6.8 \cdot 10^{-7}$
6 Lleida	0.005	0.089	-0.037	0.125	9.92	10.50	$1.4 \cdot 10^{-8}$	$1.3 \cdot 10^{-6}$
7 Ascó	-0.007	0.053	-0.017	0.106	6.59	7.15	$3.2 \cdot 10^{-9}$	$9.3 \cdot 10^{-7}$
8 Vandellòs	0.040	0.049	0.014	0.069	2.85	1.95	$-7.0 \cdot 10^{-9}$	$4.8 \cdot 10^{-7}$
9 Vielha	-0.020	0.061	-0.003	0.088	4.52	3.78	$-4.3 \cdot 10^{-9}$	$9.6 \cdot 10^{-7}$

**Table 4**

Mean and standard deviation of the dose rates (Geiger monitors) and the concentrations of activity (river stations) for the period September 2006–October 2010. The last column shows the relative standard deviations.

Geiger monitors			
Station	$\bar{x}$ ( $\mu\text{Sv}/\text{h}$ )	$\sigma$ ( $\mu\text{Sv}/\text{h}$ )	$\sigma/\bar{x}$ (%)
1	0.111	0.004	4.0
2	0.120	0.004	3.4
3	0.111	0.004	3.8
4	0.114	0.004	3.6
5	0.107	0.004	3.4
6	0.120	0.005	3.8
7	0.107	0.005	4.6
9	0.111	0.004	3.5
River monitors			
Station	$\bar{x}$ ( $\text{Bq L}^{-1}$ )	$\sigma$ ( $\text{Bq L}^{-1}$ )	$\sigma/\bar{x}$ (%)
8	0.264	0.219	82.8
10	0.211	0.210	99.9

wide variability of data is a consequence of the measurement of artificial emitters (that is not an absolute measurement), which in normal conditions is expected to be nil. Even so, although the relative variations observed seem to be huge (2200%) the absolute radiological variations are very small (less than  $0.02 \text{ Bq}/\text{m}^3$ ).

For the Geiger monitors these values do not vary much compared with those of shorter periods. Several comparisons were made for different periods (12, 18, 25 and 36 months) and gave results with discrepancies lower than 0.3% for the means and 7.5% for the standard deviations, respectively. As it does not rain often, the distributions of the obtained values with the Geiger monitors are nearly Gaussian, thus, taking  $k = 2$  only 2.25% of the values are expected to be above the interval as false positives.

The measurements in the river monitors are sensitive to external causes such as algae, sediments and river flow variations. Hence, comparisons between the studied period (50 months) and shorter ones (12, 18, 25 and 36 months) gave discrepancies up to 48% for the means and 29% for standard deviations, giving better agreements for the longer periods.

## 4. Discussion

### 4.1. Geiger monitors

Data calculations for the Geiger monitors show mean values between 0.107 and 0.120  $\mu\text{Sv}/\text{h}$  (0.9–1.1  $\text{mSv}/\text{y}$ ), which are below the worldwide average background dose of  $2.4 \text{ mSv}/\text{y}$  (UNSCEAR, 2000) and the Spanish nationwide average effective dose of  $1.6 \text{ mSv}/\text{y}$  (García-Talavera et al., 2007). In practice, the values in the debugged database can be considered as natural background. The reason is that on the one hand, the anomalous values (representing

less than 0.7% of the total received values) are removed and on the other, those associated to incidents and other external causes affecting the radiological natural background are negligible when considering long calculation periods.

The interpretation of the criterion when applied to the Geiger monitors can be directly related to the annual dose limit for the public of  $1 \text{ mSv}$  (ICRP 103, 2007). Therefore, if a station gave the constant value of  $\bar{x} + 2\sigma$  over the whole year, the annual effective dose that a person standing beside the monitor would receive over one year would be less than 10% of the annual limit (noticing that the ambient dose equivalent is a conservative estimate of the effective dose (ICRP 103, 2007)).

In order to classify radiological increments, the values are considered normal until an increment of  $\bar{x} + 2\sigma$  is produced, that is used to define an *investigation level*. This level, which is quite restrictive, is suitable for the real-time detection of increments between measured and mean data values (caused either by the malfunction of the station or by external radiological increases). Two additional levels above  $\bar{x}$  are defined according to legislation: *alert level*, set to  $1 \text{ mSv}/\text{y}$  ( $0.114 \mu\text{Sv}/\text{h}$ ), (ICRP 103, 2007), and *alarm level*, set to  $8.8 \text{ mSv}/\text{y}$  ( $1 \mu\text{Sv}/\text{h}$ ) (CSN IS-10, 2006).

The mentioned incident in Ascó provided us with a lot of information on the capabilities of the network. Thus, taking into account the *investigation level* of performance described before, the incident was properly detected by the Geiger detector nearest to the nuclear power plant. The *investigation level*, that may seem very restrictive, was the only criterion that made it possible to detect the incident, since the maximum value registered was about  $\bar{x} + 13\sigma$ , and so the second and the third levels were above this value. In another study (Baeza et al., 1993), a similar criterion was implemented as a radiological pre-alert in another network with  $k = 15$  and with the mean calculated for the last 30 days values. Hence, in this case, this other criterion would not be suitable to detect the incident.

### 4.2. Aerosol monitors

The criterion described for these monitors is very difficult to interpret for damage assessment because the legal limits established for the concentrations of activity are only set for individual isotopes (RD-783/2001, 2001), (96/29/Euratom, 1996). Even so, the criterion has been found to be useful to detect abnormal operation of the equipment and to remove the not radiologically significant (being the 3.2% of all received values).

It is important to notice that during the Ascó incident, none of the Berthold aerosol monitors detected anything abnormal. This fact, together with the big percentage of missing data due to equipment failure or technical interventions and the difficulties in data interpretation makes it necessary to carry out a future full inspection of these monitors.

### 4.3. River monitors

In the river monitors, the values above the *investigation level* are usually caused either by punctual rain periods or by continuous increments in the activity concentrations produced by the sludge or algae deposited in the sample recipient. Thus, the criterion is used by the network operator to determine when a vessel cleaning is necessary. Unfortunately, the radiological values obtained cannot easily be interpreted in terms of the legislation RD-140/2003 (based on the World Health Organization Recommendations (World Health Organization, 2008)) because total gamma activity concentrations are not considered in them. In this way, as in the aerosol monitors, it would be desirable to obtain more complete information, such as the activity concentration of each individual isotope.

## 5. Conclusions

The accurate analysis of the values obtained in a real-time monitoring network depends on several factors, among others: frequency and transmission speed of new data, experience and training of the staff operating the network, stability of measuring equipment in continuous operation and the reliability of the obtained data. In this sense, an exhaustive maintenance of the measuring equipment and data transmission systems is required. The full remote control applied to all network systems reduced costs and visits to the stations and increased the data availability. However, the network system sometimes produces suspicious values which can be either anomalous (due to equipment malfunction) or caused by true radiological increases which, in turn, can be produced by natural causes (those correlated with meteorological data) or artificial causes (due to external artificial activities).

In order to identify these suspicious data, a simple statistical criterion was presented. This criterion is easily implementable since it involves simple calculations over the database. However, it is sufficiently restrictive and adequate to notice anomalous events. In addition, it can be combined with meteorological information to generate automatic warnings or alerts that can be sent via email, SMS, etc. The criterion was found to be useful in a broad range of situations that produce radiological increments, such as natural causes, equipment failure, incidents at the nuclear power plants and other artificial causes.

The criterion is clearly interpreted when applied to Geiger monitors because radioactivity increases can be related to legal limits, whereas, aerosol and river monitors do not permit this interpretation. Therefore, it would be advisable a revision of the latest and the implementation of new detection systems with major capabilities. This renewal of the network equipment should be carried out taking into account important features like real-time measurements, remote control (restart, calibrations, etc.), software calculations, data transmission and meteorological data availability.

The installation of in-situ gamma ray spectrometry, together with the proposed statistical criterion, would allow the implementation of accurate alarms limiting the concentrations of activity for the different isotopes, or at least, it would help to discriminate natural causes from artificial emissions, since the involved isotopes in both cases would not be the same. In this case, the criterion could be a useful tool to perform a preliminary automatic analysis and would help in the fast identification of abnormal increases related to each individual isotope. This would enable a comparison with the legal limits established for activity concentrations in air or in water (drinking water standards). Finally, the proposed criterion would also allow an early generation of automatic alerts in spectrometric systems, enabling a better and a faster response in case of a possible accident scenario.

## References

- 96/29/Euratom, 29 June 1996. Commission Recommendation of 13 May 1996, Official Journal of the European Commission, No. 159. Available: [http://ec.europa.eu/energy/nuclear/radioprotection/doc/legislation/9629\\_en.pdf](http://ec.europa.eu/energy/nuclear/radioprotection/doc/legislation/9629_en.pdf).
- 2000/473/Euratom, 27 July 2000. Commission Recommendation of 8 June 2000, Official Journal of the European Commission, No. 191. Available: [http://ec.europa.eu/energy/nuclear/radioprotection/doc/legislation/00473\\_en.pdf](http://ec.europa.eu/energy/nuclear/radioprotection/doc/legislation/00473_en.pdf).
- Abida, R., Bocquet, M., Vercauteren, N., Isnard, O., 2008. Design of a monitoring network over France in case of a radiological accidental release. *Atmos. Env* 42, 5205–5219.
- Baeza, A., del Puerto, J.A., del Rio, M., Miró, C., Ortiz, F., Paniagua, J.M., 1993. Development and Operativity of a real-time radiological monitoring network Centred on the nuclear power plant of Almaraz (Spain). *IEEE Trans. Nucl. Sci.* 40 (6), 2014–2020.
- Blaauboer, R.O., Smetsers, R.C.G.M., 1997. Outdoor concentrations of the Equilibrium equivalent decay products of  $^{222}\text{Rn}$  in the Netherlands and the effect of meteorological Variables. *Radiat. Prot. Dosim.* 69, 7–18.
- Consejo de Seguridad Nuclear (CSN), 2008. Informe sobre notificación de sucesos en centrales nucleares. Available (in Spanish): <http://www.csn.es/descarga/INFSUC1ersem08.pdf>.
- De Felice, P., 2001. The quality Assurance Programme for the national radioactivity surveillance network in Italy. *Radiat. Prot. Dosim.* 97, 313–316.
- García-Talavera, M., Matarranz, J.L., Martínez, M., Salas, R., Ramos, L., 2007. Natural ionizing radiation exposure of the Spanish population. *Radiat. Prot. Dosim* 124, 353–359.
- Gómez, V., Vera, F., Martín, A., 1996. Gross alpha- and beta-activities in Rainwater and Airbone particulate Samples. Influence of rainfall and radon. *J. Environ. Radioact.* 31, 273–285.
- Instrucción IS-10, de 25 de julio de 2006, del Consejo de Seguridad Nuclear, por la que se establecen los criterios de notificación de sucesos al Consejo por parte de las centrales nucleares. BOE Núm. 263 23 noviembre 2006. Available (in Spanish): [http://www.csn.es/descarga/IS\\_10.pdf](http://www.csn.es/descarga/IS_10.pdf).
- ICRP, 2007. The 2007 recommendations of the International Commission on radiological protection. Ann. ICRP 37 (2–4) ICRP Publication 103.
- Jackson, R.L., 1993. Rimnet: the United Kingdom government system for response to Overseas nuclear Accidents. *Radiat. Prot. Dosim.* 50, 171–176.
- Madruga, M.J., 2008. Environmental radioactivity monitoring in Portugal. *Appl. Radiat. Isot* 66, 1639–1643.
- Mercier, J.F., Tracy, B.L., d'Amours, R., Chagnon, F., Hoffman, I., Korpach, E.P., 2009. Increased environmental gamma-ray dose rate during precipitation: a strong correlation with contributing air mass. *J. Environ. Radioact* 100, 527–533.
- Programas de vigilancia radiológica ambiental. Resultados 2008, 2009. Colección de Informes Técnicos Núm. 23.2009. Consejo de Seguridad Nuclear. Available (in Spanish): [http://www.csn.es/images/stories/publicaciones/unitarias/informes\\_tecnicos/pvra2008ok.pdf](http://www.csn.es/images/stories/publicaciones/unitarias/informes_tecnicos/pvra2008ok.pdf).
- Red de estaciones automáticas de vigilancia radiológica ambiental (REA) del CSN, 2009. Operación y resultados años 2006 y 2007. Colección de Informes Técnicos CSN 22.2009. Consejo de Seguridad Nuclear. Available (in Spanish): [http://www.csn.es/images/stories/publicaciones/unitarias/informes\\_tecnicos/re0607.pdf](http://www.csn.es/images/stories/publicaciones/unitarias/informes_tecnicos/re0607.pdf).
- Real Decreto 140/2003, de 7 de febrero, por el que se establecen los criterios sanitarios de la calidad del agua de consumo humano. BOE núm. 45, 21 febrero 2003. Available (in Spanish): [http://www.msc.es/ciudadanos/saludAmbLaboral/docs/rd\\_140\\_2003.pdf](http://www.msc.es/ciudadanos/saludAmbLaboral/docs/rd_140_2003.pdf).
- Real Decreto 783/2001, de 6 de julio, por el que se aprueba el Reglamento sobre protección sanitaria contra radiaciones ionizantes. BOE núm. 178, 26 julio 2001. Available (in Spanish): [http://www.csn.es/images/stories/publicaciones/unitarias/normativa/reglamento\\_proteccion.pdf](http://www.csn.es/images/stories/publicaciones/unitarias/normativa/reglamento_proteccion.pdf).
- Smetsers, R.C.G.M., Blaauboer, R.O., 1994. Time-Resolved monitoring of Outdoor radiation levels in the Netherlands. *Radiat. Prot. Dosim* 55, 173–181.
- Smetsers, R.C.G.M., Blaauboer, R.O., 1997. A Dynamic Compensation Method for natural ambient dose rate based on 6 Years data from the Dutch radioactivity monitoring network. *Radiat. Prot. Dosim.* 69, 19–31.
- Sombré, L., Lambotte, J.M., 2004. Overview of the Belgian Programme for the surveillance of the Territory and the Implications of the International Recomendations or Directives on the monitoring Programme. *J. Environ. Radioact.* 72, 75–87.
- Štuhec, M., Zorko, B., Mitic, D., Miljanić, S., Ranogajec-Komor, M., 2006. Quality Assurance of environmental gamma radiation monitoring in Slovenia. *Radiat. Prot. Dosim.* 121, 191–194.
- United Nations Scientific Committee on the Effects of Atomic Radiation, 2000. Sources and Effects of Ionizing Radiation. Report to General Assembly (New York: UNSCEAR). Available: <http://www.unscear.org/docs/reports/gareport.pdf>.
- Vargas, A., Arnold, D., Ortega, X., Parages, C., 2008. Influence of natural radioactive aerosols on artificial radioactivity detection in the Spanish surveillance networks. *Appl. Radiat. Isot* 66, 1627–1631.
- Wallberg, P., Moberg, L., 2002. Evaluation of 20 Years of environmental monitoring data around Swedish nuclear installations. *J. Environ. Radioact* 63, 117–133.
- World Health Organization, 2008. Guidelines for Drinking-water Quality [electronic Resource]: Incorporating 1st and 2nd Addenda, vol. 1, Recommendations, third ed., ISBN 9789241547611. Available: [http://www.who.int/water\\_sanitation\\_health/dwq/fulltext.pdf](http://www.who.int/water_sanitation_health/dwq/fulltext.pdf).

## Chapter 3

# Calibration methods and spectra stabilisation

### 3.1 Energy and resolution calibration of NaI(Tl) and LaBr<sub>3</sub>(Ce) scintillators and validation of an EGS5 Monte Carlo user code for efficiency calculations

#### Abstract

The radiation detectors yield the optimal performance if they are accurately calibrated. This paper presents the energy, resolution and efficiency calibrations for two scintillation detectors, NaI(Tl) and LaBr<sub>3</sub>(Ce). For the two former calibrations, several fitting functions were tested. To perform the efficiency calculations, a Monte Carlo user code for the EGS5 code system was developed with several important implementations. The correct performance of the simulations was validated by comparing the simulated spectra with the experimental spectra and reproducing a number of efficiency and activity calculations.



Contents lists available at SciVerse ScienceDirect

## Nuclear Instruments and Methods in Physics Research A

journal homepage: [www.elsevier.com/locate/nima](http://www.elsevier.com/locate/nima)



# Energy and resolution calibration of NaI(Tl) and LaBr<sub>3</sub>(Ce) scintillators and validation of an EGS5 Monte Carlo user code for efficiency calculations

R. Casanovas <sup>a,\*</sup>, J.J. Morant <sup>b</sup>, M. Salvadó <sup>a</sup>

<sup>a</sup> Unitat de Física Mèdica, Facultat de Medicina i Ciències de la Salut, Universitat Rovira i Virgili, ES-43201 Reus (Tarragona), Spain

<sup>b</sup> Servei de Protecció Radiològica, Facultat de Medicina i Ciències de la Salut, Universitat Rovira i Virgili, ES-43201 Reus (Tarragona), Spain

## ARTICLE INFO

### Article history:

Received 30 December 2011

Received in revised form

23 January 2012

Accepted 5 February 2012

Available online 10 February 2012

### Keywords:

Scintillation gamma-ray spectrometry

NaI(Tl)

LaBr<sub>3</sub>(Ce)

Energy calibration

Resolution calibration

Monte Carlo simulation

Efficiency calculation

## ABSTRACT

The radiation detectors yield the optimal performance if they are accurately calibrated. This paper presents the energy, resolution and efficiency calibrations for two scintillation detectors, NaI(Tl) and LaBr<sub>3</sub>(Ce). For the two former calibrations, several fitting functions were tested. To perform the efficiency calculations, a Monte Carlo user code for the EGS5 code system was developed with several important implementations. The correct performance of the simulations was validated by comparing the simulated spectra with the experimental spectra and reproducing a number of efficiency and activity calculations.

© 2012 Elsevier B.V. All rights reserved.

## 1. Introduction

Scintillation detectors, with a special emphasis on the NaI(Tl) detectors, have been broadly used in many fields over the last 50 years [1]. Recently, the new lanthanum-based scintillators have become commercially available [2]. Compared with the NaI(Tl) detectors, the lanthanum detectors have better scintillation properties, including energy resolution, temperature performance, decay time, light yield and material density [2]. All of these capabilities make lanthanum detectors good candidates to substitute the NaI(Tl) scintillators in most applications.

Nonetheless, the correct performance of all radiation detectors requires the correct calibration. When the scintillation detectors are used for gamma spectrometry, the calibration procedure can be divided into three sub-calibrations [3]: the energy calibration, the resolution calibration and the efficiency calibration. These calibrations make it possible to correctly identify and determine the activity of the involved isotopes.

However, while the energy and the resolution calibrations are easily performed experimentally, the efficiency calibration can be a demanding task, especially for complex and extended source geometries. Thus, a common approach to perform the efficiency calibration is to use the Monte Carlo (MC) simulation techniques,

which must be experimentally validated at least for the simple source geometries. This validation enables one to extrapolate the simulations to obtain the efficiency curves for other sources that would be difficult or impossible to obtain in a laboratory.

In this study, we perform the energy and the resolution calibrations for the NaI(Tl) and LaBr<sub>3</sub>(Ce) scintillators, and we test several fitting functions used in both calibrations. For the efficiency calculations, we present an MC user code, which is validated with certified calibration sources. The details of the more important implementations of the MC code are also discussed.

## 2. Materials and methods

### 2.1. Experimental setup

The detectors used in this study were a 2" × 2" NaI(Tl) and a 2" × 2" LaBr<sub>3</sub>(Ce) scintillation detectors. The NaI(Tl) detector was an ORTEC® Model 905-3 and the LaBr<sub>3</sub>(Ce) detector was a BrilLanCe™380 from Saint-Gobain Crystals. Both detectors were coupled to a preamplifier (ORTEC® Model 276) and an amplifier (ORTEC® Model 575A), which were connected to a multichannel pulse-height analyser ORTEC® TRUMP™-PCI-2k. The spectrum analysis software that we used was ScintiVision™ from ORTEC®.

The experimental data were obtained from five radioactive sources that allowed the coverage of all gamma energies up to 1408 keV. Table 1 shows the current activity (deduced from the

\* Corresponding author. Tel.: +34977759382; fax: +34977759322.  
E-mail address: ramon.casanovas@urv.cat (R. Casanovas).

### 3.1. ENERGY, RESOLUTION AND EFFICIENCY CALIBRATION METHODS 21

R. Casanovas et al. / Nuclear Instruments and Methods in Physics Research A 675 (2012) 78–83

79

**Table 1**

Radioactive sources used in this study with their current activity and their active dimensions.

Radionuclide	Current activity <sup>a</sup> (kBq)	Source shape	Active dimensions (mm)
<sup>241</sup> Am	3.2 ± 0.3	Squared	Side=55
<sup>133</sup> Ba	1.0 ± 0.1	Circular	Radius=47
<sup>137</sup> Cs	4.0 ± 0.4	Circular	Radius=0.5
<sup>60</sup> Co	1.40 ± 0.14	Circular	Radius=1.0
<sup>152</sup> Eu	Unknown	Unknown	Unknown

<sup>a</sup> At the time of measurement.

certifications) and the active dimensions of each source. In all measurements, the background spectra were subtracted. The data related to the decay, the energies and the emission probabilities were taken from [4].

#### 2.1.1. Energy calibrations

The energy calibration consists of establishing a relationship between the channels  $C$  and the corresponding gamma-ray energies  $E$  in the spectrum. Because this relationship is not always linear [5], as expected, its nonlinearity may produce inaccuracies in the determination of the peak energies and the comparison of real spectra with the MC simulations. This nonlinearity is produced as a consequence of the different uncertainties introduced in the measured energies that come from the different processes involved in the detection of gamma-rays [1].

Thus, the relationship between the energy  $E$  and the peak position  $C$  should be extended to a polynomial with  $n > 1$ :

$$E = \sum_{k=0}^n a_k \cdot C^k \quad (1)$$

where  $n$  is the degree of the polynomial.

#### 2.1.2. Resolution calibrations

The non-proportional light response in scintillation detectors is the main cause of the limited energy resolution [1,6–8]. This limitation makes it necessary to perform a peak width calibration, which establishes a correspondence between the peak width and its energy. Resolution calibrations are necessary as an input not only for the peak-analysis software but also for the MC simulations to obtain realistic spectra. Because the peak width is often given by the Full Width at Half Maximum (FWHM), this calibration establishes the dependence of the FWHM on the energy  $E$ , i.e., it sets the function  $\text{FWHM}(E)$ . However, there is no consensus in the literature on the mathematical form of this function. Thus, we tested several functions to identify one that provides the best fit (see Table 3).

#### 2.1.3. Experimental efficiency calibrations

The relationship between the number of counts under a peak and the activity of a radioactive source is set by the efficiency calibration. Whereas the two previous calibrations only depended on the gamma-ray energy, the efficiency calibration depends on many other factors, such as the source-to-detector distance, the source geometry and the materials surrounding the setup. Consequentially, the efficiency calibration is only valid for identical calibration and measuring conditions.

If the efficiency calibrations are performed with certified sources, the experimental efficiencies  $\varepsilon_{\text{exp}}$  are calculated using the following equation:

$$\varepsilon_{\text{exp}} = \frac{N}{A \cdot t \cdot p} \quad (2)$$

where  $N$  is the number of net counts under the full-energy peak,  $A$  is the known radionuclide activity,  $t$  is the counting time and  $p$  is the emission probability of the particular gamma-ray being measured.

The uncertainty propagation gives the following equation for the efficiency uncertainty  $\delta\varepsilon_{\text{exp}}$ :

$$\delta\varepsilon_{\text{exp}} = \varepsilon_{\text{exp}} \sqrt{\left(\frac{\delta N}{N}\right)^2 + \left(\frac{\delta A}{A}\right)^2 + \left(\frac{\delta p}{p}\right)^2} \quad (3)$$

#### 2.2. Monte Carlo simulation

The MC simulations were performed with the EGS5 code system [9]. This general-purpose package enables the simulation of the coupled transport of electrons and photons in an arbitrary geometry. The EGS5 subroutines are controlled by a user code, which must be written in Fortran 77. The user code must contain all of the information about the radiation source (the type of particles, the energy and the probabilities of emission, the position and the geometry, the direction of emission, etc.) and the detector geometry (the components, the sizes, the materials, etc.). In addition, the user code must contain all of the calculations related to the quantities to be obtained.

In this study, we were interested in reproducing real gamma-ray spectra and performing the efficiency calculations. A user code for EGS5 was prepared for this purpose, where the radioactive isotopes comprising the emitting source were modelled through their gamma emission energies and associated probabilities. The source spatial distribution and the emitting directions are set in each simulated history (i.e., in each simulation of the primary source-particles and all of the secondary particles produced by it). Thus, it is possible to define extended sources that emit in the desired directions. Meanwhile, the geometry where the radiation interacts was defined using the combinational geometry package [9], which allows the definition of multiple geometries by combining 14 elemental bodies.

Fig. 1 shows the geometry of the NaI/LaBr<sub>3</sub> detectors. The dimensions were adapted to the manufacturer technical specifications. Basically, the geometry was modelled with the corresponding scintillation crystal with a case of 0.5 mm of aluminium. The space between the case and the crystal was filled with air. A glass light guide after the crystal was also considered, and the photomultiplier tube was modelled as a filled-of-air cylinder of aluminium. The material information (density and composition) were taken from [10], and the cut-off energy for the photons and the electrons was set at 10 keV.

#### 2.2.1. Simulation of gamma-ray spectra

When some energy  $E'$  is deposited into the detector, a count in the corresponding channel of the spectrum is recorded. However, the gamma-ray spectra obtained in the simulations are very

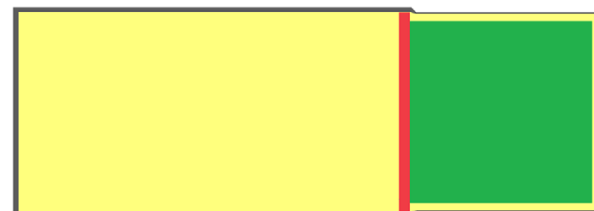


**Fig. 1.** Cross-section of the detector geometry used in the simulations. The modelled parts are: scintillation crystal (green), aluminium (grey), glass light guide (red) and air (yellow). (For interpretation of the references to color in this figure legend, the reader is referred to the web version of this article.)

## 22 CHAPTER 3. CALIBRATION METHODS AND SPECTRA STABILISATION

80

R. Casanovas et al. / Nuclear Instruments and Methods in Physics Research A 675 (2012) 78–83

different from the spectra obtained with the detectors due to their finite resolution. Thus, the resolution calibration in the user code must be accounted for obtaining the realistic spectra.

The relationship between the calculated energy deposition spectrum  $S_0$  and the real spectrum  $S$ , which would be observed in a real detector, can be represented through the following convolution [11]:

$$S(E) = \int S_0(E') \cdot G(E-E') dE' \quad (4)$$

where  $S_0(E')$  is the probability that a photon deposits the energy  $E'$  in the detector crystal per unit energy  $E'$  and per incident fluence, and  $G(E-E')$  is the probability per unit pulse height that a deposited energy  $E'$  will give counts on the energy channel  $E$ .

The resolution function  $G(E-E')$  is generally approximated by a Gaussian distribution [11]:

$$G(E-E') = \frac{1}{\sqrt{2\pi}\sigma^2} e^{-(E-E')^2/2\sigma^2} \quad (5)$$

It is important to remark that in Eq. (5), the standard deviation  $\sigma$  is not constant because it is a function of the photon energy, i.e.,  $\sigma=\sigma(E')$ .

The convolution described by Eq. (4) was implemented in the user code using the Box-Muller algorithm [12] to sample the Gaussian functions. Thus, the gamma-particle-deposited energy  $E'$  was readjusted using the following equation:

$$E = E' + \sigma(E') \cdot \sin(2\pi\xi_1) \cdot \sqrt{-2 \ln \xi_2} \quad (6)$$

where  $\xi_1$  and  $\xi_2$  are independent random variables uniformly distributed in the interval [0,1]. In practice, Eq. (6) is rewritten in terms of the FWHM using the following relationship:

$$\sigma = \frac{\text{FWHM}}{2\sqrt{2\ln 2}} \quad (7)$$

### 2.2.2. Statistical uncertainty calculations

The results are obtained after the simulation of  $N_{\text{hist}}$  histories. To estimate the statistical uncertainties, we split these  $N_{\text{hist}}$  histories into  $m$  statistical batches of  $N_{\text{hpb}}=N_{\text{hist}}/m$  histories. Then, the expected value  $\langle x \rangle$  of a certain quantity of interest  $x$  is estimated by its average:

$$\bar{x} = \frac{1}{m} \sum_{i=1}^m \bar{x}_i \quad (8)$$

where  $\bar{x}_i$  is the average of the quantity  $x_i$  over the  $N_{\text{hpb}}$  histories in the  $i$ -th batch.

According to the central limit theorem, when  $N_{\text{hist}} \rightarrow \infty$ , the distribution of  $\bar{x}$  is Gaussian. Thus, an unbiased estimator of the variance of  $\bar{x}$  is

$$s_x^2 = \frac{s_x^2}{m} \quad (9)$$

with

$$s_x^2 = \frac{1}{m-1} \sum_{i=1}^m (\bar{x}_i - \bar{x})^2. \quad (10)$$

For our purposes, the use of the method of statistical batches is unaffected by the problems described in [13] and is fully equivalent to the approach described in [14].

### 2.2.3. Monte Carlo efficiency calculations

The MC efficiency  $\varepsilon_{\text{MC}}$  calculations were performed by reproducing the experimental setup for each radioactive source (to account the different source sizes and source-detector distances). For the efficiency calculations, a monoenergetic source was considered to avoid unnecessary interferences in the spectrum.

Thus, the MC efficiency was calculated in each statistical batch as

$$\varepsilon_{\text{MC}} = \frac{N_{\text{counts}}}{N_{\text{hpb}}} \quad (11)$$

where  $N_{\text{counts}}$  is the number of counts under the full energy peak, and  $N_{\text{hpb}}$  is the number of photons emitted by the source per batch. Then, the MC efficiency and its uncertainty were obtained from Eqs. (8) and (9).

### 2.2.4. Variance reduction

To obtain better statistics with fewer simulations, a variance reduction method, the direction bias method [14], was implemented, which only considers the photons that are emitted against the detector. In this method, the scored quantities must be weighted with the corresponding statistical weight  $w$ . The weight is defined in each history as

$$w = \frac{\text{true probability}}{\text{sampled probability}} \quad (12)$$

## 2.3. Activity calculation

Once the MC efficiencies  $\varepsilon_{\text{MC}}$  are calculated, it is possible to estimate the activity of any radioactive isotope. If we use  $n_p$  peaks for the calculation, the activity  $A_{\text{calc}}$  of the given isotope is the weighted mean of all  $k$ -peak activities  $A_{\text{calc},k}$ :

$$A_{\text{calc}} = \frac{\sum_k^n A_{\text{calc},k} \cdot w_k}{\sum_k^n w_k} \quad (13)$$

with the weights

$$w_k = \frac{1}{(\delta A_{\text{calc},k})^2} \quad (14)$$

Then, the uncertainty of Eq. (13) is evaluated using the following relationship:

$$\delta A_{\text{calc}} = \frac{1}{\sqrt{\sum_k^n w_k}} \quad (15)$$

The activity related to the  $k$ -peak is calculated by rearranging Eq. (2) as

$$A_{\text{calc},k} = \frac{N_k}{\varepsilon_{\text{MC},k} \cdot t \cdot p_k} \quad (16)$$

where  $N_k$  is the number of counts under the  $k$ -peak,  $p_k$  the probability and  $\varepsilon_{\text{MC},k}$  is the corresponding efficiency.

Finally, the uncertainty for the  $k$ -peak corresponding activity is given by

$$\delta A_{\text{calc},k} = A_{\text{calc},k} \sqrt{\left(\frac{\delta N_k}{N_k}\right)^2 + \left(\frac{\delta \varepsilon_{\text{MC},k}}{\varepsilon_{\text{MC},k}}\right)^2 + \left(\frac{\delta p_k}{p_k}\right)^2} \quad (17)$$

## 3. Results and discussion

### 3.1. Energy calibrations

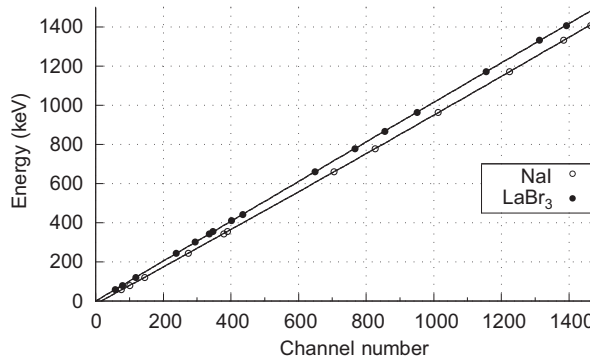
To set the suitable  $n$  for Eq. (1) and to obtain the fitting coefficients, several data points were obtained with the available radioactive sources described in Table 1. Fig. 2 shows the data used for NaI(Tl) and LaBr<sub>3</sub>(Ce) in the energy calibrations.

Table 2 shows the results of the data fit to Eq. (1) for  $n=1, 2, 3$  and 4. The goodness of fit was evaluated with the adjusted coefficient of determination  $\bar{R}^2$  instead of the usual coefficient of determination  $R^2$ . This coefficient takes into account whether the additional fitting parameters in fact improve the fit.

### 3.1. ENERGY, RESOLUTION AND EFFICIENCY CALIBRATION METHODS 23

R. Casanovas et al. / Nuclear Instruments and Methods in Physics Research A 675 (2012) 78–83

81



**Fig. 2.** Data points used for the energy calibration of both the NaI(Tl) and the LaBr<sub>3</sub>(Ce) detectors. The continuous lines correspond to a 2nd-order polynomial fit.

**Table 2**  
 Fitting functions for the energy calibration with their corresponding adjusted coefficient of determination for both detectors.

Fitted $E(C)$ function	$\bar{R}^2$	
	NaI	LaBr <sub>3</sub>
$E = a_0 + a_1 C$	0.999968	0.999995
$E = a_0 + a_1 C + a_2 C^2$	0.999994	0.999996
$E = a_0 + a_1 C + a_2 C^2 + a_3 C^3$	0.999994	0.999996
$E = a_0 + a_1 C + a_2 C^2 + a_3 C^3 + a_4 C^4$	0.999993	0.999997

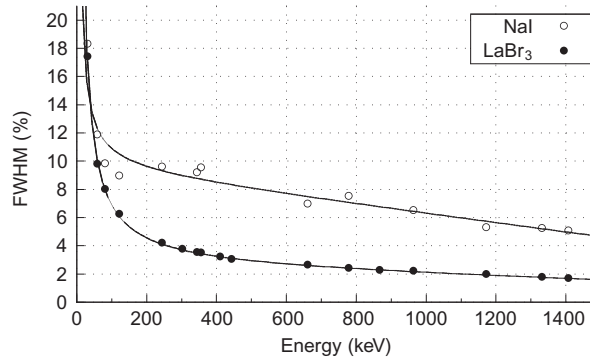


**Fig. 3.** Data points used in the resolution calibration of both the NaI(Tl) and the LaBr<sub>3</sub>(Ce) detectors. The continuous lines correspond to a 2nd-order polynomial fit.

The results in Table 2 show that a 2nd-order polynomial ( $n=2$ ) is the best option for the energy calibration. However, for  $n=1$ , the detectors showed a good linearity in all ranges. The highest deviation from linearity was produced at the lowest energy (59.5 keV), but it was less than 12% and 4% for NaI and LaBr<sub>3</sub>, respectively. Finally, for  $n > 2$ , the fit did not improve significantly, but deviations lower than 2% for the lowest energy point could be achieved.

#### 3.2. Resolution calibrations

To identify the best FWHM( $E$ ) function, different functions were tested to fit the data in Fig. 3. Again, the accuracy of the fit was evaluated with the adjusted coefficient of determination  $\bar{R}^2$ . The results of different fits are shown in Table 3.

**Table 3**

Fitted functions with their corresponding adjusted coefficient of determination for both detectors. The references of the functions found in the literature for different types of gamma-spectrometers are also provided.

Fitted FWHM function	Literature	$\bar{R}^2$		
	Detector	References	NaI	LaBr <sub>3</sub>
FWHM( $E$ ) = $a + bE$	Ge	[3,21]	0.98011	0.99301
FWHM( $E$ ) = $a + b\sqrt{E}$	Ge	[3]	0.99534	0.99904
FWHM( $E$ ) = $a \cdot E^b$	NaI	[15]	0.99310	0.99884
FWHM( $E$ ) = $a + b\sqrt{E + cE^2}$	NaI, LaCl <sub>3</sub>	[16–18]	0.99581	0.99900
FWHM( $E$ ) = $a\sqrt{E + bE}$	NaI, LaBr <sub>3</sub>	[3,19]	0.99138	0.99873
FWHM( $E$ ) = $a\sqrt{E}$	NaI	[20]	0.98729	0.99850
FWHM( $E$ ) = $\sqrt{a + bE}$	NaI, Ge	[3,21]	0.97922	0.99923
FWHM( $E$ ) = $\sqrt{a + bE + cE^2}$	Ge	[3,21]	0.91769	0.99917
FWHM( $E$ ) = $a + bE + cE^2$	NaI, LaBr <sub>3</sub>	[22]	0.99713	0.99979
FWHM( $E$ ) = $a + b\sqrt{E + c}$	NaI, LaBr <sub>3</sub>	This study	0.99492	0.99922
FWHM( $E$ ) = $a + bE + cE^2 + d\sqrt{E}$	NaI, LaBr <sub>3</sub>	This study	0.99699	0.99980
FWHM( $E$ ) = $a + bE + c\sqrt{E}$	NaI, LaBr <sub>3</sub>	This study	0.99550	0.99904
FWHM( $E$ ) = $aE + bE^2$	NaI, LaBr <sub>3</sub>	This study	0.99695	0.98146

From the results of Table 3, the relationship that best fits the experimental data for both detectors is

$$\text{FWHM}(E) = a + bE + cE^2 \quad (18)$$

Eq. (18) also has a more user-friendly mathematical form than other equations, which makes it more usable. The results in Table 3 show that the data points from the LaBr<sub>3</sub> detector provide better fits in comparison with the NaI detector. This result is obvious from the distribution of the data points observed in Fig. 3, which is more irregular for NaI. Similar results were obtained by other authors [8].

From Fig. 3, the energy resolution is clearly better for the LaBr<sub>3</sub> detector than for the NaI detector all over the energy range. In particular, the obtained resolutions for the 661.7 keV  $\gamma$ -rays of the <sup>137</sup>Cs source were 7.0% for the NaI detector and 2.6% for the LaBr<sub>3</sub> detector. However, at low energies the differences become smaller. This can be explained by considering that the energy resolution improves when the light yield increases. Thus, at low energies NaI crystals show an excess of light [1,8], while the LaBr<sub>3</sub> ones show a reduced light yield in this region [6]. And so, this non-proportionality of the light yield explains the observed behaviour.

#### 3.3. Spectra simulations

The resolution function obtained from the fit of Eq. (18) for each detector was incorporated into the MC code. As the fit can only be trusted in the energy region  $[E_{\min}, E_{\max}]$  defined by the calibration sources, we impose a linear interpolation from  $\text{FWHM}(0)=0$  to  $\text{FWHM}(E_{\min})$ . The correct performance of the implemented algorithm can be observed in Fig. 4 for an <sup>152</sup>Eu source.

#### 3.4. Efficiency calculations

The efficiency calculations of the MC code were tested with the certified sources described in Table 1. Table 4 shows the source-detector distance considered, the experimental and the calculated efficiencies,  $\varepsilon_{\text{exp}}$  and  $\varepsilon_{\text{MC}}$ , and the relative differences RD (%) for both detectors.

From Table 4, we observe that the simulations are in good agreement with the experimental measurements. The discrepancies between the experimental and the calculated efficiencies can

## 24 CHAPTER 3. CALIBRATION METHODS AND SPECTRA STABILISATION

82

R. Casanovas et al. / Nuclear Instruments and Methods in Physics Research A 675 (2012) 78–83

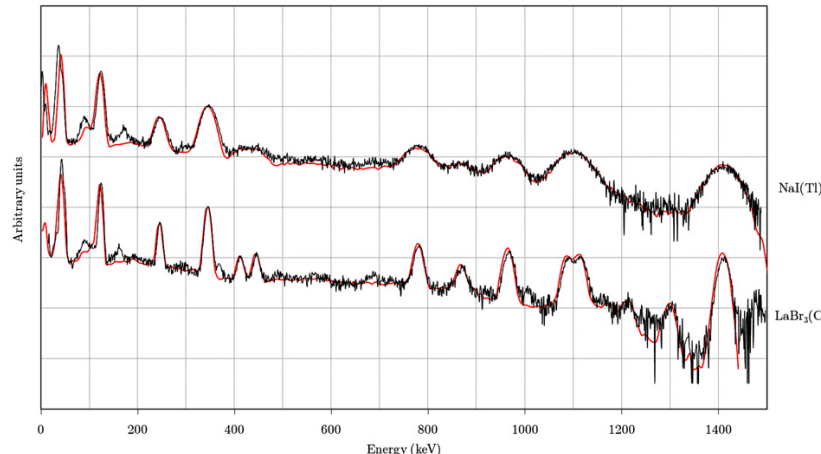


**Fig. 4.** Experimental (black) and simulated (red) spectra for both detectors, NaI(Tl) and LaBr<sub>3</sub>(Ce). For purposes of comparison, the spectra are displayed in arbitrary units. (For interpretation of the references to color in this figure legend, the reader is referred to the web version of this article.)

**Table 4**  
 Comparison of the experimental and the MC-simulated efficiencies of both detectors.

Radionuclide	Source-detector distance (cm)	Energy (keV)	NaI			LaBr <sub>3</sub>		
			$\varepsilon_{\text{exp}}$ (%)	$\varepsilon_{\text{MC}}$ (%)	RD (%) <sup>b</sup>	$\varepsilon_{\text{exp}}$ (%)	$\varepsilon_{\text{MC}}$ (%)	RD (%) <sup>b</sup>
<sup>241</sup> Am	5	59.541	2.5(3)	2.570(4)	-2.9	3.0(3)	3.090(7)	-2.8
		80.998 <sup>a</sup>	3.2(3)	3.141(6)	1.5	3.8(4)	3.576(6)	7.0
	5	302.851	n.a.	n.a.	n.a.	2.0(2)	2.013(6)	-1.6
		356.013	1.5(2)	1.506(5)	-0.5	1.8(2)	2.013(6)	-14.2
<sup>137</sup> Cs	5	661.657	1.0(1)	1.045(3)	-2.4	1.3(1)	1.308(4)	-0.9
		1173.228	1.3(1)	1.302(6)	-3.0	2.1(2)	2.149(8)	-3.2
	2	1332.492	1.2(1)	1.141(5)	1.7	2.0(2)	1.897(9)	3.4

<sup>a</sup> For the 80.998 keV energy of <sup>133</sup>Ba, we also took into account the contribution of the 79.61 keV line.

<sup>b</sup> RD(%) =  $\frac{\varepsilon_{\text{exp}} - \varepsilon_{\text{MC}}}{\varepsilon_{\text{exp}}} \times 100$ .

be associated with many factors such as source positioning, detector modelling, the inaccuracy of the manufacturer parameters, the activities of the reference sources and true coincidence summing. Consequently, these factors may make our simulation results for the LaBr<sub>3</sub>(Ce) not as accurate as the NaI(Tl) results.

Most of these discrepancies could be reduced by positioning the radioactive reference sources farther away from the detector; thus, it would be desirable to have reference sources of higher activity.

Finally, it is important to remark that the MC uncertainties are small because they are only statistical. In fact, they can be reduced even by increasing the number of simulated histories. Thus, MC uncertainties must be only taken as indicators of good statistics in the simulations.

### 3.5. Activity calculations

From the MC efficiencies given in Table 4, we used Eq. (13) to estimate the activities of the radioactive sources. Table 5 shows the calculated activities and the relative differences RD (%) for both detectors.

The results included in Table 5 show good agreement between the certified activity of the radiation sources and the calculated activities obtained from the MC efficiencies. Thus, the maximum relative differences between the current and the calculate activity were less than 3.4% in absolute value. The observed discrepancies can be attributed to the same factors discussed in Section 3.4.

The uncertainties provided with the calculated activities are low due to the small uncertainties associated with MC efficiencies. Thus, if the method was used to estimate unknown activities,

**Table 5**  
 Comparison of the certified activities with the activity calculations for both detectors.

Radionuclide	Current activity <sup>a</sup> (kBq)	NaI		LaBr <sub>3</sub>	
		Calculated activity (kBq)	RD(%) <sup>b</sup>	Calculated activity (kBq)	RD(%) <sup>b</sup>
<sup>241</sup> Am	3.2 ± 0.3	3.12 ± 0.03	2.8	3.12 ± 0.03	2.7
<sup>133</sup> Ba	1.0 ± 0.1	1.02 ± 0.02	-1.1	0.97 ± 0.01	3.4
<sup>137</sup> Cs	4.0 ± 0.4	3.93 ± 0.05	2.3	3.98 ± 0.04	0.9
<sup>60</sup> Co	1.40 ± 0.14	1.40 ± 0.02	0.2	1.41 ± 0.01	-0.5

<sup>a</sup> At the time of measurement.

<sup>b</sup> RD(%) =  $\frac{A - A_{\text{calc}}}{A} \times 100$ .

it would be necessary to assume a higher uncertainty to take into account the other possible sources of uncertainty.

## 4. Conclusions

In this study, we presented a complete calibration (energy, resolution and efficiency calibrations) of two scintillation detectors, NaI(Tl) and LaBr<sub>3</sub>(Ce), to be used in gamma-spectrometry.

For the energy calibration, we found that the best function to establish the energy-channel relation is a 2nd-degree polynomial. After testing several fitting functions for the resolution calibration, we found that the best fitting function for the FWHM(E) relation was also a 2nd-degree polynomial.

### 3.1. ENERGY, RESOLUTION AND EFFICIENCY CALIBRATION METHODS 25

R. Casanovas et al. / Nuclear Instruments and Methods in Physics Research A 675 (2012) 78–83

83

Additionally, an MC user code for the EGS5 code system was developed and validated to reproduce a realistic gamma-ray spectra and efficiency calculations for both the NaI(Tl) and LaBr<sub>3</sub>(Ce) detectors. The correct implementation of the FWHM function in the MC code was tested across all the energy ranges by comparing the simulated spectra with the experimental spectra. We also validated the code by calculating the efficiency of simple source geometries, and the calculated efficiencies were in good agreement with the experimental values obtained from certified radioactive sources. Finally, using the calculated efficiencies in the activity calculations also provided good results.

The validation of this MC user code for simple source geometries will permit one to extrapolate the calculations to other distributions of radioactive sources. Thus, the code can be used to calculate the efficiencies for different kinds of extended sources and to estimate their activities.

#### Acknowledgements

Part of this research has been performed using the resources of CESCA (Centre de Supercomputació de Catalunya).

#### References

- [1] M. Moszyński, Nuclear Instruments and Methods A 505 (2003) 101–110.  
[2] BrillLanCe™ Scintillators Performance Summary (Revision: January, 2009). Saint-Gobain Crystals, Scintillation Products. Available: <[http://www.detectors.saint-gobain.com/uploadedFiles/SGdetectors/Documents/Technical\\_Information\\_Notes/BrillLanCe-Scintillators-Performance-Summary.pdf](http://www.detectors.saint-gobain.com/uploadedFiles/SGdetectors/Documents/Technical_Information_Notes/BrillLanCe-Scintillators-Performance-Summary.pdf)>.  
[3] G. Gilmore, Practical Gamma-Ray Spectrometry, 2nd edn., John Wiley & Sons Ltd, England, 2008.  
[4] Update of X Ray and Gamma Ray Decay Data Standards for Detector Calibration and Other Applications. Volume 1: Recommended Decay Data, High Energy Gamma Ray Standards and Angular Correlation Coefficients. International Atomic Energy Agency, Vienna, 2007. Available: <[http://www-pub.iaea.org/MTCD/publications/PDF/Pub1287\\_Vol1\\_web.pdf](http://www-pub.iaea.org/MTCD/publications/PDF/Pub1287_Vol1_web.pdf)>.  
[5] F. Quarati, A.J.J. Bos, S. Brandenburg, C. Dathy, P. Dorenbos, S. Kraft, R.W. Ostendorf, V. Ouspenski, A. Owens, Nuclear Instruments and Methods A 574 (2007) 115–120.  
[6] M. Moszyński, L. Świderski, T. Szczęśniak, A. Nassalski, A. Syntfeld-Kažuch, W. Czarnacki, G. Pausch, J. Stein, P. Lavoute, F. Lherbert, F. Kniest, IEEE Transactions on Nuclear Science 55 (2008) 1774–1780.  
[7] M. Moszyński, A. Nassalski, A. Syntfeld-Kažuch, L. Świderski, T. Szczęśniak, IEEE Transactions on Nuclear Science 55 (2008) 1062–1068.  
[8] M. Balcerzyk, M. Moszyński, M. Kapusta, Nuclear Instruments and Methods A 537 (2005) 50–56.  
[9] H. Hirayama, Y. Namito, A.F. Bielajew, S.J. Wilderman, W.R. Nelson, The EGS5 Code System, SLAC-R-730 and KEK Report 2005-8, 2005.  
[10] M.J. Berger, J.S. Coursey, M.A. Zucker, J. Chang, ESTAR, PSTAR, and ASTAR: Computer Programs for Calculating Stopping-Power and Range Tables for Electrons, Protons, and Helium Ions (version 1.2.3), National Institute of Standards and Technology, Gaithersburg, 2005. Available: <<http://physics.nist.gov/Star>>.  
[11] ICRU Report 53, International Commission on Radiation Units and Measurements, Bethesda, Maryland, 1994.  
[12] G.E.P. Box, M.E. Muller, Annals of Mathematical Statistics 29 (1958) 610–611.  
[13] B.R.B. Walters, I. Kawrakow, D.W.O. Rogers, Medical Physics 29 (2002) 2745–2752.  
[14] S. Hurtado, M. García-León, R. García-Tenorio, Nuclear Instruments and Methods A 518 (2004) 764–774.  
[15] H.X. Shi, B.X. Chen, T.Z. Li, D. Yun, Applied Radiation and Isotopes 57 (2002) 517–524.  
[16] K. Amgarou, C. Domingo, T. Bouassoule, F. Fernandez, Nuclear Instruments and Methods B 267 (2009) 2944–2951.  
[17] V. Kovaltchouk, R. Machrafi, Annals of Nuclear Energy 38 (2011) 788–793.  
[18] S. Baccouche, D. Al-Azmi, N. Karunakara, A. Trabelsi, Applied Radiation and Isotopes 70 (2012) 227–232.  
[19] G. Anil-Kumar, I. Mazumdar, D.A. Gothe, Nuclear Instruments and Methods A 609 (2009) 183–186.  
[20] S. Ashrafi, S. Anvarian, S. Sobhanian, Journal of Radioanalytical and Nuclear Chemistry 269 (2006) 95–98.  
[21] S. Hurtado, M. García-León, R. García-Tenorio, Nuclear Instruments and Methods A 564 (2006) 295–299.  
[22] G. Su, Z. Zeng, J. Cheng, Radiation Protection Dosimetry 146 (2011) 103–106.

26 CHAPTER 3. CALIBRATION METHODS AND SPECTRA STABILISATION

## 3.2 Temperature peak-shift correction methods for NaI(Tl) and LaBr<sub>3</sub>(Ce) gamma-ray spectrum stabilisation

### Abstract

NaI(Tl) and LaBr<sub>3</sub>(Ce) detectors are frequently operated under unstable temperature conditions when used in an open environment. These temperature changes result in a peak shift and spectral distortion during measurement. Two methods are proposed to stabilise the measured spectra; they are applied using a software algorithm, without the necessity of adjusting the gain. Both methods are based on the experimental observation that the relative channel displacement due to temperature changes is approximately the same for all channels. The first method corrects the spectrum using experimental data obtained under controlled conditions in the laboratory, and thus it only depends on the detector temperature. The second method uses one known peak in the spectrum to correct all of the channels: the NORM <sup>40</sup>K peak for the NaI(Tl) detector, the internal contaminant peak of <sup>138</sup>La for the LaBr<sub>3</sub>(Ce), or an external source when these two cannot be easily identified.

### 3.2. SPECTRUM STABILISATION METHODS

27

Radiation Measurements 47 (2012) 588–595



Contents lists available at SciVerse ScienceDirect

## Radiation Measurements

journal homepage: [www.elsevier.com/locate/radmeas](http://www.elsevier.com/locate/radmeas)



# Temperature peak-shift correction methods for NaI(Tl) and LaBr<sub>3</sub>(Ce) gamma-ray spectrum stabilisation

R. Casanovas <sup>a,\*</sup>, J.J. Morant <sup>b</sup>, M. Salvadó <sup>a</sup>

<sup>a</sup> Unitat de Física Mèdica, Facultat de Medicina i Ciències de la Salut, Universitat Rovira i Virgili, ES-43201 Reus, Tarragona, Spain

<sup>b</sup> Servei de Protecció Radiològica, Facultat de Medicina i Ciències de la Salut, Universitat Rovira i Virgili, ES-43201 Reus, Tarragona, Spain

### HIGHLIGHTS

- NaI(Tl) and LaBr<sub>3</sub>(Ce) scintillation detectors are used for gamma-ray spectrometry.
- Environmental temperature changes result in a peak shift and spectral distortion.
- Two methods are proposed to stabilise the measured spectra.
- These methods are applied using a software algorithm, without adjusting the gain.
- Both methods are tested in the laboratory under controlled temperature conditions.

### ARTICLE INFO

*Article history:*  
Received 24 February 2012  
Received in revised form  
26 May 2012  
Accepted 1 June 2012

*Keywords:*  
NaI(Tl)  
LaBr<sub>3</sub>(Ce)  
Scintillation gamma-ray spectrometry  
Temperature dependence  
Peak-shift correction  
Spectra stabilisation

### ABSTRACT

NaI(Tl) and LaBr<sub>3</sub>(Ce) detectors are frequently operated under unstable temperature conditions when used in an open environment. These temperature changes result in a peak shift and spectral distortion during measurement. Two methods are proposed to stabilise the measured spectra; they are applied using a software algorithm, without the necessity of adjusting the gain. Both methods are based on the experimental observation that the relative channel displacement due to temperature changes is approximately the same for all channels. The first method corrects the spectrum using experimental data obtained under controlled conditions in the laboratory, and thus it only depends on the detector temperature. The second method uses one known peak in the spectrum to correct all of the channels: the NORM <sup>40</sup>K peak for the NaI(Tl) detector, the internal contaminant peak of <sup>138</sup>La for the LaBr<sub>3</sub>(Ce), or an external source when these two cannot be easily identified.

© 2012 Elsevier Ltd. All rights reserved.

### 1. Introduction

The calibration methodology for NaI(Tl) and LaBr<sub>3</sub>(Ce) scintillation detectors in the laboratory is well known (Casanovas et al., 2012). However, when used in an open environment, the detectors frequently operate under unstable temperature conditions. This affects the performance of the detectors either in the crystal itself, such as their light yield or decay time constants (Ivanakiev et al., 2009; Moszyński et al., 2006), or the electronics (ICRU 53, 1994). For environmental monitoring, where the main interest is focused on isotope identification rather than exact activity determination, it is important to account for the effect of temperature on electronics. It is known that temperature changes may lead to gain instabilities and result in a peak shift and spectral distortion during

measurement (ICRU 53, 1994). This can lead to the misidentification of some isotopes.

Several methods are commonly used to stabilise the gain, and thus the gamma-ray spectra. Some examples of this are as follows: using an electronic reference pulse that produces a known equivalent energy in the spectrum (Shepard et al., 1997), attaching an external radioactive source to the detector (Shepard et al., 1997; Pausch et al., 2005), using isotopes from the natural background (Pausch et al., 2005), using the temperature dependence of the light pulse decay time (Pausch et al., 2005) and using LEDs as reference light sources (Pausch et al., 2005; Saucke et al., 2005). However, all of these methods are based on automatically adjusting the gain. Therefore, they are not valid for systems with an analogue gain control.

In this study, we present two methods to correct the peak shift without continuously adjusting the gain. The spectra are corrected by a software implementation of an algorithm that compensates for

\* Corresponding author. Tel.: +34 977759382; fax: +34 977759322.  
E-mail address: [ramon.casanovas@urv.cat](mailto:ramon.casanovas@urv.cat) (R. Casanovas).

## 28 CHAPTER 3. CALIBRATION METHODS AND SPECTRA STABILISATION

R. Casanovas et al. / Radiation Measurements 47 (2012) 588–595

589

gain drifts due to temperature variations. The methods were tested in the laboratory under controlled temperature conditions. The results indicate that the methods are valid approaches to peak shift corrections in the gamma-ray spectra produced by temperature changes.

### 2. Materials and methods

#### 2.1. Experimental set-up

The detectors used in this study were a 2" × 2" NaI(Tl) and a 2" × 2" LaBr<sub>3</sub>(Ce) scintillation detectors. The NaI(Tl) detector was an ORTEC® Model 905-3, and the LaBr<sub>3</sub>(Ce) detector was a Bril-LanCe™380 from Saint-Gobain Crystals. Both detectors were coupled to a preamplifier (ORTEC® Model 276) and an amplifier (ORTEC® Model 575A) with shaping time constants adjusted to 1.5 μs, which were connected to a Multi-Channel pulse-height Analyser (MCA) ORTEC® TRUMPTM-PCI-2k. The spectrum analysis software that we used was Scintivision™ from ORTEC®. A refrigerator and an oven were used to control the temperature changes, and all of the temperatures were measured using a temperature probe (Brodersen Controls Model PXT-10/11). The experimental data were obtained using four radioactive sources: <sup>152</sup>Eu, <sup>241</sup>Am, <sup>137</sup>Cs and <sup>60</sup>Co. These sources emit gamma-rays over a range of energies up to 1408 keV.

#### 2.2. Data collection

To validate the methods, we collected two sets of 18 spectra for each detector (72 spectra) in the approximate temperature range of 0 °C to 50 °C, which is the manufacturer's recommended operating range. The first set of spectra was collected using the <sup>152</sup>Eu source and the second set using a combined source containing <sup>241</sup>Am, <sup>137</sup>Cs and <sup>60</sup>Co. Each spectrum was collected after thermal stability was achieved (at least 1 h of constant temperature), and the corresponding temperature was noted.

#### 2.3. Description of the methods

At a constant reference temperature  $T_0$  (e.g.,  $T_0 = 25$  °C) of the detector, the position  $C_{i0}$  of the  $i^{\text{th}}$ -channel of the MCA is constant. Thus, the energy calibration is constant. However, temperature changes lead to a channel shift that may invalidate the energy calibration and lead to the misidentification of radionuclides. Thus, the  $i^{\text{th}}$ -channel position  $C_{ik}$  in a gamma-ray spectrum measured at the temperature  $T_k$  is displaced with respect to the reference position at  $T_0$ ,  $C_{i0}$ .

If we assume, for a fixed voltage and gain, that the channel positions only depend on the temperature, we can establish a simple relationship between  $C_{ik}$  and  $C_{i0}$ :

$$C_{ik} = C_{i0} \cdot f_i(T_k) \quad (1)$$

where  $f_i(T_k)$  is a function that depends only on the temperature.

Based on experimental evidence (see Section 3.1), we assume that the relative channel displacement due to temperature changes is approximately the same for all of the  $N$  channels conforming the spectrum. Thus, the  $f_i(T_k)$  functions become:

$$f_1(T_k) \approx f_2(T_k) \approx \dots \approx f_N(T_k) \equiv f(T_k) \quad (2)$$

To stabilise the spectrum, we displace the  $C_{ik}$  channel position to its corrected value  $C_{ik}^{\text{corrected}}$ , which is the reference position at  $T_0$ , i.e.,  $C_{ik}^{\text{corrected}} = C_{i0}$ .

Using the assumption of Equation (2) in Equation (1), the corrected channel position is given by:

$$C_{ik}^{\text{corrected}} = \frac{C_{ik}}{f(T_k)} \quad (3)$$

With the corrected spectrum, the energy calibration obtained at the reference temperature  $T_0$  is still valid. Thus, the objective of the two proposed methods is to find an approximation to  $f(T_k)$  that corrects the measured spectrum.

#### 2.3.1. Method 1

Method 1 corrects the measured spectrum using an algorithm based on previous measurements in the laboratory. Thus, no radioactive or pulse reference is needed during the measurements. However, data must be collected in the laboratory under controlled temperature conditions, which is not always possible.

This method assumes a second-order polynomial approximation to the functions  $f_i(T_k)$ . Thus, Equation (1) becomes:

$$\frac{C_{ik}}{C_{i0}} = \sum_{j=0}^2 a_{ij} \cdot T_k^j = a_{i0} + a_{i1} \cdot T_k + a_{i2} \cdot T_k^2 \quad (4)$$

The parameters of the second-order polynomial  $a_{ij}$  are fit using the 72 spectra (acquired using the different detectors and sources at various temperatures). For each of the main peaks we fit the  $a_{ij}$  coefficients. By virtue of Equation (2), we have:

$$a_{1j} \approx a_{2j} \approx \dots \approx a_{Nj} \equiv a_j \quad (5)$$

where  $a_j$  is calculated by averaging the  $a_{ij}$  coefficients for the  $N_p$  peaks considered:

$$a_j \equiv \frac{\sum_{i=1}^{N_p} a_{ij}}{N_p} \quad (6)$$

Equation (4) becomes:

$$\frac{C_{ik}}{C_{i0}} = \sum_{j=0}^2 a_j \cdot T_k^j = a_0 + a_1 \cdot T_k + a_2 \cdot T_k^2 \quad (7)$$

The spectrum is corrected using:

$$C_{ik}^{\text{corrected}} = C_{i0} = \frac{C_{ik}}{\sum_{j=0}^2 a_j \cdot T_k^j} = \frac{C_{ik}}{(a_0 + a_1 \cdot T_k + a_2 \cdot T_k^2)} \quad (8)$$

#### 2.3.2. Method 2

Method 2 uses a single known peak in the spectrum to correct all of the channels. With this method, no previous measurements in the laboratory are needed, and temperature measurements are not required. However, the known peak should be in all of the spectra, either produced by natural background or by an inner contaminant as for the LaBr<sub>3</sub>(Ce) detector. If this is not possible, the method requires an external source, which will cause additional undesired counts in the obtained spectra.

This method is based on the assumption made in Equation (2). Thus, it is only necessary to determine  $f(T_k)$  for one peak in the spectrum and the spectra can be corrected by following the position of only this one known peak.

Using Equation (3) for the known peak, we have:

$$f(T_k) \equiv \frac{C_{ik}^{\text{known}}}{C_{i0}^{\text{known}}} \quad (9)$$

### 3.2. SPECTRUM STABILISATION METHODS

29

590

R. Casanovas et al. / Radiation Measurements 47 (2012) 588–595

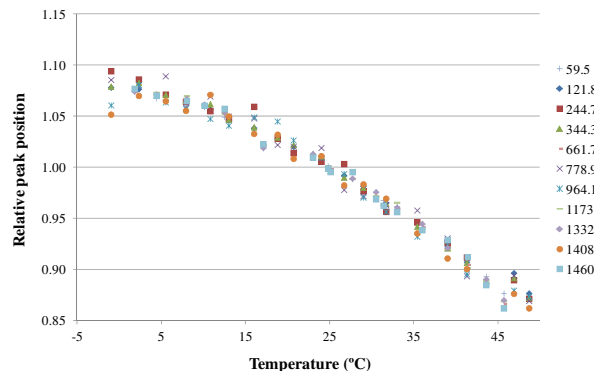


**Fig. 1.** Relative peak-shift as a function of temperature for the NaI(Tl) detector. The peak positions are normalised to unity at  $T_0 = 25^\circ\text{C}$  and are named according to their gamma-ray energy in keV.

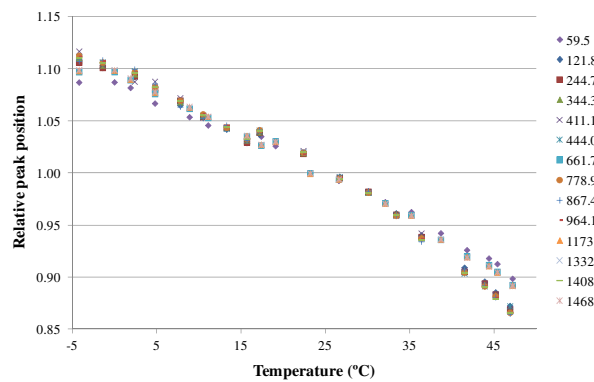


**Fig. 2.** Relative peak-shift as a function of temperature for the LaBr<sub>3</sub>(Ce) detector. The peak positions are normalised to unity at  $T_0 = 25^\circ\text{C}$  and are named according to their gamma-ray energy in keV.

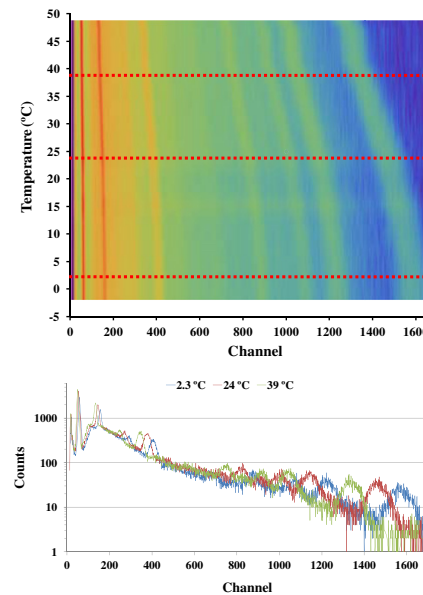


**Fig. 3.**  $^{152}\text{Eu}$  spectra as a function of temperature for the NaI(Tl) detector. The raw measured spectra (left) are corrected (right) using the data obtained from the source composed of  $^{241}\text{Am}$ ,  $^{137}\text{Cs}$  and  $^{60}\text{Co}$ . The red dotted lines on the waterfall plots (top) indicate which pulse height spectra (bottom) are represented by way of example. (For interpretation of the references in colour in this figure legend, the reader is referred to the web version of this article.)

Combining Equations (3) and (9), all of the channels in the spectrum can be corrected using:

$$C_{ik}^{\text{corrected}} \equiv C_{ik0} = C_{ik} \frac{C_{ik}^{\text{known}}}{C_{ik}^{\text{known}}} \quad (10)$$

The spectra of the NaI(Tl) detector were corrected using either the known peak position of the NORM  $^{40}\text{K}$  or that produced by an external  $^{241}\text{Am}$  source. For the LaBr<sub>3</sub>(Ce) detector, we used the internal contaminant peak from  $^{138}\text{La}$  present in all of the spectra.

### 3. Results and discussion

#### 3.1. Temperature dependence of the relative peak positions

Figs. 1 and 2 show the variation in the relative peak positions as a function of temperature for all of the measured isotopes for the NaI(Tl) and the LaBr<sub>3</sub>(Ce) detectors, respectively. The data follow the same curve over the range of temperatures studied. Therefore, the assumption made in Equation (2) is reasonable and feasible. The temperature dependence of the relative peak positions is approximately the same for all channels in the spectrum. Despite the different temperature dependences of the studied crystals (Moszyński et al., 2006), no significant differences are observed between the peak shifts in the NaI(Tl) and the LaBr<sub>3</sub>(Ce) detectors. Thus, it suggests that the main component of instability is caused by photomultipliers when the temperature changes affect all the detection system.

#### 3.2. Validation of method 1

To test the validity of method 1, for each detector we used the data of one set of measurements to correct the other set. Specifically, we took the data obtained from the second source ( $^{241}\text{Am} + ^{137}\text{Cs} + ^{60}\text{Co}$ ) to correct the spectra obtained with the first source ( $^{152}\text{Eu}$ ) and vice versa. Figs. 3 to 6 compare the waterfall plots (top) for the uncorrected and corrected spectra for both

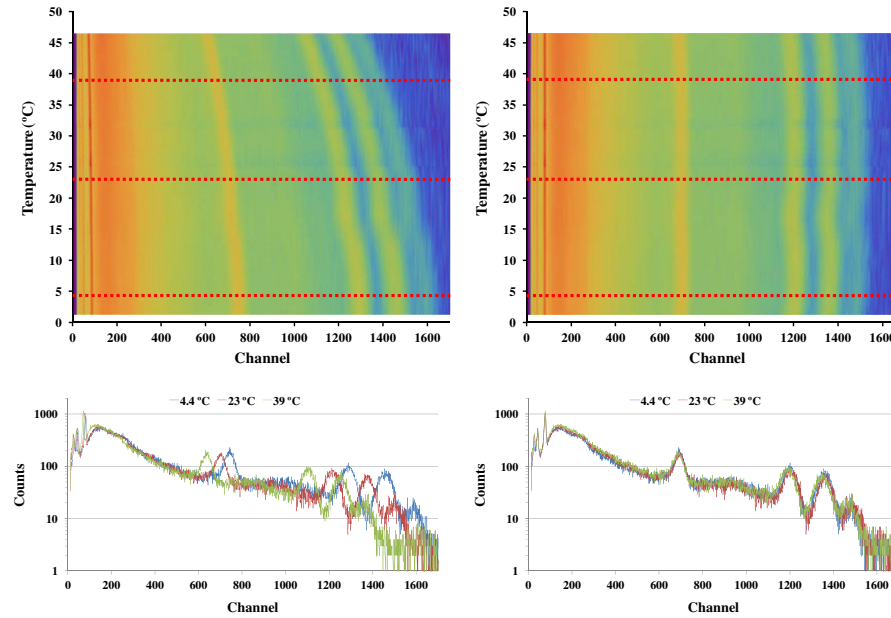


**Fig. 4.**  $^{241}\text{Am}$ ,  $^{137}\text{Cs}$  and  $^{60}\text{Co}$  spectra as a function of temperature for the NaI(Tl) detector. The raw measured spectra (left) are corrected (right) using the data obtained from the  $^{152}\text{Eu}$  source. The red dotted lines on the waterfall plots (top) indicate which pulse height spectra (bottom) are represented by way of example. (For interpretation of the references to colour in this figure legend, the reader is referred to the web version of this article.)

detectors. In these spectra, the horizontal axis represents the channel number, the vertical axis the temperature at acquisition and the colour scale indicates the logarithm of the pulse height, which is red for higher values and purple for lower ones. By way of example, some pulse height spectra (bottom) are also represented at different temperatures, which are marked with a red dotted line on the waterfall plots.

The corrected spectra obtained using method 1 are, in general, stable. The corrected peak positions are significantly more constant against temperature variations. The largest discrepancies between the corrected peak positions and the reference peak positions occur at the extremes of the temperature. The method performs well between 0 °C and 40 °C, which is the normal operating range for the detectors. The fluctuations observed in Figs. 3 to 6 near 15 °C are

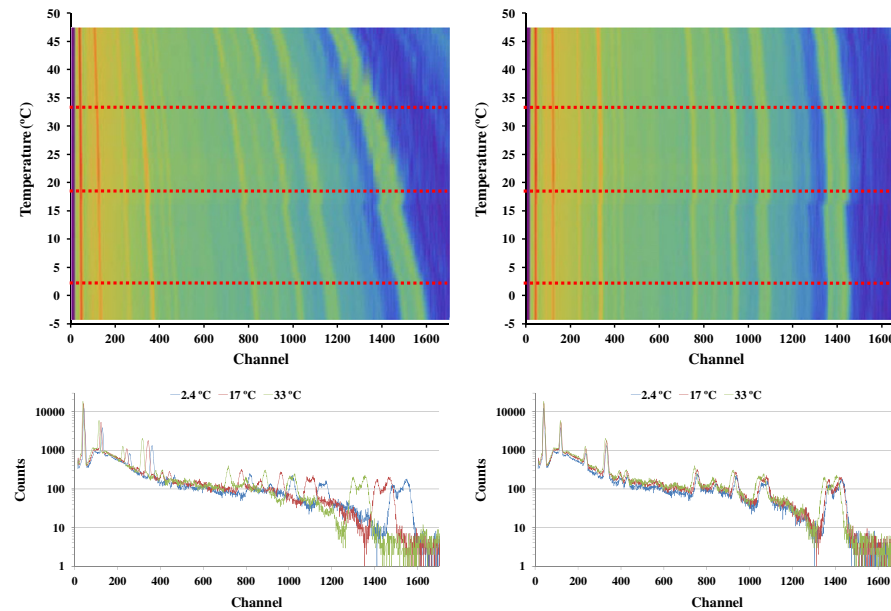


**Fig. 5.**  $^{152}\text{Eu}$  spectra as a function of temperature for the LaBr<sub>3</sub>(Ce) detector. The raw measured spectra (left) are corrected (right) using the data obtained from the source composed of  $^{241}\text{Am}$ ,  $^{137}\text{Cs}$  and  $^{60}\text{Co}$ . The red dotted lines on the waterfall plots (top) indicate which pulse height spectra (bottom) are represented by way of example. (For interpretation of the references to colour in this figure legend, the reader is referred to the web version of this article.)

### 3.2. SPECTRUM STABILISATION METHODS

31

592

R. Casanovas et al. / Radiation Measurements 47 (2012) 588–595

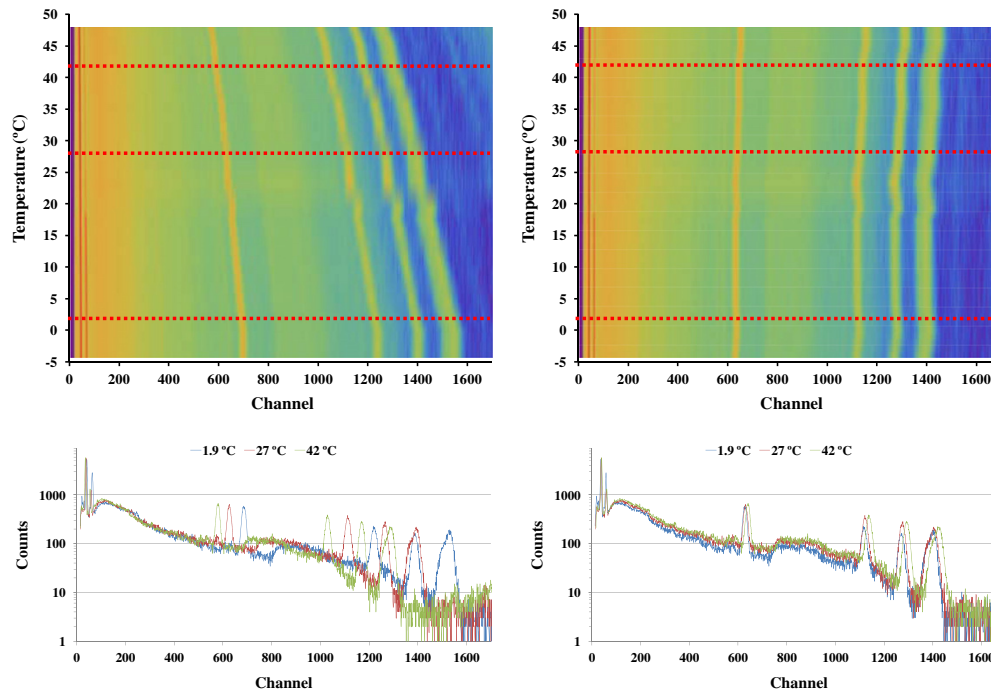


**Fig. 6.**  $^{241}\text{Am}$ ,  $^{137}\text{Cs}$  and  $^{60}\text{Co}$  spectra as a function of temperature for the  $\text{LaBr}_3(\text{Ce})$  detector. The raw measured spectra (left) are corrected (right) using the data obtained from the  $^{152}\text{Eu}$  source. The red dotted lines on the waterfall plots (top) indicate which pulse height spectra (bottom) are represented by way of example. (For interpretation of the references to colour in this figure legend, the reader is referred to the web version of this article.)

due to the transfer of the detectors from the refrigerator to the oven. However, the spectra correction in the environment will not be affected by this phenomenon because the fitting functions are soft and this fluctuation is due to a problem in data collection in the laboratory. Further measurements should be performed using a better environmental chamber.

After testing method 1, we used the data of the two sets of measurements to correct all of the spectra. Figs. 7 and 8 show the relative deviation of the corrected peak positions with respect to the reference position for the  $\text{NaI}(\text{Tl})$  and the  $\text{LaBr}_3(\text{Ce})$  detectors, respectively.

The spread of points observed at the extremes of the studied temperature could be attributed to some kind of thermal inertia

in the detectors. In fact, it can be observed in Figs. 1 and 2 that the measurements with the first source of  $^{241}\text{Am}$ ,  $^{137}\text{Cs}$  and  $^{60}\text{Co}$  have a slightly different tendency than those obtained with the second one of  $^{152}\text{Eu}$ . This is more pronounced in Fig. 2 for the  $\text{LaBr}_3(\text{Ce})$ , where a bifurcation between the first and the second source can be observed at the extremes of temperatures. However, the differences are, in absolute value, less than 3% in the temperature range of  $-5\text{ }^\circ\text{C}$  and  $50\text{ }^\circ\text{C}$  and a smaller relative deviation (below 2% in absolute value) in the normal operating range of  $0\text{ }^\circ\text{C}$  to  $40\text{ }^\circ\text{C}$ , which is an acceptable correction for both detectors. These figures also validate that the relative channel displacement due to temperature changes is approximately the same for all channels.

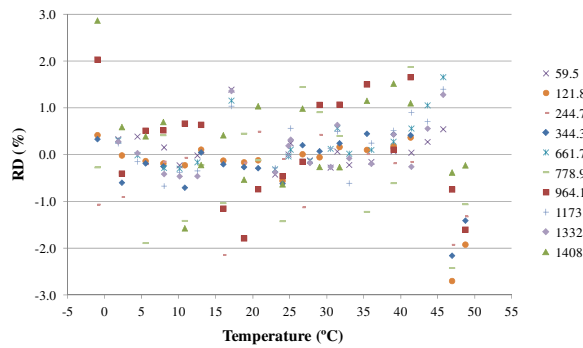


**Fig. 7.** Relative deviation ( $\text{RD}\% = (C_{10} - C_{ik})/C_{10} \cdot 100$ ) of the corrected peak positions as compared to their reference positions for the  $\text{NaI}(\text{Tl})$  detector. The correction was calculated using all of the data shown in Fig. 1. The peaks are named according to their gamma-ray energy in keV.

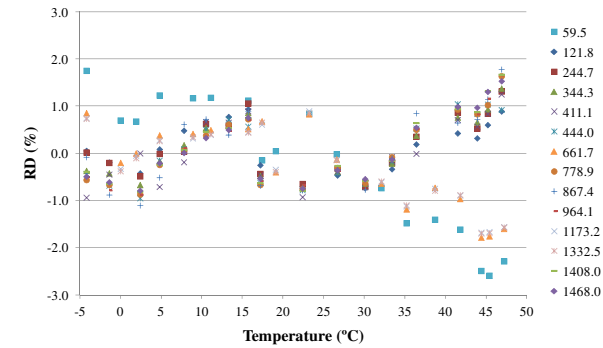


**Fig. 8.** Relative deviation ( $\text{RD}\% = (C_{10} - C_{ik})/C_{10} \cdot 100$ ) of the corrected peak positions as compared to their reference positions for the  $\text{LaBr}_3(\text{Ce})$  detector. The correction was calculated using all of the data shown in Fig. 2. The peaks are named according to their gamma-ray energy in keV.

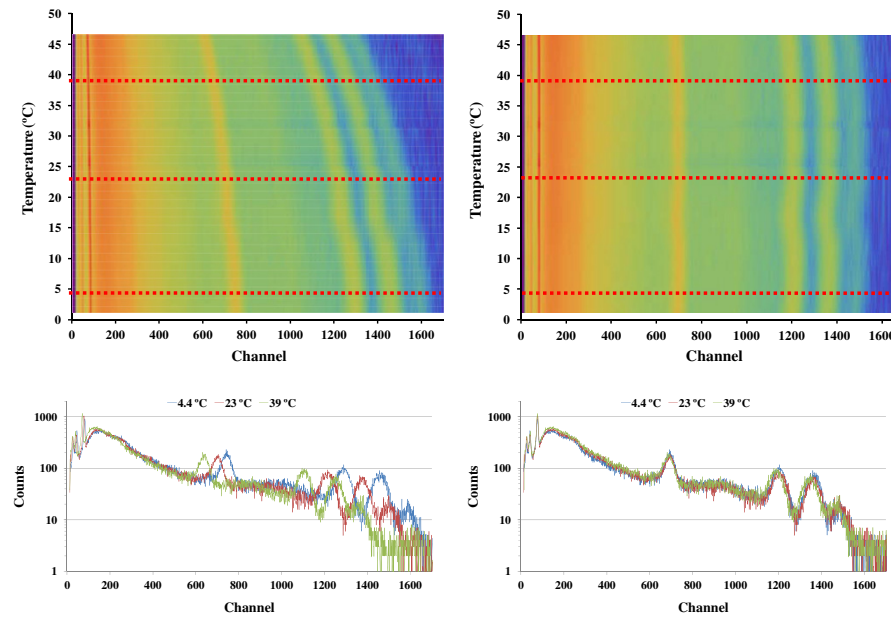


**Fig. 9.**  $^{241}\text{Am}$ ,  $^{137}\text{Cs}$  and  $^{60}\text{Co}$  spectra as a function of temperature for the Nal(Tl) detector. The raw measured spectra (left) are corrected (right) using the data obtained from the NORM  $^{40}\text{K}$  peak. The red dotted lines on the waterfall plots (top) indicate which pulse height spectra (bottom) are represented by way of example. (For interpretation of the references to colour in this figure legend, the reader is referred to the web version of this article.)

### 3.3. Validation of method 2

#### 3.3.1. Nal(Tl) spectrum correction using $^{40}\text{K}$ peak

Fig. 9 shows the correction of the  $^{241}\text{Am} + ^{137}\text{Cs} + ^{60}\text{Co}$  spectrum using the  $^{40}\text{K}$  peak. The quality of the correction depends on the quality of the  $^{40}\text{K}$  peak. The correction is acceptable over the range

of temperatures. The  $^{40}\text{K}$  content in the laboratory is small compared to the environment; the method is expected to perform better when used outdoors.

Unfortunately, this method cannot be used when the reference peak cannot be identified, either due to low activity or low detector resolution. The latter is why the  $^{152}\text{Eu}$  spectrum cannot be

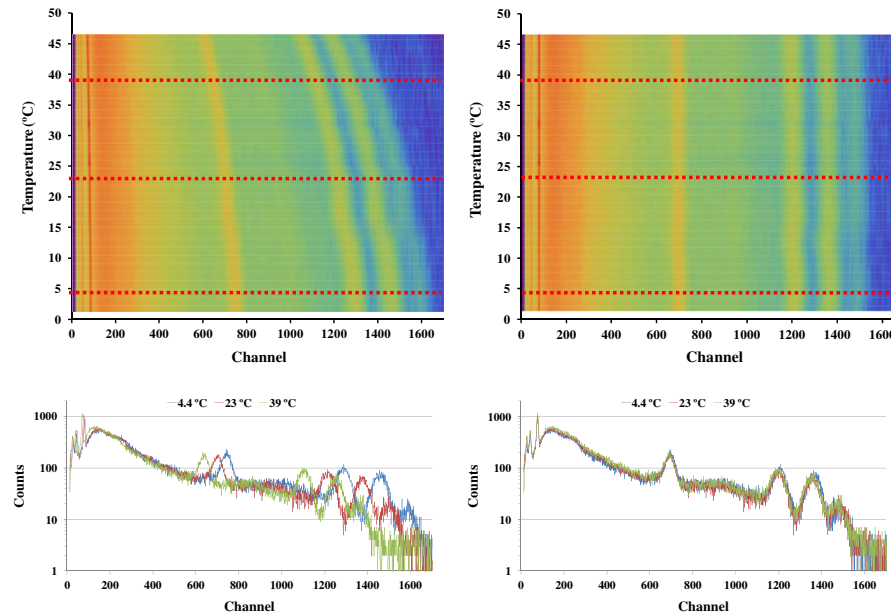


**Fig. 10.**  $^{241}\text{Am}$ ,  $^{137}\text{Cs}$  and  $^{60}\text{Co}$  spectra as a function of temperature for the Nal(Tl) detector. The raw measured spectra (left) are corrected (right) using the data obtained from the  $^{241}\text{Am}$  peak. The red dotted lines on the waterfall plots (top) indicate which pulse height spectra (bottom) are represented by way of example. (For interpretation of the references to colour in this figure legend, the reader is referred to the web version of this article.)

### 3.2. SPECTRUM STABILISATION METHODS

33

594

R. Casanovas et al. / Radiation Measurements 47 (2012) 588–595

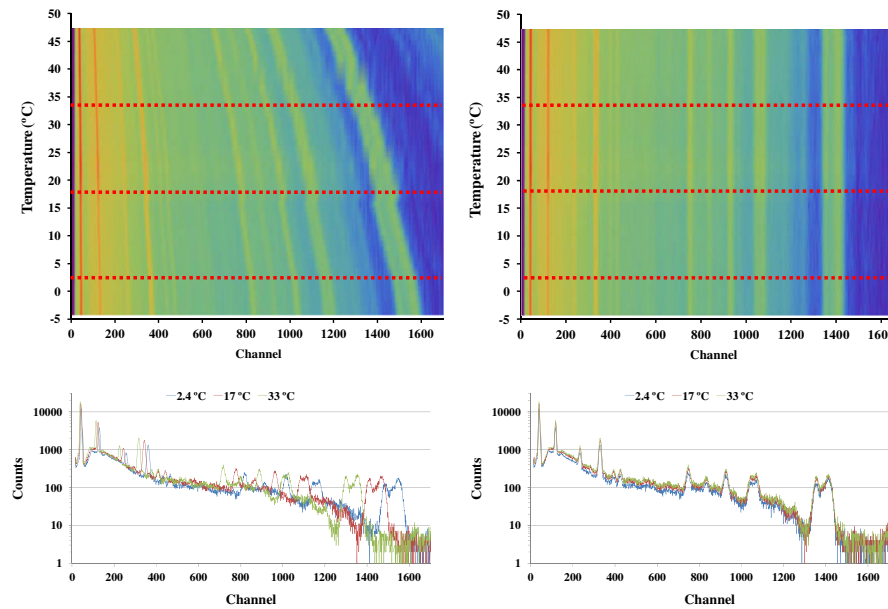


**Fig. 11.**  $^{152}\text{Eu}$  spectra as a function of temperature for the  $\text{LaBr}_3(\text{Ce})$  detector. The raw measured spectra (left) are corrected (right) using the data obtained from the  $^{138}\text{La}$  internal contaminant peak. The red dotted lines on the waterfall plots (top) indicate which pulse height spectra (bottom) are represented by way of example. (For interpretation of the references to colour in this figure legend, the reader is referred to the web version of this article.)

corrected by this method. In this case, the  $^{40}\text{K}$  peak is hidden by the  $^{152}\text{Eu}$  1408 keV peak.

#### 3.3.2. $\text{NaI}(\text{Tl})$ spectrum correction using $^{241}\text{Am}$ peak

The previous  $\text{NaI}(\text{Tl})$  spectra corrected using  $^{40}\text{K}$  are not accurate enough due to the peak quality, which depends on the concentration of potassium in the environment. To overcome this, it is necessary to add an external radioactive source to the detector. To

avoid peak interferences, the source should not emit gamma-rays in the energy range of interest. In our case,  $^{241}\text{Am}$  was used as an external source, adding extra counts only in the spectra below 60 keV. Thus, the spectra may be trusted only above this energy if no extra analysis is performed. In Fig. 10 we show the correction of the  $^{241}\text{Am} + ^{137}\text{Cs} + ^{60}\text{Co}$  spectrum using the  $^{241}\text{Am}$  peak. Because the  $^{241}\text{Am}$  peak is better identified than the  $^{40}\text{K}$  peak, the correction is more stable.

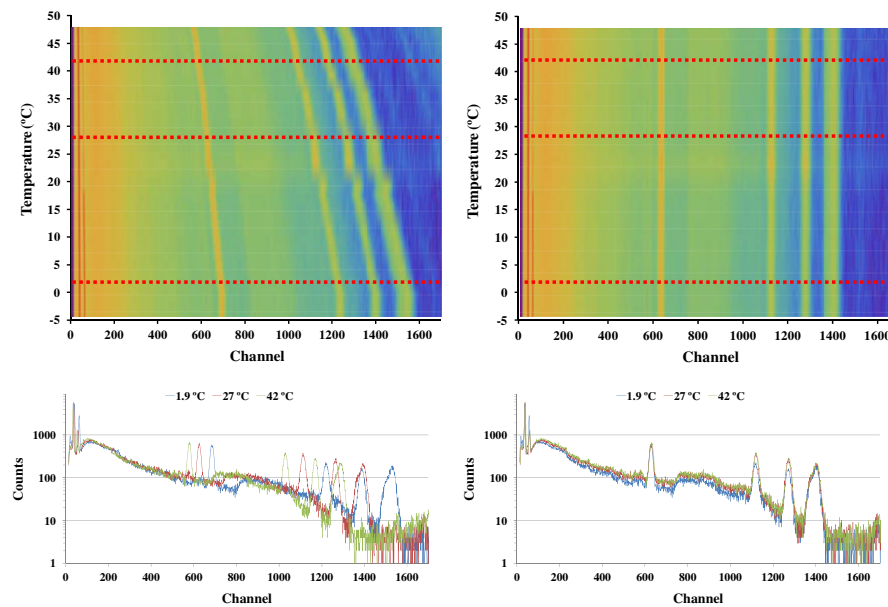


**Fig. 12.**  $^{241}\text{Am}$ ,  $^{137}\text{Cs}$  and  $^{60}\text{Co}$  spectra as a function of temperature for the  $\text{LaBr}_3(\text{Ce})$  detector. The raw measured spectra (left) are corrected (right) using the data obtained from the  $^{138}\text{La}$  internal contaminant peak. The red dotted lines on the waterfall plots (top) indicate which pulse height spectra (bottom) are represented by way of example. (For interpretation of the references to colour in this figure legend, the reader is referred to the web version of this article.)

### 3.3.3. *LaBr<sub>3</sub>(Ce)* spectra correction using <sup>138</sup>La internal contamination

The internal contaminant of the LaBr<sub>3</sub>(Ce) detector can be used for spectrum stabilisation. Figs. 11 and 12 show the <sup>152</sup>Eu and <sup>241</sup>Am + <sup>137</sup>Cs + <sup>60</sup>Co spectra stabilised using the <sup>138</sup>La peak. The usual disadvantage of radioactive contamination plays a positive role in spectrum stabilisation.

## 4. Conclusions

In this study, we presented two methods to correct the peak shift that do not require adjustment of the gain. Thus, both methods are useful to stabilise gamma-ray spectra obtained under unstable temperature conditions.

The first method provides spectrum stabilisation in the absence of known peaks, especially when alternative methods are not available. However, it requires some measurements under controlled temperature conditions, which cannot always be performed and may be specific to each detector. Besides, some internal thermal inertia are observed, worsening the peak-shift correction. Even so, the results show a relative deviation of less than 2%, in absolute value, in the peak correction in the normal operating range of 0 °C to 40 °C for both detectors.

The second method does not require previous measurements in the laboratory, so it can be generally applied. In addition, it provides better results than method 1 since the thermal inertia do not affect the corrections. However, this method depends on a known peak in all of the spectra, which is not always available or identifiable, especially in the NaI(Tl) detector. For the LaBr<sub>3</sub>(Ce) detector, the internal contaminant, <sup>138</sup>La, together with the better energy resolution of the detector, make it easy to apply this method.

The second method can also be applied using an external radioactive source (for example, <sup>241</sup>Am). This is especially useful to stabilise the NaI(Tl) spectra in environments with low <sup>40</sup>K content. However, adding an external radioactive source causes undesired counts in the spectra. Fortunately, they can be minimised using mechanical devices to shield the source when it is not in use.

Both methods were tested under stable temperature conditions that may not reflect real scenarios in the environment. Additionally, when used in an open environment, both methods are applied by software after the spectra acquisition (instead of adjusting the gain during the measurements). For these reasons, it is desirable to use short integration times (e.g., 10 min) during the spectra acquisition and correct the spectra after each integration.

We recommend using method 2 as the default method and implementing method 1 only when the known peak cannot be identified or is not significant (usually in NaI(Tl) detectors). When the known peak cannot be detected, it is possible to implement the second method by adding an external radioactive source.

Finally, these methods cannot replace the conventional methods used with digital systems. In fact, in analogue systems, the number of available channels decreases when the temperature rises, and resolution may be lost. This should not be a problem for MCA with a large number of channels, but it is an important distinction between the analogue and digital correction methods.

## References

- Casanovas, R., Morant, J.J., Salvadó, M., 2012. Energy and resolution calibration of NaI(Tl) and LaBr<sub>3</sub>(Ce) scintillators and validation of an EGSS Monte Carlo user code for efficiency calculations. Nucl. Inst. Meth. Phys. Res. A 675, 78–83.
- Ianakiev, K.D., Alexandrov, B.S., Littlewood, P.B., Browne, M.C., 2009. Temperature behaviour of NaI(Tl) scintillation detectors. Nucl. Instrum. Methods. Phys. Res. A 607, 432–438.
- ICRU 53, 1994. Gamma-ray Spectrometry in the Environment. International Commission on Radiation Units and Measurements, Bethesda, Maryland. Report 53.
- Moszyński, M., Nassalski, A., Syntfeld-Kažuch, A., Szczęśniak, T., Czarnacki, W., Wolski, D., Pausch, G., Stein, J., 2006. Temperature dependences of LaBr<sub>3</sub>(Ce), LaCl<sub>3</sub>(Ce) and NaI(Tl) scintillators. Nucl. Instrum. Methods. Phys. Res. A 568, 739–751.
- Pausch, G., Stein, J., Teofilov, N., 2005. Stabilizing scintillation detector systems by exploiting the temperature dependence of the light pulse decay time. IEEE Trans. Nucl. Sci. 52, 1849–1855.
- Saucke, K., Pausch, G., Stein, J., Ortlepp, H.G., Schotanus, P., 2005. Stabilizing scintillation detector systems with pulsed LEDs: a method to derive the LED temperature from pulse height spectra. IEEE Trans. Nucl. Sci. 52, 3160–3165.
- Shepard, R., Wawrowski, S., Charland, M., Roberts, H., Möslinger, M., 1997. Temperature stabilization of a field instrument for uranium enrichment measurements. IEEE Trans. Nucl. Sci. 44, 568–571.

## Chapter 4

# Development and calibration

### 4.1 Implementation of gamma-ray spectrometry in two real-time water monitors using NaI(Tl) scintillation detectors

#### Abstract

In this study, the implementation of gamma-ray spectrometry in two real-time water monitors using 2"x2" NaI(Tl) scintillation detectors is described. These monitors collect the water from the river through a pump and it is analyzed in a vessel, which is shielded with Pb. The full calibration of the monitors was performed experimentally, except for the efficiency curve, which was set using validated Monte Carlo simulations with the EGS5 code system.

After the calibration, the monitors permitted the identification and quantification of the involved isotopes in a possible radioactive increment and made it possible to discard possible leaks in the nuclear plants. As an example, a radiological increment during rain is used to show the advantages of gamma-ray spectrometry. To study the capabilities of the monitor, the minimum detectable activity concentrations for  $^{131}\text{I}$ ,  $^{137}\text{Cs}$  and  $^{40}\text{K}$  are presented for different integration times.



Contents lists available at SciVerse ScienceDirect

## Applied Radiation and Isotopes

journal homepage: [www.elsevier.com/locate/apradiso](http://www.elsevier.com/locate/apradiso)



# Implementation of gamma-ray spectrometry in two real-time water monitors using NaI(Tl) scintillation detectors



R. Casanovas <sup>a,\*</sup>, J.J. Morant <sup>b</sup>, M. Salvadó <sup>a</sup>

<sup>a</sup> Unitat de Física Mèdica, Facultat de Medicina i Ciències de la Salut, Universitat Rovira i Virgili, ES-43201 Reus (Tarragona), Spain

<sup>b</sup> Servei de Protecció Radiològica, Servei de Recursos Científics i Tècnics, Universitat Rovira i Virgili, ES-43007 Tarragona, Spain

## HIGHLIGHTS

- Gamma-ray spectrometry with NaI(Tl) detectors was implemented in two water monitors.
- The monitors were calibrated using experimental data and Monte Carlo simulations.
- The efficiency calculations and MDAC values are given.
- Advantages of using gamma-ray spectrometry are discussed.
- The monitors permit the identification and quantification of isotopes in water.

## ARTICLE INFO

### Article history:

Received 17 January 2013

Received in revised form

30 May 2013

Accepted 4 June 2013

Available online 13 June 2013

### Keywords:

Scintillation gamma-ray spectrometry

NaI(Tl)

Monte Carlo simulation

Efficiency calculation

## ABSTRACT

In this study, the implementation of gamma-ray spectrometry in two real-time water monitors using 2 in. × 2 in. NaI(Tl) scintillation detectors is described. These monitors collect the water from the river through a pump and it is analyzed in a vessel, which is shielded with Pb. The full calibration of the monitors was performed experimentally, except for the efficiency curve, which was set using validated Monte Carlo simulations with the EGSS code system.

After the calibration, the monitors permitted the identification and quantification of the involved isotopes in a possible radioactive increment and made it possible to discard possible leaks in the nuclear plants. As an example, a radiological increment during rain is used to show the advantages of gamma-ray spectrometry. To study the capabilities of the monitor, the minimum detectable activity concentrations for <sup>131</sup>I, <sup>137</sup>Cs and <sup>40</sup>K are presented for different integration times.

© 2013 Published by Elsevier Ltd.

## 1. Introduction

The nuclear power plant in Ascó, Catalonia (ES-E, Spain-East), consists of two pressurized water nuclear reactors cooled with water from the Ebre River. This water is also used for human consumption and crop watering. Thus, to conduct real-time monitoring of the radioactivity levels in water, two monitors have been providing the total gamma activity concentration in water before and after the river passes by both nuclear reactors at Ascó.

However, the obtained radiological values cannot easily be interpreted in terms of the Spanish legislation ([Royal Decree 140/2003](#)) (based on the World Health Organization Recommendations ([World Health Organization, 2008](#))) because it fails to consider total gamma activity concentrations. In addition, when

some radiological increments occur, it is impossible to distinguish whether they were caused by natural causes (e.g., rain) or artificial emissions (e.g., incidents in nuclear plants). Thus, a previous study identified the implementation of in-situ real-time gamma-ray spectrometry as a possible solution ([Casanovas et al., 2011](#)).

The use of gamma-ray spectrometry for real-time water monitoring has become fairly common. Several types of detectors have been used, including NaI(Tl) detectors as the most common example ([Bagatelas et al., 2010](#); [Povinec et al., 1996](#); [Tsabarlis, 2008](#); [Tsabarlis and Ballas, 2005](#); [Tsabarlis et al., 2008](#); [Van Put et al., 2004](#); [Vlastou et al., 2006](#); [Vojtyla, 2001](#); [Wedekind et al., 1999](#)), although HPGe ([Povinec et al., 1996](#)) and LaBr<sub>3</sub>(Ce) detectors ([Su et al., 2011](#)) have been used as well.

Commonly, real-time water monitoring using gamma-ray spectrometry is conducted by means of direct measurements, i.e. with detectors mounted in floating buoys or with detectors in contact with the sea floor or very close to it ([Jones, 2001](#)). When direct measurements are performed, some assumptions concerning the distribution of the source term must be done. Thus, the efficiency

\* Corresponding author. Tel.: +34 977759382.

E-mail address: [ramon.casanovas@urv.cat](mailto:ramon.casanovas@urv.cat) (R. Casanovas).

## 4.1. GAMMA-RAY SPECTROMETRY IN TWO WATER MONITORS

37

50

R. Casanovas et al. / Applied Radiation and Isotopes 80 (2013) 49–55

calculation is only an approximation that can introduce extra uncertainties in the activity concentrations quantification.

In this paper, the implementation of gamma-ray spectrometry in two river monitors using NaI(Tl) detectors is described. Each of them collect water from the river through a pump and it is analyzed in a vessel. Thus, the counting geometry is always the same and efficiency calibrations can be performed accurately. Besides, the vessel is shielded with Pb, enabling a low background environment that permits better measurement capabilities.

The implementation of gamma-ray spectrometry was conducted through the installation of a parallel spectrometric module in the initial design of the monitor, ensuring its compatibility with other previously installed features. The calibration of the monitor was performed experimentally, except for the efficiency curve, which was set using the Monte Carlo (MC) simulations with the EGS5 code system, which were, in turn, validated with some experimental measurements.

After the presented implementation, the monitor enabled the real-time identification and quantification of radioactive isotope content in the river water. Thus, valuable extra information was obtained at a reasonable cost that guided decisions regarding limits based on current legislation.

## 2. Materials

### 2.1. Original system

The original system in both river stations was a Berthold LB/BAI 9110 (Berthold Technologies GmbH & Co. KG, Germany) equipped with a 2 in. × 2 in. NaI(Tl) scintillation detector from ORTEC® (Model 905-3). The system includes a 25 L vessel with a Pb shield (see Fig. 1). A single channel analyzer (SCA) allows one to compute the total concentration of gamma activity ( $\text{Bq L}^{-1}$ ) in water, which is measured real-time and integrated every 10 min.

### 2.2. New system

To implement gamma-ray spectrometry in the water monitor, a parallel spectrometric module was added to the initial design of the monitor. This module consists of a NaI(Tl) detector and a preamplifier (ORTEC® Model 276) that are connected to an amplifier (ORTEC® Model 575A), which, in turn, is connected to a multichannel pulse-height analyzer (MCA) ORTEC® TRUMP™-PCI-2k.

The spectrometric module was integrated with other previously installed features, resulting in the overall functioning scheme shown in Fig. 2. Thus, the measurement process starts at

the vessel (1), where water is collected with a pump from the river. The measurements are conducted with a NaI(Tl) detector (2) connected in parallel to two acquisition cards, an SCA (3) and an MCA (4). The cards are, in turn, connected to their respective associated computers (5) and (6). All data are then transferred to an external server with an SQL database (7) for their storage and processing. An external computer (8) also allows remote interaction with the server or local interaction with the monitor. The system was also improved via the installation of two recipients of 15 L each (9) that can be used to sample water for later analysis in the laboratory. The recipients can be manually or automatically, as well as partially or totally, filled by using several predefined radiological criteria. Finally, the monitor comprises a pneumatic system that allows the insertion and removal of a radioactive test source (10) inside Pb. The source, which can be controlled locally or remotely, can be used to check the spectra stability or energy calibration.

The obtained data are transmitted to the server through an ADSL connection, and the remote control of the system is performed using the TCP/IP protocol. The monitor has different electronic checking sensors that ensure the proper operation of the system. The most relevant are a flow meter (i.e., for the control of the pumped water), a detector temperature probe and an integrated meteorological station (i.e., allowing the measurement of wind speed and direction, as well as air temperature, humidity, barometric pressure, rainfall and solar radiation). From the main

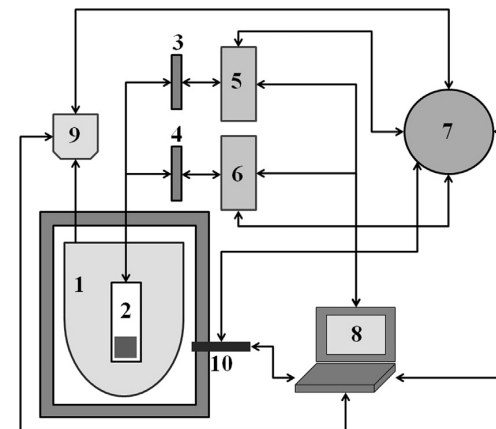


**Fig. 2.** Schematic showing data acquisition, transfer and processing in the spectrometric water monitoring system. (1) Vessel; (2) NaI(Tl) detector; (3) SCA; (4) MCA; (5) SCA computer; (6) MCA computer; (7) SQL server; (8) external computer; and (9) sampling recipients; and (10) test source.

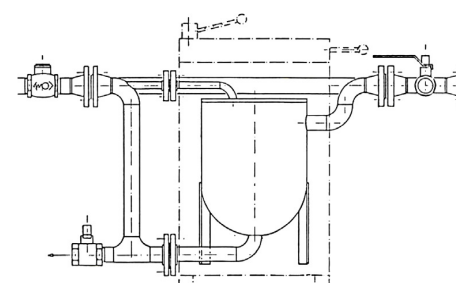


**Fig. 1.** Image (left) and scheme (right) of the water monitor. The Pb shielding is in the box represented by the dashed lines.

server, it is possible to send automatic messages (SMS or emails) to a predefined contact list, depending on either radiological criteria or different sensor signals.

### 3. Methods

#### 3.1. Calibration

The calibration methodology for a NaI(Tl) detector has been described in detail in a previous paper (Casanovas et al., 2012a) and adapted specifically for this river monitor. This methodology encompasses energy, resolution and efficiency calibrations.

##### 3.1.1. Energy and resolution calibrations

The energy and resolution calibrations were established using five radioactive point-sources containing  $^{241}\text{Am}$ ,  $^{133}\text{Ba}$ ,  $^{137}\text{Cs}$ ,  $^{60}\text{Co}$  and  $^{152}\text{Eu}$ . The former was set using the following equation:

$$E = a_0 + a_1 C + a_2 C^2 \quad (1)$$

where  $C$  is the channel number,  $E$  is the energy and  $a_k$  are the fitting coefficients.

The spectra stability is high because the temperature of water varies few along the day. However, to ensure long time measurements, spectra are stabilized. The stabilization is performed fitting a Gaussian curve to the  $^{40}\text{K}$  peak at 1460.8 keV to find its position and correcting the entire spectrum using the method described in Casanovas et al. (2012b).

For resolution calibration, the following 2nd-order polynomial was also used to fit the experimental data:

$$FWHM(E) = b_0 + b_1 E + b_2 E^2 \quad (2)$$

where  $FWHM(E)$  is the Full Width at Half Maximum,  $E$  is the energy and  $b_k$  are the fitting coefficients.

##### 3.1.2. Experimental efficiencies

The experimental efficiencies were calculated from the manufacturer's calibration report of the original monitor, which was performed using  $^{131}\text{I}$  and  $^{137}\text{Cs}$  (364.5 keV and 661.7 keV peaks, respectively). The available data were gross counts in the peak regions instead of net counts under the full-energy peaks. The reported background values were low enough to distinguish any discrepancies between them. However, the discrepancies between net areas and gross areas in normal operation spectra are around

20% as a consequence of the different Compton events that occurred in the crystal. And thus, we assumed an uncertainty level of 20% in the experimental data to account for this deficiency.

To obtain an extra efficiency point at 1460.8 keV, a solution of KCl containing  $^{40}\text{K}$  was also prepared. The activity of  $^{40}\text{K}$  was estimated from the amount of potassium chloride and its isotopic natural abundance (0.0117%), and the uncertainty was also considered to be 20%.

The experimental efficiencies  $\varepsilon_{\text{exp}}$  were calculated using

$$\varepsilon_{\text{exp}} = \frac{N}{Atp_{\gamma}} \quad (3)$$

where  $N$  is the number of the net counts under the full-energy peak,  $A$  is the known radionuclide activity,  $t$  is the counting time and  $p_{\gamma}$  is the emission probability of the particular gamma-ray being measured.

##### 3.1.3. Monte Carlo simulated efficiencies

To obtain a complete efficiency curve, efficiency calibration was performed using MC simulations. The MC simulations were performed with a previously validated EGS5 user code (Casanovas et al., 2012a). This user code contains all of the information about the radiation source (diluted in water) and the involved geometry (e.g., vessel, detector, Pb, etc.).

Thus, a model of the monitor was implemented for the MC simulations based on the real dimensions and materials. Fig. 3 shows the implemented geometry model and the materials that were used in each of the regions. The material information (e.g., density and composition) was taken from Berger et al. (2005), and the cut-off energy for the photons and the electrons was set at 10 keV. For the efficiency calculations, each point of the efficiency curve was calculated by considering a monoenergetic source (in the range of 20–2000 keV) that was distributed homogeneously in the water volume. The obtained spectra for the simulated monoenergetic sources were convoluted with the resolution function described by Eq. (2) using the method described in Casanovas et al. (2012a). Then, the broadened spectra were used to calculate the efficiencies using the spectra analysis software ScintiVision™ from ORTEC®.

The efficiency was calculated as

$$\varepsilon_{\text{MC}} = \frac{N_{\text{counts}}}{N_{\text{hist}}} \quad (4)$$

where  $N_{\text{counts}}$  is the number of net counts under the full-energy peak and  $N_{\text{hist}}$  is the number of simulated histories (i.e., the

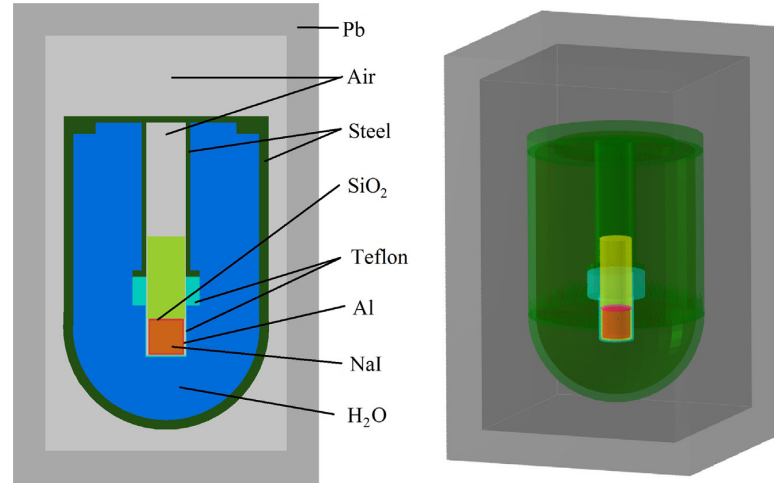


**Fig. 3.** Geometric model of the monitor (in scale) used in the MC simulations.

## 4.1. GAMMA-RAY SPECTROMETRY IN TWO WATER MONITORS

39

52

R. Casanovas et al. / Applied Radiation and Isotopes 80 (2013) 49–55

number of primary source-particles simulated and all of the secondary particles produced by it), which was set at  $10^7$ .

### 3.2. Activity calculations

The activity related to each peak was calculated using

$$A = \frac{N}{\epsilon t p_\gamma} \quad (5)$$

where  $N$  is the number of counts under the peak,  $t$  is the counting time,  $p_\gamma$  is the emission probability of the gamma-ray and  $\epsilon$  is the peak-efficiency.

Using Eq. (5), the activity concentration (e.g.,  $\text{Bq L}^{-1}$ ) can be written as

$$a = \frac{N}{\epsilon_V t p_\gamma} \quad (6)$$

where  $\epsilon_V \equiv \epsilon V$  is the volumetric efficiency and  $V$  is the volume of the vessel, which was 25 L in our case.

### 3.3. Minimum Detectable Activity Concentration (MDAC)

The detection capabilities of a system are usually evaluated with the detection limit  $L_D$ , or the minimum number of counts under a peak that one can be confident of detecting with a certain probability.

Then, the Minimum Detectable Activity Concentration (MDAC) is the activity concentration equivalent to the detection limit  $L_D$ . Thus, from Eq. (6) we get

$$\text{MDAC} = \frac{L_D}{\epsilon_V t p_\gamma} \quad (7)$$

If the measured spectrum is assumed to be only background, the detection limit  $L_D$  (with a 95% confidence limit) for a certain Region of Interest (ROI) in the spectrum can be calculated using the following single-count Currie expression (Currie, 1968):

$$L_D = 2.71 + 4.65\sqrt{B} \quad (8)$$

where  $B$  is the number of counts produced by the background in the considered ROI.

The width of the ROI is determined by the width of the expected peak, which is proportional to the  $\text{FWHM}(E)$  function

$$n = n(E) = k \text{FWHM}(E) \quad (9)$$

where  $k$  is the proportionality constant to set the desired peak coverage and  $\text{FWHM}(E)$  is obtained using Eq. (2). For example,  $k = 2.548$  for 99.73% peak area coverage.

## 4. Results and discussion

### 4.1. Energy and resolution calibrations

The data used for the energy calibration of the system are shown in Fig. 4. The data were fitted to Eq. (1) and it gave a coefficient of determination of  $R^2 = 0.99999$ . Similar results were obtained in both monitors, and therefore, only data from one of them are shown.

The maximum relative drift of the  $^{40}\text{K}$  peak position is lower than 3% for 1 month period if stabilization methods are not applied. The stabilization method performs well for spectra integrations of 2 h. If shorter integration periods are considered, the location of the  $^{40}\text{K}$  peak is not warranted. After the stabilization, the displacement is almost zero and quality of the energy calibration is high.

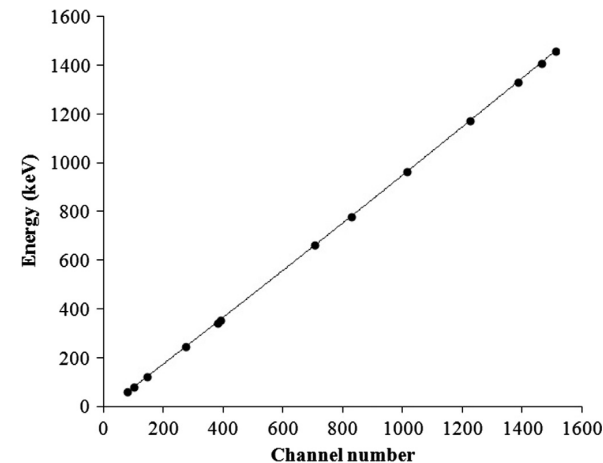


Fig. 4. Energy calibration of the NaI(Tl) detector. The solid line represents the fit of the data to Eq. (1).

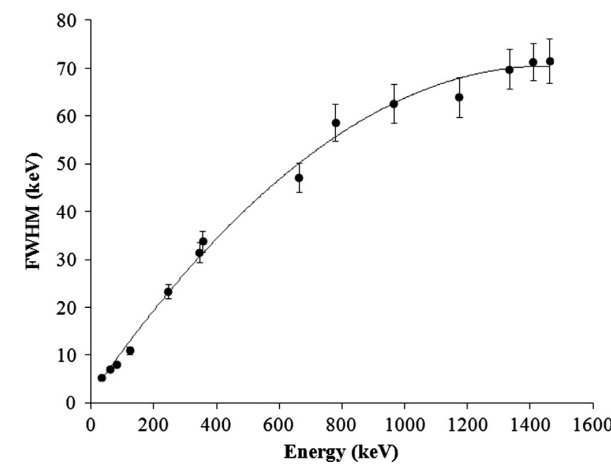


Fig. 5. Resolution calibration of the NaI(Tl) detector. The solid line represents the fit of the data to Eq. (2).

The energy resolution curve was set using Eq. (2) and it gave a coefficient of determination  $R^2 = 0.995$ . The data used for this calibration together with the statistical uncertainties are drawn in Fig. 5.

### 4.2. Efficiency calculations

The efficiency curve calculated from the MC simulations and the obtained experimental efficiency values are shown in Fig. 6. The MC simulations provided higher efficiency values than did the experimental measurements. This discrepancy could be attributed to the simplification introduced when modeling the photomultiplier tube, which was assumed to be an aluminum cylinder filled with air. In fact, some tests were performed with different materials inside the photomultiplier that resulted in values closer to the experimental data. In this sense, the geometric model could be improved by studying in detail the structure and materials of the photomultiplier tube. However, as was discussed in Section 3.1.2, the quality of the experimental data was low; thus, before the detector model can be improved, new experimental data must be obtained using certified radioactive solutions.

An uncertainty of approximately 20% in the efficiencies implies an uncertainty of approximately 20% in the activity calculations

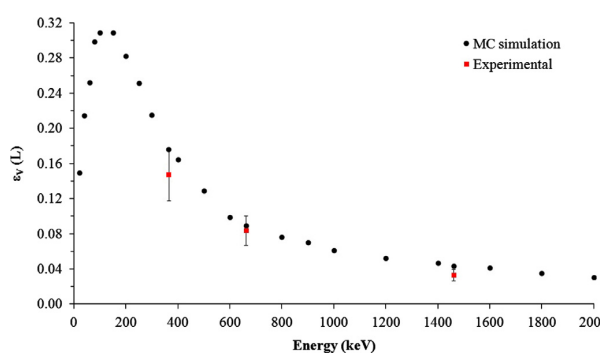


**Fig. 6.** Efficiency curve calculated using the MC simulations (dots) and experimental efficiencies (squares).

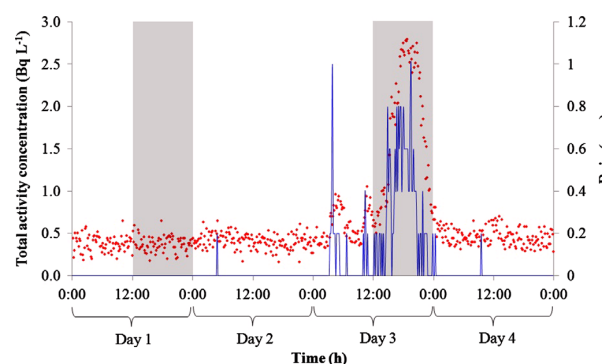


**Fig. 7.** Radiological increments in the total activity concentration (dots) during Day 3, correlated with rainfall (solid lines). The gray shadows indicate the time intervals considered for the comparison of the 12 h-spectra in Fig. 8.

because the other contributions to the uncertainty are estimated to be lower. Even so, an uncertainty of approximately 20% in real-time spectrometry is assumable because the overall uncertainty can be even higher due to the uncertainty associated with the distribution of the radioactivity in river water, which is assumed to be uniform.

In this sense, the system permits the identification of the isotopes and the estimation of their activity concentration values, which is useful to establish alarm levels. According to this, when significant radiological increments are produced, the monitor has two independent recipients of 15 L each that can sample the water for post-analysis in the laboratory.

#### 4.3. Gamma-ray spectrometry advantages

In this section, an example of the advantages of the implementation of gamma-ray spectrometry is provided. Fig. 7 shows an increment of the total activity concentration in the SCA at Day 3. This radiological increment is clearly time-correlated with a rain episode and was most likely produced by the wash-out of the atmosphere during precipitation. However, it is impossible to know whether it contained an artificial radioactive component.

The data obtained from the spectrometric module provides more radiological information. By way of example, Fig. 8 shows two superposed 12 h-spectra acquired on Day 1 and Day 3, one before the rainfall (Day 1, from 12:00 to 24:00) and the other during it (Day 3, from 12:00 to 24:00). The time intervals of the spectra acquisitions are represented with gray shadows in Fig. 7. The displayed spectra in Fig. 8 are from 2000 channels. The spectra

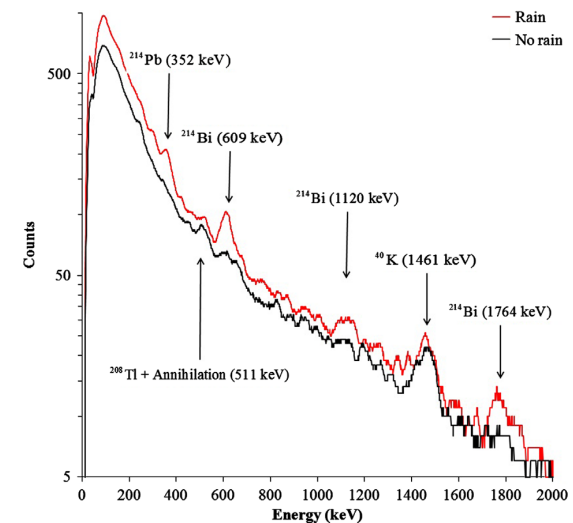


**Fig. 8.** The 12 h-spectra obtained before the rain episode (Day 1, black lines) and during it (Day 3, red lines). The arrows indicate the isotopes (and their corresponding levels of gamma-ray energy) that produced some of the observed peaks. (For interpretation of the references to color in this figure legend, the reader is referred to the web version of this article.)

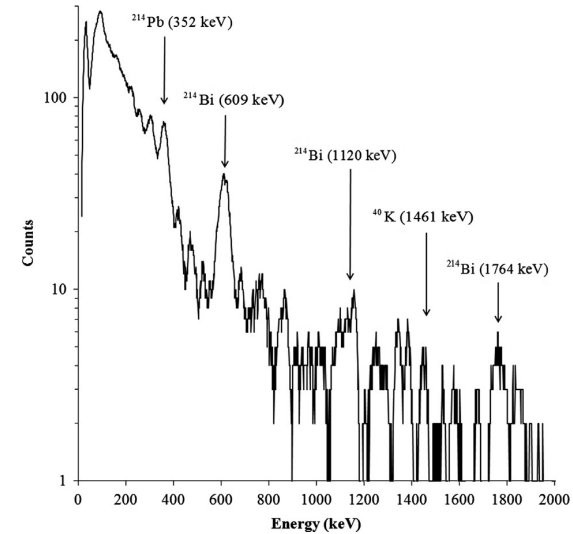


**Fig. 9.** The subtracted spectrum of Day 3 (rain episode) from the spectrum of Day 1 (normal background). The arrows indicate the isotopes (and their corresponding levels of gamma-ray energy) that produced some of the observed peaks.

were smoothed to depict the peaks clearly. Comparing both spectra, one can clearly see that the radiological increment is basically produced by  $^{222}\text{Rn}$  and  $^{232}\text{Th}$  daughters (i.e.,  $^{214}\text{Pb}$ ,  $^{214}\text{Bi}$  and  $^{208}\text{Tl}$ ) as a consequence of atmospheric wash-out during the rain. The pure increment produced in this case can be observed after subtracting both spectra (see Fig. 9). The other significant peak that can be observed was produced by the NORM  $^{40}\text{K}$ . Hence, because no artificial isotopes were detected, a nuclear plant leak during the rain can be discarded in this case.

#### 4.4. Activity calculations

The activity concentrations of some isotopes are calculated from the 12 h-spectra of Fig. 8. The results of the analysis are

## 4.1. GAMMA-RAY SPECTROMETRY IN TWO WATER MONITORS

41

54

R. Casanovas et al. / Applied Radiation and Isotopes 80 (2013) 49–55

**Table 1**

Activity concentrations of some isotopes before the rain episode.

Energy (keV)	Isotope	Net area (counts)	Activity concentration ( $\text{Bq L}^{-1}$ )
352	$^{214}\text{Pb}$	480	$0.16 \pm 0.03$
511	$^{208}\text{Tl}$	699	$0.6 \pm 0.1$
609	$^{214}\text{Bi}$	664	$0.3 \pm 0.1$
1120	$^{214}\text{Bi}$	n.a.	n.a.
1461	$^{40}\text{K}$	662	$3.3 \pm 0.7$
1764	$^{214}\text{Bi}$	94	$0.4 \pm 0.1$

**Table 2**

Activity concentrations of some isotopes during the rain episode.

Energy (keV)	Isotope	Net area (counts)	Activity concentration ( $\text{Bq L}^{-1}$ )
352	$^{214}\text{Pb}$	1403	$0.5 \pm 0.1$
511	$^{208}\text{Tl}$	834	$0.7 \pm 0.1$
609	$^{214}\text{Bi}$	2463	$1.3 \pm 0.3$
1120	$^{214}\text{Bi}$	428	$1.2 \pm 0.2$
1461	$^{40}\text{K}$	742	$3.7 \pm 0.7$
1764	$^{214}\text{Bi}$	279	$1.1 \pm 0.2$

shown in Table 1 (Day 1, before the rain episode) and Table 2 (Day 3, during the rain episode).

In both tables, it can be observed that the  $^{214}\text{Pb}$  activity concentration is systematically lower than the  $^{214}\text{Bi}$  one, showing a clear disequilibrium between these two  $^{222}\text{Rn}$  daughters. The observed increment in the activity concentration of  $^{40}\text{K}$  could be attributed to the accumulation of sludge in the vessel, which is frequent during rainfall.

### 4.5. MDAC

During the day, the variability of the background spectra can be considerable, especially at low integration times. However, regarding the measurement capabilities of the monitor, Table 3 shows the MDAC for the different isotopes and integration times. The spectra are calculated as averages of different spectra (more than 20,000) throughout the day to account for their variability. The MDAC is calculated using Eqs. (7)–(9) (with  $k = 2.548$ ) by assuming that spectra are only background spectra.

The MDAC for  $^{40}\text{K}$  was an order of magnitude higher than the MDAC for  $^{131}\text{I}$  and  $^{137}\text{Cs}$  isotopes because the background spectra have always an important content of  $^{40}\text{K}$ . For this reason, the isotopes with energy levels near 1461 keV should be detected using, if possible, other gamma emission lines.

Other MDAC values for 2 in.  $\times$  2 in. NaI(Tl) detectors in fresh water were not found in the literature, and thus, direct comparison was not possible. However, the typical MDAC for  $^{137}\text{Cs}$  in a 3 in.  $\times$  3 in. NaI(Tl) detector measuring directly during 24 h in fresh water is  $0.035 \text{ Bq L}^{-1}$  (Bagatelas et al., 2010), which is clearly higher than the  $0.009 \text{ Bq L}^{-1}$  achieved in the 2 in.  $\times$  2 in. NaI(Tl) used in the presented monitor. This is an expected result since the Pb shield in the vessel enables lower background measurements in comparison with the other monitor measuring directly in water. Nevertheless, the monitor can only detect those isotopes collected with the pump whereas other monitors measuring directly do not have this restriction.

The monitor capabilities may be improved by using longer and larger NaI(Tl) detectors, which would enable a more efficient system, thus lowering MDACs. Another important improvement to the monitor would be the use of LaBr<sub>3</sub>(Ce) detectors. These detectors have, in general, worse MDACs compared with NaI(Tl) ones because of their intrinsic self-activity (Su et al., 2011). However, they present good energy resolution that can be an important factor when several isotopes are detected.

**Table 3**

MDAC for the different isotopes and integration times.

Isotope	Energy (keV)	MDAC ( $\text{Bq L}^{-1}$ )				
		10 min	1 h	4 h	12 h	24 h
$^{131}\text{I}$	364.5	0.9	0.2	0.04	0.01	0.007
$^{137}\text{Cs}$	661.7	1.2	0.2	0.05	0.02	0.009
$^{40}\text{K}$	1460.8	13.2	2.2	0.55	0.18	0.092

## 5. Conclusions

Two real-time water monitors using 2 in.  $\times$  2 in. NaI(Tl) scintillation detectors were improved by installing a gamma-ray spectrometric module, which was implemented to ensure its compatibility with other previously installed features. The new feature provided valuable extra information at a reasonable cost, which enables the establishment of decision limits based on current legislation. The monitors were calibrated using experimental data, except for the efficiency curve, which was set using the Monte Carlo simulations with the EGS5 code system.

The spectrometric module presented clear advantages in comparison with the old system. For example, it enabled the identification of the involved isotopes in radiological increments and made it possible to discard a possible artificial cause. The capabilities of the new monitor were evaluated with some MDAC calculations over average spectra, which showed a good performance, especially for  $^{131}\text{I}$  and  $^{137}\text{Cs}$  isotopes. In comparison to other monitors that measure directly in water, the obtained MDAC values were lower, and thus, a faster identification can be performed. In addition, the quantification of the activity can be more precise because the counting geometry is always the same and no assumptions about the source term geometry must be done. However, the system can only detect those isotopes collected with the pump and alternative systems measuring directly in the river could be also useful.

As shown via its implementation and calibration, the monitor enables the real-time identification and quantification of radioactive isotope content in river water. This functionality enables a comparison of the obtained data with the legal limits established for the activity concentrations in water, thereby allowing one to establish alarm levels for early warning. As such, valuable extra information could be obtained by comparing both monitors, which are before and after the nuclear plant.

## Acknowledgments

Part of this research was performed using the resources of CESCA (Centre de Supercomputació de Catalunya).

## References

- Bagatelas, C., Tsabarlis, C., Kokkoris, M., Papadopoulos, C.T., Vlastou, R., 2010. Determination of marine gamma activity and study of the minimum detectable activity (MDA) in 4pi geometry based on Monte Carlo simulation. Environ. Monit. Assess. 165, 159–168.
- Berger, M.J., Coursey, J.S., Zucker, M.A., Chang, J., 2005. ESTAR, PSTAR, and ASTAR: Computer Programs for Calculating Stopping-Power and Range Tables for Electrons, Protons, and Helium Ions (version 1.2.3). National Institute of Standards and Technology, Gaithersburg. Available from: <http://physics.nist.gov/Star>.
- Casanovas, R., Morant, J.J., Lopez, M., Hernandez-Giron, I., Batalla, E., Salvado, M., 2011. Performance of data acceptance criteria over 50 months from an automatic real-time environmental radiation surveillance network. J. Environ. Radioact. 102, 742–748.
- Casanovas, R., Morant, J.J., Salvadó, M., 2012a. Energy and resolution calibration of NaI(Tl) and LaBr<sub>3</sub>(Ce) scintillators and validation of an EGS5 Monte Carlo user

- code for efficiency calculations. *Nucl. Instrum. Methods Phys. Res. Sect. A* 675, 78–83.
- Casanovas, R., Morant, J.J., Salvadó, M., 2012b. Temperature peak-shift correction methods for NaI(Tl) and LaBr<sub>3</sub>(Ce) gamma-ray spectrum stabilisation. *Radiat. Meas.* 47, 588–595.
- Currie, L.A., 1968. Limits for qualitative detection and quantitative determination. *Anal. Chem.* 40, 586–593.
- Jones, D.G., 2001. Development and application of marine gamma-ray measurements: a review. *J. Environ. Radioact.* 53, 313–333.
- Povinec, P.P., Osvath, I., Baxter, M.S., 1996. Underwater gamma-spectrometry with HPGe and NaI(Tl) detectors. *Appl. Radiat. Isot.* 47, 1127–1133.
- Royal Decree 140/2003 of 7 February by Which Health Criteria for the Quality of Water Intended for Human Consumption are Established. Available from: [http://www.msc.es/profesionales/saludPublica/docs/royal\\_decree\\_140\\_2003.pdf](http://www.msc.es/profesionales/saludPublica/docs/royal_decree_140_2003.pdf).
- Su, G., Zeng, Z., Cheng, J., 2011. Monte Carlo simulation of in situ LaBr gamma-ray spectrometer for marine environmental monitoring. *Radiat. Prot. Dosim.* 146, 103–106.
- Tsabaris, C., 2008. Monitoring natural and artificial radioactivity enhancement in the Aegean Sea using floating measuring systems. *Appl. Radiat. Isot.* 66, 1599–1603.
- Tsabaris, C., Ballas, D., 2005. On line gamma-ray spectrometry at open sea. *Appl. Radiat. Isot.* 62, 83–89.
- Tsabaris, C., Bagatelas, C., Dakladas, Th., Papadopoulos, C.T., Vlastou, R., Chronis, G.T., 2008. An autonomous in situ detection system for radioactivity measurements in the marine environment. *Appl. Radiat. Isot.* 66, 1419–1426.
- Van Put, P., Debauche, C., De Llelis, C., Adam, V., 2004. Performance level of an autonomous system of continuous monitoring of radioactivity in seawater. *J. Environ. Radioact.* 72, 177–186.
- Vlastou, R., Ntzou, I.Th., Kokkoris, M., Papadopoulos, C.T., Tsabaris, C., 2006. Monte Carlo simulation of gamma-ray spectra from natural radionuclides recorded by a NaI detector in the marine environment. *Appl. Radiat. Isot.* 64, 116–123.
- Vojtyla, P., 2001. Calibration of monitors used for surveillance of radioactivity in effluent water from CERN's accelerator installations. *Appl. Radiat. Isot.* 55, 81–88.
- Wedeckind, Ch., Schilling, G., Grüttmüller, K., Becker, K., 1999. Gamma-radiation monitoring network at sea. *Appl. Radiat. Isot.* 50, 73–741.
- World Health Organization, 2008. Guidelines for Drinking-Water Quality [Electronic Resource]: Incorporating 1st and 2nd Addenda, Vol. 1. 3rd ed. Recommendations. isbn:9789241547611. Available from: [http://www.who.int/water\\_sanitation\\_health/dwq/fulltext.pdf](http://www.who.int/water_sanitation_health/dwq/fulltext.pdf).

4.2. GAMMA-RAY SPECTROMETRY ON A PARTICULATE FILTER

43

## 4.2 Development and calibration of a real-time airborne radioactivity monitor using gamma-ray spectrometry on a particulate filter

### Abstract

In this work, we present the development and calibration of a Real-time Airborne Radioactivity Monitor using gamma-ray spectrometry on a particulate Filter (RARM-F) to be used in an automatic environmental radiation surveillance network. The RARM-F collects a constant flow of air that passes across a particulate filter, where airborne aerosols are collected. Then, the filter is faced toward a NaI(Tl) or LaBr<sub>3</sub>(Ce) scintillation detector that is used for gamma-ray spectrometry. This permits the identification and quantification of airborne radioactive isotopes in real time. The RARM-F was fully calibrated with a combination of experimental data and Monte Carlo simulations. For the simulations, a user code, including a model of the system geometry, was prepared for the EGS5 code system and validated with experimental measurements. The calibration methodology is independent of the scintillation crystal used; however, the measurement capabilities and the performance of the RARM-F are not. Thus, we also discuss some characteristics of the RARM-F when using different crystals.

# Development and Calibration of a Real-Time Airborne Radioactivity Monitor Using Gamma-Ray Spectrometry on a Particulate Filter

R. Casanovas, J. J. Morant, and M. Salvadó

**Abstract**—In this work, we present the development and calibration of a Real-time Airborne Radioactivity Monitor using gamma-ray spectrometry on a particulate Filter (RARM-F) to be used in an automatic environmental radiation surveillance network. The RARM-F collects a constant flow of air that passes across a particulate filter, where airborne aerosols are collected. Then, the filter is faced toward a NaI(Tl) or LaBr<sub>3</sub>(Ce) scintillation detector that is used for gamma-ray spectrometry. This permits the identification and quantification of airborne radioactive isotopes in real time. The RARM-F was fully calibrated with a combination of experimental data and Monte Carlo simulations. For the simulations, a user code, including a model of the system geometry, was prepared for the EGSS code system and validated with experimental measurements. The calibration methodology is independent of the scintillation crystal used; however, the measurement capabilities and the performance of the RARM-F are not. Thus, we also discuss some characteristics of the RARM-F when using different crystals.

**Index Terms**—Calibration, environmental radiation monitoring, gamma-ray scintillation detectors, Monte Carlo methods, spectroscopy, surveillance.

## I. INTRODUCTION

THE main objective of an automatic real-time environmental radiation surveillance network is to detect anomalous levels of radioactivity in the environment as quickly as possible. The Spanish automatic network is essentially composed of two types of monitors [1]: aerosol and Geiger monitors. On the one hand, the aerosol monitors give artificial alpha and beta, radon and gamma (due mainly to the iodine isotopes) activity concentrations. On the other hand, the Geiger monitors give the ambient dose equivalent rate.

However, the obtained radiological values in the aerosol monitors cannot easily be interpreted in terms of the Spanish legislation because the legal limits established for the concentrations of activity are only set for individual isotopes.

Manuscript received June 28, 2012; revised October 24, 2012; accepted January 06, 2014. Date of publication February 21, 2014; date of current version April 10, 2014.

R. Casanovas and M. Salvadó are with the Unitat de Física Mèdica, Facultat de Medicina i Ciències de la Salut, Universitat Rovira i Virgili, ES-43201 Reus (Tarragona), Spain (e-mail: ramon.casanovas@urv.cat).

J. J. Morant is with the Servei de Protecció Radiològica, Servei de Recursos Científics i Tècnics, Universitat Rovira i Virgili, ES-43007 Tarragona, Spain.

Color versions of one or more of the figures in this paper are available online at <http://ieeexplore.ieee.org>.

Digital Object Identifier 10.1109/TNS.2014.2299715

Therefore, the implementation of automatic in-situ gamma-ray spectrometry was identified as a possible solution in a previous study [1]. When gamma-ray spectrometry is used instead of gross counting, it is possible not only to identify the involved isotopes in a radiation level increment but also to quantify their activity concentrations. Hence, this enables the discrimination of naturally occurring radionuclides from artificial ones and the establishment of automatic alerts based on the limits provided by legislation.

The use of automatic in-situ gamma-ray spectrometry is fairly common in radiation surveillance networks. Two examples of this are the International Monitoring System (IMS) of the Comprehensive Test Ban Treaty Organization with the Radionuclide Aerosol Sampler/Analyzer (RASA) [2] and the LaBr<sub>3</sub>(Ce) nationwide radiation monitoring network of Finland [3].

On the one hand, the RASA is an automated high volume (500 m<sup>3</sup>/h) aerosol collector equipped with a high-purity germanium (HPGe) detector that provides high-resolution gamma-ray spectrometry. The overall duration of a measurement cycle is 72 h, and thus, it cannot be used as an early warning system. Concerning this, an upgrade including a NaI/CsI detector inside the sample head has been recently proposed [4].

On the other hand, the Finnish nationwide radiation monitoring network is composed of LaBr<sub>3</sub>(Ce) detectors measuring directly the environmental radioactivity. The spectra are collected and analyzed every 10 minutes, and thus, the data can be used for early warning.

To develop an early warning system with better measurement capabilities than those obtained by direct measurement, a Real-time Airborne Radioactivity Monitor using gamma-ray spectrometry on a particulate Filter (RARM-F) was developed by Universitat Rovira i Virgili, Universitat Politècnica de Catalunya and Raditel Serveis i Subministraments Tecnològics S.L. The RARM-F is basically composed of an aerosol collector and a scintillation detector, either a NaI(Tl) or a LaBr<sub>3</sub>(Ce) detector.

The use of scintillators, instead of HPGe detectors, avoids failures related to the mechanical coolers, which have been identified as a significant portion of missing data in RASA [4]. In this paper, we describe the general aspects of the RARM-F development, as well as its full calibration procedure, which is performed by combining experimental measurements with Monte Carlo (MC) simulations.

## 4.2. GAMMA-RAY SPECTROMETRY ON A PARTICULATE FILTER

45

728

IEEE TRANSACTIONS ON NUCLEAR SCIENCE, VOL. 61, NO. 2, APRIL 2014

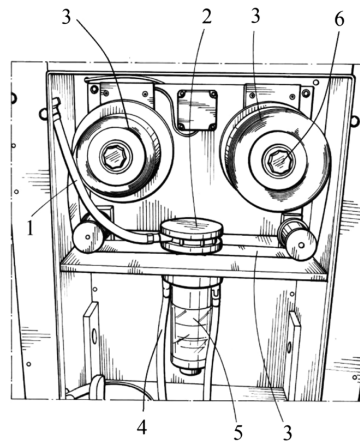


Fig. 1. Front view scheme of the RARM-F without Pb shielding. The main elements are: inlet duct (1), head collector (2), fiber glass filter (3), outlet duct (4), scintillation detector (5) and motorized roller (6).

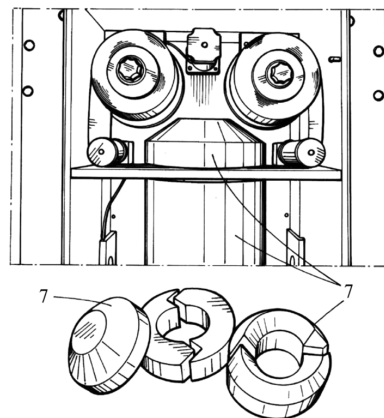


Fig. 2. Front view scheme of the RARM-F with the Pb shielding (7).

## II. MATERIALS

### A. Description of the RARM-F

A general scheme of the developed monitor [5] is shown in Fig. 1 and Fig. 2. The system comprises a suction pump that collects a constant flow of air that can be preset by the user. The air is circulated through an inlet duct (1) towards a head collector (2). The head collector homogenizes and distributes the air flux in a circle 45 mm in diameter that passes across the particulate filter (3). The filter is used to retain the airborne particles and to accumulate the radioactive isotopes. Once the air has passed through the filter, it is expelled via an outlet duct (4).

The active part of the filter is faced toward a 2" x 2" NaI(Tl) or LaBr<sub>3</sub>(Ce) detector (5) connected to a multichannel analyzer, which permits the measurement of the gamma particle energy

spectrum. After the selected integration time, the head collector is elevated and the filter is displaced with a motorized roller (6) to obtain the next set of measurements on a clean sheet of filter.

Both the detector and the active part of the filter are inside a cylindrical Pb shielding (7) 50 mm thick, which is used to reduce the surrounding background radiation and to avoid cross-contamination from the sheet of filter that is not being measured.

The NaI(Tl) detector was Model 905-3 from ORTEC and the LaBr<sub>3</sub>(Ce) detector was BrillLaCe380 from Saint-Gobain Crystals. The Pb shielding was specifically designed for this monitor and was manufactured by TECNIBUSA Protección Radiológica S.L.

The RARM-F has multiple control sensors (crystal temperature, air temperature, temperature in the rack, air flow, amount of filter available, positioning and traveling distance of the filter, filter break sensor, etc.). Software was specifically designed for local or remote control to manage data collection and storage, information transmission, sensor management, information on operating parameters, graphical representations of spectra, calculations, etc. The system also includes a meteorological station for observing atmospheric conditions. In addition, the RARM-F can easily integrate several devices, such as Geiger detectors or proportional counters, to complement the radiological measurements.

The obtained data are transmitted to a main server via an ADSL connection (using the SSL/TLS protocol), and remote control of the system is carried out using the TCP/IP protocol. However, other redundant means of communications are possible (GSM, radiofrequency, satellite, etc.). From the main server, it is also possible to activate alternative measurement systems (e.g. high flow filters for laboratory analysis) and to send automatic messages (SMS or emails) to a predefined contact list in response to either radiological criteria or different sensor signals.

Two prototypes of the RARM-F were constructed, one with a NaI(Tl) detector and the other with a LaBr<sub>3</sub>(Ce) detector, and have been continuously working in test phase since late 2009 and late 2010, respectively. Both monitors are housed inside a modular building, which permits a better control of their environmental conditions, but they take the air from outside. The modular building is located in the vicinity of a nuclear power plant.

### B. Radioactive Calibration Sources

The experimental data were obtained from five certified radioactive point-sources that spanned the range of gamma energies up to 1408 keV. The available sources were <sup>241</sup>Am, <sup>133</sup>Ba, <sup>137</sup>Cs, <sup>60</sup>Co and <sup>152</sup>Eu. However, to reproduce the real counting geometry of the RARM-F, two calibration filters containing <sup>241</sup>Am and <sup>137</sup>Cs were prepared in the laboratory with an active diameter of 45 mm and a total activity of 20 Bq. To prepare each calibration filter, 2 mL of a certified liquid sample were uniformly distributed over the active part of the filter and dried at 45°C.

### III. METHODS

#### A. Experimental Setup

**Calibration Methodology:** The calibration methodology for NaI(Tl) and LaBr<sub>3</sub>(Ce) detectors has been described in detail in a previous paper [6] and was adapted specifically for this monitor. This methodology encompasses the energy, resolution and efficiency calibrations. The experimental efficiencies were calculated from the <sup>241</sup>Am and <sup>137</sup>Cs calibration filters, which were prepared in the laboratory. These isotopes have simple decay schemes, emitting monoenergetic gamma rays, and therefore true coincidence summing is avoided.

The spectra stabilization against temperature changes is performed by means of software algorithms [7]. Besides, some digital systems with automatic gain correction have been tested for future upgrades.

**Minimum Detectable Activity Concentration (MDAC):** After calibration, the detection capabilities can be evaluated with the Minimum Detectable Activity Concentration (MDAC). The MDAC was determined using the following adaptation of the Currie expression [8] (for a detection limit with a 95% confidence limit):

$$MDAC = \frac{2.71 + 4.65\sqrt{B}}{\varepsilon \cdot V \cdot t \cdot p_\gamma} \quad (1)$$

where  $B$  is the number of background counts produced in a certain region of the spectrum (set symmetrically to the considered gamma ray),  $\varepsilon$  is the efficiency,  $V$  the aspirated air volume,  $t$  the counting time and  $p_\gamma$  is the emission probability of the particular gamma ray being considered.

The radiation background is dominated by the ambient radon and thoron concentration, which is not constant along the day. To account this, we studied the real background of the monitors at different moments to provide a range of values of the MDACs. Thus, we calculated the minimum and maximum MDACs, in different integration times, corresponding with the minimum and maximum radon concentrations measured by the monitors.

#### B. Monte Carlo Simulations

The MC simulations were performed with the EGS5 code system [9]. This general-purpose package enables the simulation of the coupled transport of electrons and photons in an arbitrary geometry. For the control of the EGS5 subroutines, a previously validated user code [6] was adapted to the particularities of the RARM-F counting geometry.

A model of the RARM-F (see Fig. 3) was implemented by accounting for the real shapes, dimensions and materials of the elements involved in the radiation detection. Thus, the NaI/LaBr<sub>3</sub> detectors were modeled with the corresponding scintillation crystal (green) in a case of aluminum 0.5 mm thick (red). The space between the case and the crystal was filled with air. A glass light guide behind the crystal (orange) was also considered, and the photomultiplier tube was modeled as a filled-of-air cylinder of aluminum (red). All of these elements were included inside a 50 mm Pb shield (blue), and

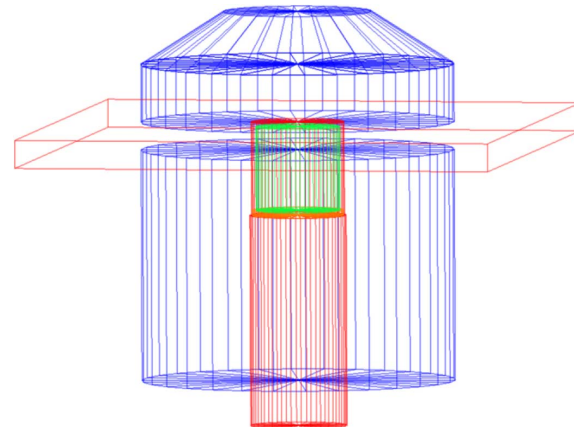


Fig. 3. Model of the RARM-F geometry (in scale) used in the MC simulations. The corresponding elements are NaI(Tl) or LaBr<sub>3</sub>(Ce) crystal (green), light guide (orange), crystal case of Al (red), aluminum plate holding the filter (red) and Pb shield (blue).

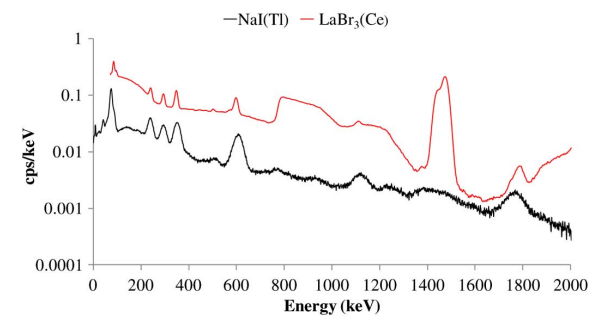


Fig. 4. Comparison of the typical background spectra obtained with both detectors in a 24 hour integration.

the aluminum plate holding the filter was also modeled (red). The information on the materials (density and composition) was taken from [10], and the cut-off energy for the photons and the electrons was set at 10 keV.

For the MC efficiency calculations, each point of the efficiency curve was calculated considering a monoenergetic source (in the range of 20 to 2000 keV) emitting in all directions with equal probability. The source was distributed homogeneously in a 45 mm diameter circle emulating the active part of the paper filter, which corresponds to the real counting geometry.

The MC efficiency  $\varepsilon_{MC}$  was calculated as:

$$\varepsilon_{MC} = \frac{N_{counts}}{N_{hist}} \quad (2)$$

where  $N_{counts}$  is the number of counts under the full energy peak and  $N_{hist}$  is the number of simulated histories (i.e., the number of primary source-particles simulated and all of the secondary particles produced by it), which was set to  $2 \cdot 10^7$ .

## 4.2. GAMMA-RAY SPECTROMETRY ON A PARTICULATE FILTER

47

730

IEEE TRANSACTIONS ON NUCLEAR SCIENCE, VOL. 61, NO. 2, APRIL 2014

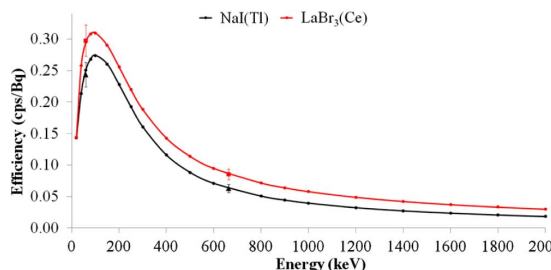


Fig. 5. Efficiency curves for the NaI(Tl) and the LaBr<sub>3</sub>(Ce) detectors. The experimental efficiencies are also shown (black triangles and red squares, respectively).

## IV. RESULTS AND DISCUSSION

### A. Comparison of the Obtained Spectra

To show the performance of the RARM-F when using either the NaI(Tl) detector or the LaBr<sub>3</sub>(Ce) detector, two 24 hour integration spectra of the typical background are compared in Fig. 4.

The background spectra depicted clearly the peaks caused by radon daughters. In particular, the contributions of <sup>214</sup>Pb (239, 295 and 352 keV) and <sup>214</sup>Bi (609, 1120 and 1764 keV) could be observed. The peaks produced by these background isotopes can be overlapped with other from certain isotopes of interest, making it difficult to detect low amounts of them. In this sense, the better resolution observed in the LaBr<sub>3</sub>(Ce) detector makes it better at resolving close peaks of most of the isotopes of interest in environmental radiation monitoring.

An important difference observed in Fig. 4 was the background shape of the LaBr<sub>3</sub>(Ce) detector compared with the NaI(Tl) detector. Specifically, important differences can be clearly observed at approximately 789 keV and 1436 keV, which are the energies of the gamma particles emitted by the internal contamination of the <sup>138</sup>La in the LaBr<sub>3</sub>(Ce) crystal. Due to this contaminant, a beta continuum is also observed between these energies. As this self-background is practically constant (the half-life of the <sup>138</sup>La is  $1.05 \cdot 10^{11}$  years), it could be removed from all the spectra after some analysis.

### B. Efficiency Calculations

The efficiency curves implemented in the NaI(Tl) and the LaBr<sub>3</sub>(Ce) monitors are shown in Fig. 5. The efficiencies calculated with the MC simulations were multiplied by 0.85 and 0.90, respectively, to fit the experimental efficiencies (black triangles and red squares, respectively). In general, the MC values were higher than the experimental ones. These differences could be attributed to some simplifications introduced in the RARM-F model used in the simulations. For example, the filter is not modeled, although it produces some attenuation to the gamma rays. However, rather than complicating the geometry model, these differences can be overcome using a simple multiplication factor. Even so, more experimental values with other radionuclides at other energies should be obtained to check the validity of this approach at more points.

TABLE I  
 COMPARISON OF THE <sup>137</sup>Cs MDACS FOR BOTH DETECTORS ACROSS  
 DIFFERENT INTEGRATION TIMES

	NaI(Tl)		LaBr <sub>3</sub> (Ce)	
	MDAC (Bq/m <sup>3</sup> )		MDAC (Bq/m <sup>3</sup> )	
	min	max	min	max
10 min	3.8 (4)	8.3 (9)	2.1 (2)	2.3 (2)
1 h	0.25 (3)	0.57 (6)	0.14 (1)	0.15 (2)
12 h	0.0070 (7)	0.0096 (10)	0.0034 (3)	0.0035 (4)

The calculated efficiencies for the LaBr<sub>3</sub>(Ce) detector were larger than those calculated for the NaI(Tl) detector over the entire energy range. This behavior can be understood by comparing the densities of both crystals, which are 3.67 g/cm<sup>3</sup> for the NaI(Tl) and 5.08 g/cm<sup>3</sup> for the LaBr<sub>3</sub>(Ce).

The efficiency curves represented in Fig. 5 do not account for the filter retention efficiency, which in practice is assumed to be 100%. It is important to remark that only particulate forms of the isotopes are captured in the filter. Thus, the real activity concentrations in air could be underestimated. In particular, iodine isotopes are of interest, and hence, some hypothesis about the percentage of particulates of iodine should be accounted to provide more realistic values of their concentration of activity in air.

### C. Measurement Capabilities

To study the measurement capabilities of each of the developed RARM-Fs, some values of the MDACs for the <sup>137</sup>Cs are reported in Table I. These values, which can vary depending on the natural background, are provided to have an estimation of the RARM-F capabilities. However, it is not possible to compare them directly because the monitors are slightly different. In fact, the LaBr<sub>3</sub>(Ce) includes some improvements in comparison with the NaI(Tl) one that have made it possible to obtain higher flows without breaking the filter. Thus, the average flows were 4.1 m<sup>3</sup>/h and 10.4 m<sup>3</sup>/h for the NaI(Tl) and LaBr<sub>3</sub>(Ce) monitors, respectively. Further work is being carried out to increase the flows even more, which will make it possible to obtain lower MDACs.

For comparison, for a 10 min measurement, the MDAC obtained with direct measurement with a 1.5" x 1.5" LaBr<sub>3</sub> for the <sup>137</sup>Cs is 30 Bq/m<sup>3</sup> [3], which is much larger than those obtained with RARM-F. Besides, these differences would be even larger if the performances would be compared at larger integration times.

Finally, the results in Table I show that the measurement capabilities of the RARM-F for <sup>137</sup>Cs are more dependent on the background when the NaI(Tl) detector is used. This is a consequence of the low resolution of this detector, which cannot clearly resolve the peak from <sup>214</sup>Bi at 609 keV from the one of <sup>137</sup>Cs at 662 keV, producing an overlap between them. This effect is no longer produced in the LaBr<sub>3</sub>(Ce) detector, where the variation on the MDAC values depends basically on the variation of the background due to Compton scattering of higher energy photons.

## V. CONCLUSIONS

A Real-time Airborne Radioactivity Monitor using gamma-ray spectrometry on a particulate Filter (RARM-F) was developed. The monitor can be operated with either a NaI(Tl) detector or a LaBr<sub>3</sub>(Ce) detector.

To achieve optimal performance, the RARM-F was fully calibrated (energy, resolution and efficiency calibrations) using experimental data and Monte Carlo simulations with the EGS5 code system.

The performance of the different RARM-Fs with different crystals was evaluated with some values of the MDACs for <sup>137</sup>Cs. The results show better performance for these monitors in comparison with other measuring directly in the environment.

Finally, the RARM-F is ready to be used in an automatic real-time environmental radiation surveillance network by allowing the isotope identification and quantifications, and thus, the establishment of automatic alerts based on the limits provided by legislation.

## ACKNOWLEDGMENT

Part of this research was performed using the resources of the CESCA (Centre de Supercomputació de Catalunya).

## REFERENCES

- [1] R. Casanovas, J. J. Morant, M. López, I. Hernández-Girón, E. Batalla, and M. Salvadó, "Performance of data acceptance criteria over 50 months from an automatic real-time environmental radiation surveillance network," *J. Environ. Radioact.*, vol. 102, pp. 742–748, 2011.
- [2] S. M. Bowyer, H. S. Miley, R. C. Thompson, and C. W. Hubbard, "Automated particulate sampler for comprehensive test ban treaty verification (the DOE radionuclide aerosol sampler/analyizer)," *IEEE Trans. Nucl. Sci.*, vol. 44, no. 3, pp. 551–556, Jun. 1997.
- [3] A. Mattila, H. Toivonen, K. Vesterbacka, M. Leppänen, S. Salmelin, and A. Pelikan, "Radiation monitoring network with spectroscopic capabilities: Implementation of LaBr<sub>3</sub> spectrometers to the Finnish network," in *Proc. 3rd Eur. IRPA Congr.*, Helsinki, Finland, 2010, pp. 1958–1966 [Online]. Available: <http://www.ipa2010europe.com/pdfs/proceedings/S12-P12.pdf>.
- [4] J. B. Forrester, F. F. Cartt, L. Comes, J. C. Hayes, H. S. Miley, S. J. Morris, M. Ripplinger, R. W. Slaugh, and P. Van Davelaar, "Engineering upgrades to the radionuclide aerosol sampler/analyzer for the CTBT international monitoring system," *J. Radioanal. Nucl. Chem.*, vol. 296, pp. 1055–1060, 2013.
- [5] R. Casanovas, M. Salvadó, M. Lopez, C. Tapia, and A. de Blas, "Estación de identificación y medida en tiempo real de la radiactividad ambiental gamma mediante espectrometría sobre filtro de papel (in Spanish)," ES Patent Application P201230408, Mar. 16, 2012 [Online]. Available: [http://www.oepm.es/pdf/ES/0000/000/02/42/58/ES-2425801\\_A1.pdf](http://www.oepm.es/pdf/ES/0000/000/02/42/58/ES-2425801_A1.pdf).
- [6] R. Casanovas, J. J. Morant, and M. Salvadó, "Energy and resolution calibration of NaI(Tl) and LaBr<sub>3</sub>(Ce) scintillators and validation of an EGS5 Monte Carlo user code for efficiency calculations," *Nucl. Instrum. Methods Phys. Res. A*, vol. 675, pp. 78–83, 2012.
- [7] R. Casanovas, J. J. Morant, and M. Salvadó, "Temperature peak-shift correction methods for NaI(Tl) and LaBr<sub>3</sub>(Ce) gamma-ray spectrum stabilization," *Radiat. Meas.*, vol. 47, pp. 588–595, 2012.
- [8] L. A. Currie, "Limits for qualitative detection and quantitative determination," *Anal. Chem.*, vol. 40, pp. 586–593, 1968.
- [9] H. Hirayama, Y. Namito, A. F. Bielajew, S. J. Wilderman, and W. R. Nelson, The EGS5 Code System Stanford, CA, USA, Rep. SLAC-R-730, Dec. 19, 2005 [Online]. Available: <http://slac.stanford.edu/cgi-wrap/getdoc/slac-r-730.pdf>.
- [10] M. J. Berger, J. S. Coursey, M. A. Zucker, and J. Chang, ESTAR, PSTAR, and ASTAR: Computer Programs for Calculating Stopping-Power and Range Tables for Electrons, Protons, and Helium Ions (version 1.2.3) [Online]. Available: <http://physics.nist.gov/Star>

#### 4.3. DIRECT GAMMA-RAY SPECTROMETRY WITH TWO DETECTORS 49

### 4.3 Development and calibration of a real-time airborne radioactivity monitor using direct gamma-ray spectrometry with two scintillation detectors

#### Abstract

The implementation of in-situ gamma-ray spectrometry in an automatic real-time environmental radiation surveillance network can help to identify and characterize abnormal radioactivity increases quickly. For this reason, a Real-time Airborne Radioactivity Monitor using direct gamma-ray spectrometry with two scintillation detectors (RARM-D2) was developed. The two scintillation detectors in the RARM-D2 are strategically shielded with Pb to permit the separate measurement of the airborne isotopes with respect to the deposited isotopes.

In this paper, we describe the main aspects of the development and calibration of the RARM-D2 when using NaI(Tl) or LaBr<sub>3</sub>(Ce) detectors. The calibration of the monitor was performed experimentally with the exception of the efficiency curve, which was set using Monte Carlo (MC) simulations with the EGS5 code system. Prior to setting the efficiency curve, the effect of the radioactive source term size on the efficiency calculations was studied for the gamma-rays from <sup>137</sup>Cs. Finally, to study the measurement capabilities of the RARM-D2, the minimum detectable activity concentrations for <sup>131</sup>I and <sup>137</sup>Cs were calculated for typical spectra at different integration times.



## Development and calibration of a real-time airborne radioactivity monitor using direct gamma-ray spectrometry with two scintillation detectors



R. Casanovas <sup>a,\*</sup>, J.J. Morant <sup>b</sup>, M. Salvadó <sup>a</sup>

<sup>a</sup> Unitat de Física Mèdica, Facultat de Medicina i Ciències de la Salut, Universitat Rovira i Virgili, ES-43201 Reus, Tarragona, Spain

<sup>b</sup> Servei de Protecció Radiològica, Servei de Recursos Científics i Tècnics, Universitat Rovira i Virgili, ES-43007 Tarragona, Spain

### HIGHLIGHTS

- A real-time airborne radioactivity monitor was developed.
- The monitor is formed using two scintillation detectors for gamma-ray spectrometry.
- The detectors are shielded with Pb. One detector is pointing up and the other down.
- The monitors were calibrated using experimental data and Monte Carlo simulations.
- The efficiency calculations and MDAC values are given.

### ARTICLE INFO

#### Article history:

Received 24 September 2013

Received in revised form

8 January 2014

Accepted 28 January 2014

Available online 12 February 2014

#### Keywords:

Scintillation gamma-ray spectrometry

Nal(Tl)

LaBr<sub>3</sub>(Ce)

Monte Carlo simulation

Efficiency calculation

### ABSTRACT

The implementation of in-situ gamma-ray spectrometry in an automatic real-time environmental radiation surveillance network can help to identify and characterize abnormal radioactivity increases quickly. For this reason, a Real-time Airborne Radioactivity Monitor using direct gamma-ray spectrometry with two scintillation detectors (RARM-D2) was developed. The two scintillation detectors in the RARM-D2 are strategically shielded with Pb to permit the separate measurement of the airborne isotopes with respect to the deposited isotopes. In this paper, we describe the main aspects of the development and calibration of the RARM-D2 when using Nal(Tl) or LaBr<sub>3</sub>(Ce) detectors. The calibration of the monitor was performed experimentally with the exception of the efficiency curve, which was set using Monte Carlo (MC) simulations with the EGS5 code system. Prior to setting the efficiency curve, the effect of the radioactive source term size on the efficiency calculations was studied for the gamma-rays from <sup>137</sup>Cs. Finally, to study the measurement capabilities of the RARM-D2, the minimum detectable activity concentrations for <sup>131</sup>I and <sup>137</sup>Cs were calculated for typical spectra at different integration times.

© 2014 Elsevier Ltd. All rights reserved.

### 1. Introduction

The Euratom Treaty requires each Member State to establish the necessary facilities to carry out real-time monitoring of the level of radioactivity in the air, water and soil and to ensure compliance with the basic standards (2000/473/Euratom, 2000). Following these requirements, there is an automatic real-time surveillance network in Catalonia (ES-E, Spain-East) that is essentially composed of two types of monitors (Casanovas et al., 2011): aerosol and Geiger monitors. The aerosol monitors provide artificial alpha and beta, radon and gamma (due mainly to the iodine

isotopes) activity concentrations. The Geiger monitors provide the ambient dose equivalent rate.

In a previous study (Casanovas et al., 2011), it was identified that the use of in-situ real-time gamma-ray spectrometry would help to identify and characterize abnormal radioactivity increases quickly. In this sense, the isotope identification can distinguish between artificial and natural radioactivity increments, and the quantification can establish alert levels based on the limits provided by legislation.

Thus, three different types of radiation monitors using either Nal(Tl) or LaBr<sub>3</sub>(Ce) scintillation detectors have been developed recently and implemented into the Catalan surveillance network: a water monitor (Casanovas et al., 2013), an aerosol monitor using a particulate filter (Casanovas et al., 2012c, 2014) and the monitor presented in this study.

Environmental monitoring with real-time gamma-ray spectrometry using scintillation detectors has become fairly common,

\* Corresponding author. Tel.: +34 977759382.  
E-mail address: [ramon.casanovas@urv.cat](mailto:ramon.casanovas@urv.cat) (R. Casanovas).

### 4.3. DIRECT GAMMA-RAY SPECTROMETRY WITH TWO DETECTORS

51

R. Casanovas et al. / Applied Radiation and Isotopes 89 (2014) 102–108

103

especially when the measurements are performed directly in the environment (i.e., without needing to concentrate the isotopes in a fiber or charcoal filter). For this purpose, either NaI(Tl) (Aage et al., 2003; Zhang et al., 2013) or LaBr<sub>3</sub>(Ce) detectors (Toivonen et al., 2008; Mattila et al., 2010) have been used.

However, when measuring directly in the environment, the characterization of the radiation source term in a nuclear release is a demanding task. In particular, it is difficult to know if the contributions to the measured spectra are from a radioactive cloud or from a deposition on the ground.

For this reason, a Real-time Airborne Radioactivity Monitor using Direct gamma-ray spectrometry with two scintillation detectors (RARM-D2) was developed. The RARM-D2 enables the discrimination between the isotopes contained in a radioactive cloud from those deposited or emerging from the ground, which enables a good primary characterization of the radioactivity source term in a nuclear release.

In this work, we describe the main aspects of the development and calibration of the RARM-D2, either using NaI(Tl) or LaBr<sub>3</sub>(Ce) detectors, with particular emphasis being placed on the efficiency calibration. In addition, several typical spectra are shown, and the measurement capabilities of this monitor were studied for <sup>131</sup>I and <sup>137</sup>Cs with different integration times and for both detector types.

## 2. Materials and methods

### 2.1. Description of the RARM-D2

A general scheme of the developed monitor (Casanovas et al., 2012b) is shown in Fig. 1. The RARM-D2 is formed using two scintillation detectors, one pointing up (1) and the other pointing down (2), which are shielded with Pb (3). This geometrical disposition together with the shielding permits the discrimination between the isotopes contained in a radioactive cloud from those deposited or emerging from the ground, which can be of interest after a nuclear accident to characterize the radiation source term.

The detectors used in this study were two 2" × 2" NaI(Tl) and two 2" × 2" LaBr<sub>3</sub>(Ce) scintillation detectors, which made it possible to have one of each pointing up and down, respectively. The NaI(Tl) detectors were Model 905-3 from ORTEC® and the LaBr<sub>3</sub>(Ce) detectors were BrillLanCe™380 from Saint-Gobain Crystals. All detectors were connected to a multichannel pulse-height analyzer of 2000 channels. The Pb shielding was specifically designed for this monitor and was manufactured by TECNIBUSA Protección Radiológica S.L.

The system integrates a meteorological station (Davis Vantage Pro2 Weather Station, Davis Instruments Corp., California, U.S.A.) that provides the following data: wind speed and direction, temperature, humidity, barometric pressure, rainfall and solar radiation. The integration of a meteorological station can provide valuable information for studying the evolution of the radiation source term, especially in cases of nuclear accidents.

The system is controlled using a specially designed software in the Delphi programming language. The obtained data are transmitted to a main server via an ADSL connection (using the SSL/TLS protocol), the system is remotely controlled using the TCP/IP protocol. However, other redundant means of communication are possible (GSM, radiofrequency, satellite, etc.). From the main server, it is also possible to activate alternative measurement systems (e.g., high flow filters for laboratory analysis) and to send automatic messages (SMS or emails) to a predefined contact list in response to either radiological criteria or different sensor signals.

### 2.2. Calibration of the RARM-D2

The calibration methodology for NaI(Tl) and LaBr<sub>3</sub>(Ce) detectors has been described in detail in a previous paper (Casanovas et al., 2012a) and adapted specifically for this monitor. This methodology encompasses energy, resolution and efficiency calibrations.

#### 2.2.1. Energy and resolution calibrations

The energy and resolution calibrations were established using five radioactive point sources (<sup>241</sup>Am, <sup>133</sup>Ba, <sup>137</sup>Cs, <sup>60</sup>Co and <sup>152</sup>Eu) and complemented with some emissions from natural background isotopes (such as <sup>214</sup>Pb, <sup>214</sup>Bi, <sup>40</sup>K or <sup>208</sup>Tl). The detectors were adjusted to cover the energy range from 0 to 3000 keV. The stability of the energy calibration in the systems without automatic gain control was controlled by means of software using the method described in (Casanovas et al., 2012d).

#### 2.2.2. Efficiency calibrations

The efficiency calibration establishes the relationship (for each energy of the gamma-rays) between the number of counts under a peak and the activity (or activity concentration) of a radioactive source. In the RARM-D2, we are interested in measuring volumetric activity (Bq m<sup>-3</sup>) with the detector pointing up and superficial activity (Bq m<sup>-2</sup>) with the detector pointing down.

To obtain a complete efficiency curve for each detector and geometrical disposition, efficiency calculations were performed

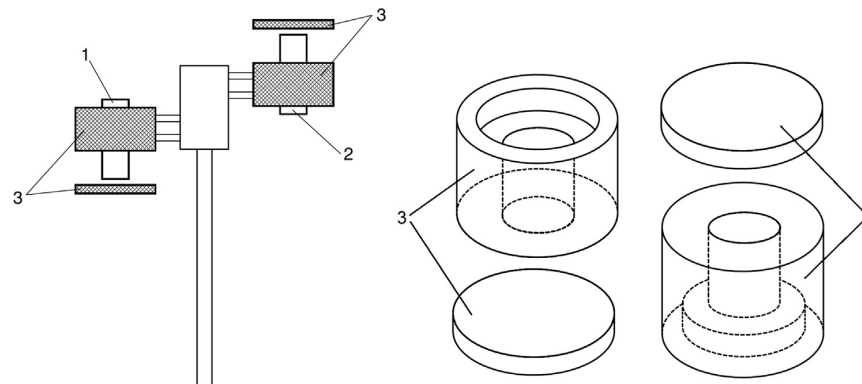


**Fig. 1.** General scheme of the RARM-D2 (left) and detailed scheme of the Pb shielding (right). The main elements are: detector pointing up (1), detector pointing down (2) and Pb shielding (3).

using MC simulations. The MC simulations were performed with a previously validated EG55 user code (Casanovas et al., 2012a). This user code contains all of the information about the radiation source (type of particles, energy of the particles, geometrical distribution of the source, etc.) and the involved detection system (type of detector, Pb shielding, etc.).

The simulations were carried out on the CESCA cluster in a Bull NovaScale machine comprised of 224 Xeon E5472 cores and 112 Xeon X5550 cores, 1.6 TB of main memory and 52.6 TB of disk memory. The simulations were performed separately but simultaneously, each using 1 processor and 4 GB of memory.

Thus, a model of the RARM-D2 (see Fig. 2) was implemented for the MC simulations based on the real dimensions and materials, which were taken from the manufacturer technical specifications. Briefly, the geometry was modeled with the corresponding scintillation crystal, either NaI(Tl) or LaBr<sub>3</sub>(Ce), with a case of 0.5 mm of Al. The space between the case and the crystal was filled with air. A glass light guide after the crystal was also considered, and the photomultiplier tube was modeled as an air-filled cylinder of Al. The tube base was modeled with a mixture of Al and Cu. The material information (density and composition) was taken from the literature (Berger et al., 2005), and the cut-off energy for the photons and the electrons was set at 10 keV.

For the efficiency calculations, each point of each efficiency curve was calculated separately by considering a monoenergetic radiation source (in the range of 20 to 3000 keV). Because the distribution of the radiation source term is not known a priori, a semi-infinite homogeneous activity concentration was assumed. However, the developed simulation user code is ready to accept any distribution of the source term, which can be of interest to provide retrospectively improved activity concentration calculations when more information on the source term evolution becomes available.

Fig. 3 shows the different geometries considered in the MC simulations for both orientations (up and down) of both the NaI (Tl) and LaBr<sub>3</sub>(Ce) detectors. The radiation source term for the up-detectors is a cylinder of radius  $R$  and height  $H = 2R$  whereas the source term for the down-detectors is a disk of radius  $R$ . To set the computational semi-infinite dimensions, the variation of the efficiency values with  $R$  was studied for a monoenergetic homogeneous source of 662 keV, which corresponds to the main <sup>137</sup>Cs gamma-ray emission. Regarding the obtained results, the final efficiency curves for the RARM-D2 were calculated using  $2R = 500$  m.

In the MC simulations, the efficiency was calculated as:

$$\epsilon = \frac{N_{\text{counts}}}{N_{\text{hist}}} \quad (1)$$

where  $N_{\text{counts}}$  is the number of net counts under the full energy peak and  $N_{\text{hist}}$  is the number of simulated histories (i.e., the number of primary source-particles simulated and all of the secondary particles produced by it), which was set at  $10^8$ .

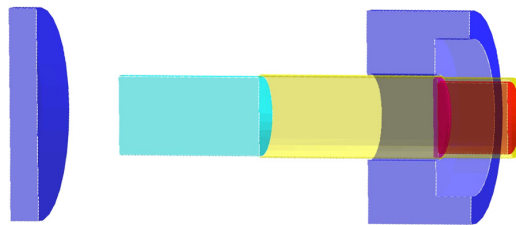


Fig. 2. Geometric model of the RARM-D2 (to scale) used in the MC simulations.

The volumetric efficiencies  $\epsilon_V$  for the up-detectors were then calculated as:

$$\epsilon_V \equiv \epsilon \times V \quad (2)$$

where  $\epsilon$  is the efficiency calculated with Eq. (1) and  $V$  the volume of the source term.

In a similar way, the superficial efficiencies  $\epsilon_S$  for the down-detectors were calculated as:

$$\epsilon_S \equiv \epsilon \times S \quad (3)$$

where  $\epsilon$  is the efficiency calculated with Eq. (1) and  $S$  the surface of the source term.

Finally, the efficiency calculations were fitted to the following function:

$$\log \epsilon_X = \sum_{n=0}^6 a_n (\log E)^n \quad (4)$$

where  $\epsilon_X$  is either the volumetric efficiency  $\epsilon_V$  or the superficial efficiency  $\epsilon_S$  at the gamma-ray energy  $E$  and  $a_n$  represents the fitting coefficients.

### 2.3. Minimum detectable activity concentration (MDAC)

The detection capabilities of a system are usually evaluated with the detection limit  $L_D$  or the minimum number of counts under a peak that one can be confident of detecting with a certain probability. Thus, the Minimum Detectable Activity Concentration (MDAC) is the activity concentration equivalent to the detection limit  $L_D$ .

After the efficiency calibration, the activity concentration  $a_X$  can be calculated as:

$$a_X = \frac{N}{\epsilon_X \times t \times p_\gamma} \quad (5)$$

where  $a_X$  can be either the volumetric activity  $a_V$  ( $\text{Bq m}^{-3}$ ) or the superficial activity  $a_S$  ( $\text{Bq m}^{-2}$ ),  $N$  is the number of counts under the peak,  $t$  the counting time,  $p_\gamma$  is the emission probability of the gamma-ray and  $\epsilon_X$  is either the volumetric efficiency  $\epsilon_V$  or the superficial efficiency  $\epsilon_S$ .

Thus, from Eq. (5):

$$\text{MDAC} = \frac{L_D}{\epsilon_X \times t \times p_\gamma} \quad (6)$$

If the measured spectrum is assumed to be only background, the detection limit  $L_D$  (with a 95% confidence limit) for a certain Region of Interest (ROI) in the spectrum can be calculated using the following single-count Currie expression (Currie, 1968):

$$L_D = 2.71 + 4.65\sqrt{B} \quad (7)$$

where  $B$  is the number of counts produced by the background in the considered ROI.

The width of the ROI is determined using the width of the expected peak, which is proportional to the  $FWHM(E)$  function (obtained from the resolution calibration) of each detector:

$$n = n(E) = k \times FWHM(E) \quad (8)$$

where  $k$  is the proportionality constant to set the desired peak coverage and  $FWHM(E)$  is obtained in the resolution calibration. For example,  $k = 2.548$  for a 99.73% peak area coverage.

### 4.3. DIRECT GAMMA-RAY SPECTROMETRY WITH TWO DETECTORS

53

R. Casanovas et al. / Applied Radiation and Isotopes 89 (2014) 102–108

105

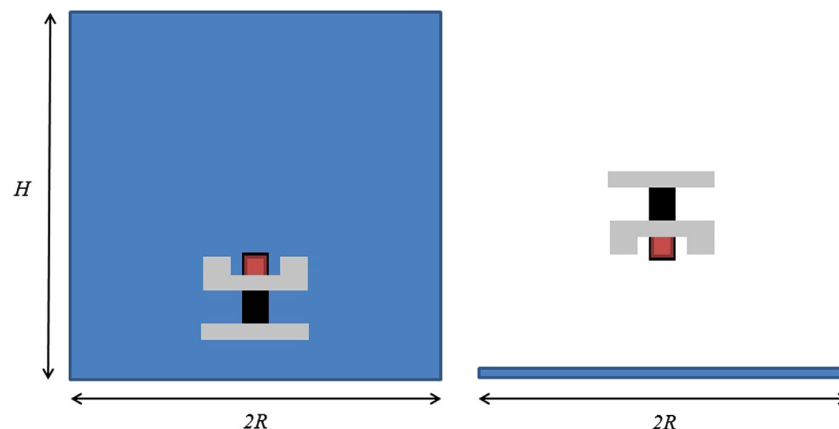


**Fig. 3.** Geometry of the source term used in the MC simulations for the up-detectors (left) and for the down-detectors (right).

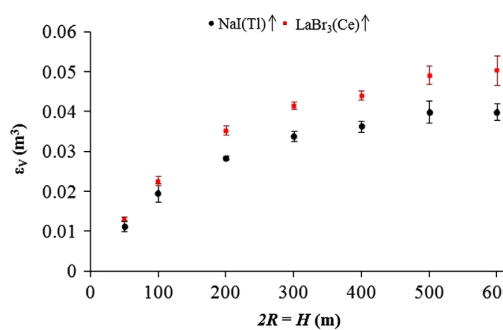


**Fig. 4.** Variation of the efficiency values with the source term size (homogeneous cylinder of radius  $R$  and height  $H$ ) for a monoenergetic source of 662 keV gamma-rays for the up-detectors.

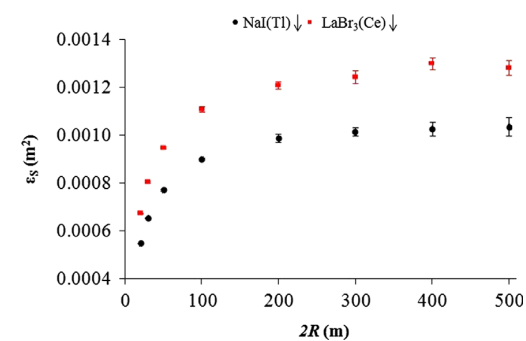


**Fig. 5.** Variation of the efficiency values with the source term size (homogeneous disk of radius  $R$ ) for a monoenergetic source of 662 keV gamma-rays for the down-detectors.

### 3. Results and discussion

#### 3.1. Source term size

The variation of the efficiency values with the source term size for a monoenergetic homogeneous source of 662 keV gamma-rays is shown in Fig. 4 for the up-detectors and in Fig. 5 for the down-detectors.

The obtained results show, in both cases, that the efficiencies increased with the size of the source term. In particular, the observed dependences of the efficiencies with the radius  $R$  of the source term were approximately  $\epsilon_V \propto R^{0.5}$  and  $\epsilon_S \propto R^{0.2}$ ; thus, the variation on the efficiency values reduces as the size of the source term increases.

This can be explained considering that the half-value layer in air for 662 keV gamma-rays is 74 m, which is related to the percentage of photons contributing to efficiency. For example, for distances larger than 250 m, less than 10% of the photons will reach the detector.

Based on these results, the final efficiency curves for the RARM-D2 (see Section 3.2) were calculated using  $2R = 500$  m for both NaI(Tl) and LaBr<sub>3</sub>(Ce) detectors in both configurations (pointing up or down).

#### 3.2. Efficiency calculations

The efficiency curves for the RARM-D2 calculated from the MC simulations are shown in Fig. 6 (up-detectors) and Fig. 7 (down-detectors). The data were well fitted to Eq. (4) (dotted lines in the

plots). The coefficients of determining  $r^2$  for the NaI(Tl) fits were 0.997 (up) and 0.9994 (down); these coefficients for the LaBr<sub>3</sub>(Ce) were 0.997 (up) and 0.9994 (down).

The computation times ranged from 45 min (for 20 keV photons) to 35 h (3000 keV photons) in the NaI(Tl) detectors and from 1.4 h (for 20 keV photons) to 45.4 h (3000 keV photons) in the LaBr<sub>3</sub>(Ce) detectors.

The calculated efficiencies for the NaI(Tl) were systematically lower than the LaBr<sub>3</sub>(Ce) efficiencies as a consequence of their different densities, which were  $3.67 \text{ g cm}^{-3}$  and  $5.08 \text{ g cm}^{-3}$ , respectively. Below 300 keV, the differences between the NaI(Tl) and LaBr<sub>3</sub>(Ce) efficiencies were shorter primarily because the attenuation of the gamma-rays in the air and in the detector covers is higher at lower energies.

#### 3.3. Typical spectra

The variability of the background spectra may strongly depend on the meteorological conditions. However (and by way of example), 24 h typical spectra obtained with the RARM-D2 are shown in Fig. 8 for the up-detectors and in Fig. 9 for the down-detectors. Similar count rates were obtained for 10 min spectra, but the quality of the peaks was lower due to low statistics.

The more important observed peaks were from <sup>222</sup>Rn and <sup>232</sup>Th daughters (such as <sup>214</sup>Pb, <sup>214</sup>Bi and <sup>208</sup>Tl) and from the NORM <sup>40</sup>K, especially on the down detectors. In addition, LaBr<sub>3</sub>(Ce) spectra showed clear evidence of its intrinsic activity, which has been discussed elsewhere (Quarati et al., 2012).

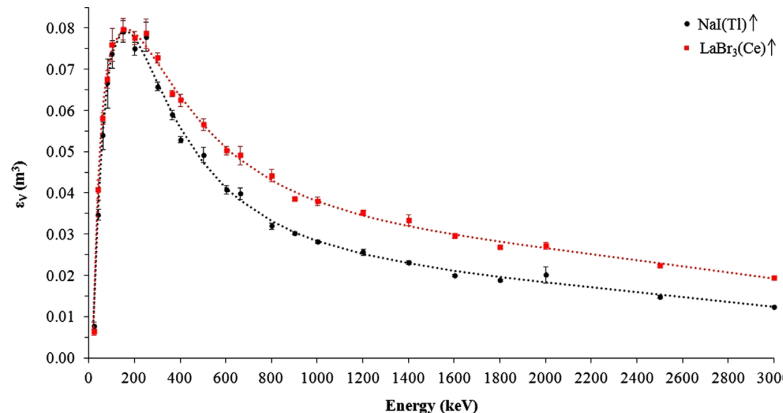


**Fig. 6.** Efficiency curves calculated using the MC simulations for up Nal(Tl) (black dots) and LaBr<sub>3</sub>(Ce) (red squares). The dotted lines correspond to the fit described by Eq. (4). (For interpretation of the references to color in this figure legend, the reader is referred to the web version of this article.)

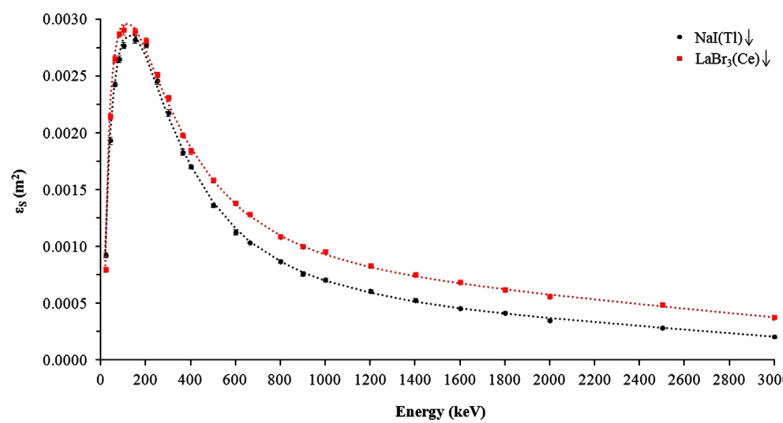


**Fig. 7.** Efficiency curves calculated using the MC simulations for down Nal(Tl) (black dots) and LaBr<sub>3</sub>(Ce) (red squares). The dotted lines correspond to the fit described by Eq. (4). (For interpretation of the references to color in this figure legend, the reader is referred to the web version of this article.)

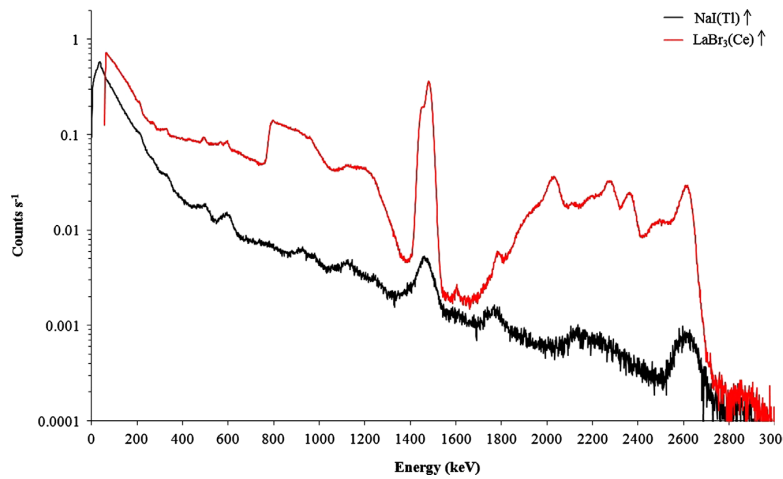


**Fig. 8.** Spectra of the typical background radiation measured with the pointing-up detectors, Nal(Tl) and LaBr<sub>3</sub>(Ce), of the RARM-D2 with an integration time of 24 h.

Better energy resolution was observed in the obtained spectra for the LaBr<sub>3</sub>(Ce) detectors than the Nal(Tl) detectors. For example, the LaBr<sub>3</sub>(Ce) could resolve the peaks from <sup>208</sup>Tl at 583 keV and <sup>214</sup>Bi at 609 keV, while the Nal(Tl) detectors could not resolve these peaks.

### 3.4. MDAC

The measurement capabilities of the RARM-D2 in terms of the MDAC are shown in Table 1 (up-detectors) and in Table 2 (down-detectors) for the <sup>131</sup>I and <sup>137</sup>Cs isotopes. MDACs were calculated

### 4.3. DIRECT GAMMA-RAY SPECTROMETRY WITH TWO DETECTORS

55

R. Casanovas et al. / Applied Radiation and Isotopes 89 (2014) 102–108

107

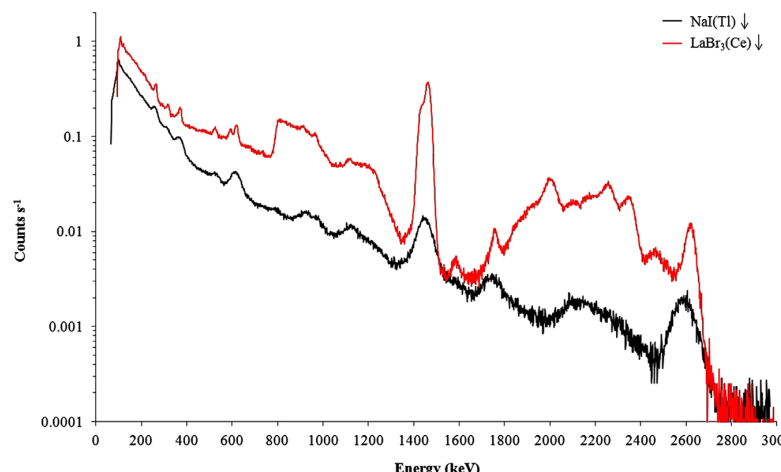


Fig. 9. Spectra of the typical background radiation measured with the pointing-down detectors, Nal(Tl) and LaBr<sub>3</sub>(Ce), of the RARM-D2 with an integration time of 24 h.

**Table 1**  
 MDAC values for the <sup>131</sup>I and <sup>137</sup>Cs isotopes in the up-detectors at different integration times.

Integration time	MDAC (Bq m <sup>-3</sup> )			
	Nal(Tl)		LaBr <sub>3</sub> (Ce)	
	<sup>131</sup> I (365 keV)	<sup>137</sup> Cs (662 keV)	<sup>131</sup> I (365 keV)	<sup>137</sup> Cs (662 keV)
10 min	4.89 ± 0.09	5.3 ± 0.2	5.25 ± 0.07	6.5 ± 0.3
1 h	1.97 ± 0.04	2.14 ± 0.07	2.12 ± 0.03	2.63 ± 0.12
4 h	0.98 ± 0.02	1.06 ± 0.04	1.05 ± 0.01	1.31 ± 0.06
12 h	0.57 ± 0.01	0.61 ± 0.02	0.61 ± 0.01	0.76 ± 0.03
24 h	0.40 ± 0.01	0.43 ± 0.01	0.43 ± 0.01	0.53 ± 0.02

**Table 2**  
 MDAC values for the <sup>131</sup>I and <sup>137</sup>Cs isotopes in the down-detectors at different integration times.

Integration time	MDAC (Bq m <sup>-2</sup> )			
	Nal(Tl)		LaBr <sub>3</sub> (Ce)	
	<sup>131</sup> I (365 keV)	<sup>137</sup> Cs (662 keV)	<sup>131</sup> I (365 keV)	<sup>137</sup> Cs (662 keV)
10 min	288 ± 4	342 ± 6	238 ± 2	278 ± 3
1 h	117 ± 2	138 ± 3	96.6 ± 0.9	112 ± 1
4 h	58.3 ± 0.8	69 ± 1	48.2 ± 0.5	56.0 ± 0.7
12 h	33.6 ± 0.5	39.8 ± 0.7	27.8 ± 0.3	32.3 ± 0.4
24 h	23.8 ± 0.2	28.1 ± 0.5	19.6 ± 0.2	22.8 ± 0.3

using Eqs. (6)–(8) over typical spectra obtained at different integration times. The spectra were assumed to be only background, and a value of  $k = 2.548$  (99.73% of the peak area coverage) was used. This value was chosen to ensure a full coverage of the hypothetical peak (smaller values could underestimate the background under it).

The most significant contribution to the MDACs uncertainty is the efficiency value component, which could be reduced using a larger number of histories in the simulations.

When comparing the MDACs for the up-detectors, the MDAC values were systematically higher for the LaBr<sub>3</sub>(Ce) detector than

for the Nal(Tl) detector. This is a consequence of the intrinsic activity of the former, which produces an additional background to the spectra that raises the number of counts in the studied ROIs. In contrast, the MDAC values in the down-detectors were systematically lower for the LaBr<sub>3</sub>(Ce) detector than for the Nal(Tl) detector; the natural background in the down-detectors is higher than in the up-detectors. Thus, the natural component of the background predominates in front of the intrinsic background of the LaBr<sub>3</sub>(Ce) in the considered ROIs and is equivalent for both detectors; hence, the better resolution and the larger efficiency of the LaBr<sub>3</sub>(Ce) improve the MDACs.

#### 4. Conclusions

A Real-time Airborne Radioactivity Monitor using Direct gamma-ray spectrometry with two scintillation detectors (RARM-D2) was developed. The RARM-D2 is formed using two scintillation detectors, either Nal(Tl) or LaBr<sub>3</sub>(Ce), with one pointing up and the other pointing down, which are shielded with Pb. This disposition permits the discrimination between the isotopes contained in a radioactive cloud from those deposited or emerging from the ground.

The RARM-D2 was fully calibrated using experimental data except for the efficiency curve, which was set using Monte Carlo simulations with the EGS5 code system that reproduced the responses of the Nal(Tl) and LaBr<sub>3</sub>(Ce) detectors. Prior to setting the efficiency curve, the effect of the radioactive source term size on the efficiency calculations was studied for the gamma-rays from <sup>137</sup>Cs, either for the up-detectors or for the down detectors. This approach made it possible to set a reasonable infinite homogeneous source, which was used to set the entire efficiency curve up to 3000 keV for all studied detectors.

Using the calculated efficiency curves, the capabilities of the RARM-D2 were evaluated with some MDAC calculations over average spectra and for different integration times. This evaluation was performed for all configurations (up and down) of Nal(Tl) and LaBr<sub>3</sub>(Ce) measuring <sup>131</sup>I and <sup>137</sup>Cs.

Finally, the RARM-D2 is ready to be used in an automatic real-time environmental radiation surveillance network. The design of the RARM-D2 enables a primary characterization of the radioactive source term and permits a comparison of the obtained data with the legal limits established for the activity concentrations, thereby allowing alarm levels for early warning to be established.

### Acknowledgements

Some of this research was performed using the resources of CESCA (Centre de Supercomputació de Catalunya).

### References

- 2000/473/Euratom, 27 July 2000. Commission Recommendation of 8 June 2000, Official Journal of the European Commission, No. 191. Available from: [http://ec.europa.eu/energy/nuclear/radioprotection/doc/legislation/00473\\_en.pdf](http://ec.europa.eu/energy/nuclear/radioprotection/doc/legislation/00473_en.pdf).
- Aage, H.K., Korsbech, U., Bargholz, K., 2003. Early detection of radioactive fallout by gamma spectrometry. *Radiat. Prot. Dosim.* **106**, 155–164.
- Berger, M.J., Coursey, J.S., Zucker, M.A., Chang, J., 2005. ESTAR, PSTAR, and ASTAR: Computer Programs for Calculating Stopping-Power and Range Tables for Electrons, Protons, and Helium Ions (version 1.2.3). National Institute of Standards and Technology, Gaithersburg. Available from: <http://physics.nist.gov/Star>.
- Casanovas, R., Morant, J.J., Lopez, M., Hernandez-Giron, I., Batalla, E., Salvadó, M., 2011. Performance of data acceptance criteria over 50 months from an automatic real-time environmental radiation surveillance network. *J. Environ. Radioact.* **102**, 742–748.
- Casanovas, R., Morant, J.J., Salvadó, M., 2012a. Energy and resolution calibration of NaI(Tl) and LaBr<sub>3</sub>(Ce) scintillators and validation of an EGSS Monte Carlo user code for efficiency calculations. *Nucl. Instrum. Methods Phys. Res., Sect. A* **675**, 78–83.
- Casanovas, R., Salvadó, M., Lopez, M. Estación de identificación y medida en tiempo real de la radiactividad ambiental gamma, mediante espectrometría con dos cristales de centelleo (in Spanish). ES Patent Application P201230236, 15th February 2012b. Available from: [http://www.oepm.es/pdf/ES/0000/000/002/42/32/ES-2423236\\_A1.pdf](http://www.oepm.es/pdf/ES/0000/000/002/42/32/ES-2423236_A1.pdf).
- Casanovas, R., Salvadó, M., Lopez, M., Tapia, C., de Blas, A. Estación de identificación y medida en tiempo real de la radiactividad ambiental gamma mediante espectrometría sobre filtro de papel (in Spanish). ES Patent Application P201230408, 16th March 2012c. Available from: [http://www.oepm.es/pdf/ES/0000/000/02/42/58/ES-2425801\\_A1.pdf](http://www.oepm.es/pdf/ES/0000/000/02/42/58/ES-2425801_A1.pdf).
- Casanovas, R., Morant, J.J., Salvadó, M., 2012d. Temperature peak-shift correction methods for NaI(Tl) and LaBr<sub>3</sub>(Ce) gamma-ray spectrum stabilisation. *Radiat. Meas.* **47**, 588–595.
- Casanovas, R., Morant, J.J., Salvadó, M. Development and calibration of a real-time airborne radioactivity monitor using gamma-ray spectrometry on a particulate filter. *IEEE Transactions on Nuclear Science* (2014). <http://dx.doi.org/10.1109/TNS.2014.2299715>.
- Casanovas, R., Morant, J.J., Salvadó, M., 2013. Implementation of gamma-ray spectrometry in two real-time water monitors using NaI(Tl) scintillation detectors. *Appl. Radiat. Isot.* **80**, 49–55.
- Currie, L.A., 1968. Limits for qualitative detection and quantitative determination. *Anal. Chem.* **40**, 586–593.
- Mattila, A., Toivonen, H., Vesterbacka, K., Leppänen, M., Salmelin, S., Pelikan, A. Radiation monitoring network with spectrometric capabilities: implementation of LaBr<sub>3</sub> spectrometers to the Finnish network. In: Proceedings of the Third European IRPA Congress, 2010, Helsinki, Finland. Available from: <http://www.irpa2010europe.com/pdfs/proceedings/S12-P12.pdf>.
- Quarati, F.G.A., Khodyuk, I.V., van Eijk, C.W.E., Quarati, P., Dorenbos, P., 2012. Study of <sup>138</sup>La radioactive decays using LaBr<sub>3</sub> scintillators. *Nucl. Instrum. Methods Phys. Res., Sect. A* **683**, 46–52.
- Toivonen, H., Vesterbacka, K., Pelikan, A., Mattila, A., Karhunen, T. LaBr<sub>3</sub> spectrometry for environmental monitoring. In: Proceedings of the 12th International Congress of the International Radiation Protection Association, 2008, Buenos Aires, Argentina. Available from: <http://www.irpa12.org.ar/fullpapers/FP0611.pdf>.
- Zhang, W., Korpach, E., Berg, R., Ungar, K., 2013. Testing of an automatic outdoor gamma ambient dose-rate surveillance system in Tokyo and its calibration using measured deposition after the Fukushima nuclear accident. *J. Environ. Radioact.* **125**, 93–98.

# Chapter 5

## Discussion

### 5.1 Results discussion

In this section, a global discussion on the contributions of the thesis is performed. Detailed discussions on the particular results of this thesis can be found in each of the papers and will not be stated here.

The main contribution of this thesis is the implementation of gamma-ray spectrometry in the automatic real-time radiation surveillance network of Catalonia. This was done via the development of three different types of environmental radioactivity monitors: one to measure radioactivity in water and the other two to measure airborne radioactivity. The airborne radioactivity monitors use two different approaches to measure: RARM-F performs measurements on a particulate filter (where radioactive isotopes are collected) and RARM-D2 measures directly in the environment.

The development of the monitors was performed simultaneously with the development of calibration methodologies and methods for spectra stabilisation, which made possible the optimal performance of the monitors. The programmed Monte Carlo user code for the EGS5 code system permitted the obtention of different results on the different monitors, with special emphasis to the efficiency calculations. The code was programmed to be versatile and easily adaptable to other types of gamma-ray detection monitors. Thus, it is possible to use it in multiple applications involving gamma-ray spectrometry, which opens a broad range of possibilities. Besides, the developed methods for spectra stabilisation were really useful to retrospectively correct all the spectra obtained with the developed monitors.

The water monitor collects water from the river through a pump and it is analyzed with a gamma-ray detector in a Pb shielded vessel. Another possibility would have been to measure directly in water, for example with the detector mounted in a floating buoy as in the KATERINA system [14]. Both approaches are complementary and they have some advantages and disadvantages. On the one hand, measuring in a vessel permits

lower MDACs and a more constant counting geometry (and radioactive source distribution) when compared with direct measurements. This provides better measurement capabilities and more accurate activity quantifications, respectively. Besides, vandalism or detector damage is more probable in the direct measurement system. On the other hand, depending on the streamlines of water, some radioactive isotopes could not arrive to the vessel through the pump, and thus, they would not be detected. Besides, the use of more mechanic and electronic devices can lead to more visits to the station for technical maintenance.

The discussion on the airborne radioactivity monitors performance is analogous to that on the water monitors. In this case, the RARM-F would play the role of the water monitor with the vessel and the RARM-D2 would play the role of the direct measurement in water system. However, the comparison is only possible between the RARM-F and the up-detector of the RARM-D2 because both give the volumetric activity concentration ( $\text{Bq}/\text{m}^3$ ) of isotopes in air.

When comparing the obtained results for the  $^{137}\text{Cs}$  MDACs in both RARM-F and up-detectors from RARM-D2 monitors, using either NaI(Tl) detectors or LaBr<sub>3</sub>(Ce) detectors, the results are clearly better for the former, specially at larger integration times. Besides, the differences would increase even more if higher suction flows could be achieved. Furthermore, the activity quantification is more accurate since the counting geometry is always the same, and thus, efficiency calculations are more precise. However, it is important to note that only particulate forms of the isotopes are captured in the filter. Thus, the real activity concentrations in air could be underestimated in certain cases. In particular, iodine isotopes are of interest. Since they can be find in gaseous forms, some hypothesis about the percentage of particulates of iodine should be accounted to provide more realistic values of their concentration of activity in air. Alternatively, additional measuring systems using charcoal filters could be used to overcome this difficulty.

The previous drawback does not apply to the RARM-D2 monitor, where all radioactive isotopes can be detected, regardless of their molecular form (i.e. independently of being in a particulate form or not). Nevertheless, the efficiency calculation depends on the radioactive source term distribution, and thus, a detailed study of the radioactive cloud geometry via dispersion models should be performed to compute correctly the efficiencies, and hence, the activity concentrations in air. In favor of the RARM-D2, the technical maintenance is low compared with the requirements of the RARM-F, which involves more electrical and mechanical parts.

Finally, it is important to remark that the implementation of gamma-ray spectrometry in the Catalan real-time radiation surveillance network has been pioneer in Spain. It started in late 2008, with the implementation of gamma-ray spectrometry in two river water monitors using NaI(Tl), which have been operative since early 2009. After these implementations, the first prototype of the RARM-F, which worked with a NaI(Tl)

5.1. RESULTS DISCUSSION

59

detector, was developed in late 2009. Simultaneously, the first prototype of the RARM-D2 using two NaI(Tl) detectors was also built. After that, in late 2010, the first prototypes of RARM-F and RARM-D2 using LaBr<sub>3</sub>(Ce) detectors were constructed. Finally, in late 2011, another RARM-F using a LaBr<sub>3</sub>(Ce) detector was developed for the *Generalitat de Catalunya*.

In Europe, the use of real-time gamma ray spectrometry is not still fairly common except in Finland, which has the largest gamma-ray spectrometry network formed by 1.5"×1.5" LaBr<sub>3</sub>(Ce) detectors measuring directly in the environment [15]. However, the tendency could change thanks to the good detection capabilities of the LaBr<sub>3</sub>(Ce) detectors, specially if their prices decrease.



# Chapter 6

## Conclusions

### 6.1 Main conclusions

Several improvements were implemented to the automatic real-time environmental radiation surveillance network of Catalonia in order to get better quality and quantity of data. For this, ADSL was installed at each monitoring place, enabling fast data transmission and remote control. Some of the improvements were the installation of meteorological stations, the installation of remotely-controlled switches or the placing of webcams for security and monitor status check.

An easily implementable statistical criterion was set for automatic data analysis and it was sufficiently restrictive and adequate to notice anomalous events. The criterion was found to be useful in a broad range of situations that produce radiological increments, such as natural causes, equipment failure, incidents at the nuclear power plants and other artificial causes.

The study of the capabilities of the Catalan network showed the need of having better radiological information in real-time. To overcome this limitation, the implementation of in-situ real-time gamma-ray spectrometry was suggested as a solution. The installation of gamma-ray spectrometry would allow the implementation of accurate alarms limiting the concentrations of activity for the different isotopes, or at least, it would help to discriminate natural causes from artificial emissions.

A complete calibration methodology of two scintillation detectors, NaI(Tl) and LaBr<sub>3</sub>(Ce), to be used in gamma-ray spectrometry was set. The calibration included energy, resolution and efficiency calibrations.

For the energy calibration, we found that the best function to establish the energy-channel relation is a 2<sup>nd</sup>-degree polynomial. In the same way, after testing several fitting functions for the resolution calibration, we found that the best fitting function for the FWHM(E) relation was also a 2<sup>nd</sup>-degree polynomial.

To perform the efficiency calculations, a Monte Carlo user code for the EGS5 code system was developed with several important implementations. The correct performance of the simulations was validated by comparing the simulated spectra with the experimental spectra and reproducing a number of efficiency and activity calculations. The user code was prepared to accept the calculation of the efficiencies in other different counting geometries, either for other radioactive source distributions or other detector arrangements.

Two correction methods for NaI(Tl) and LaBr<sub>3</sub>(Ce) gamma-ray spectrum stabilisation were established. The methods permit the correction of the peak shift produced when the detectors operate under unstable temperature conditions. Both methods are applied by software after the spectra acquisition and do not require adjustment of the gain during the measurements, which is of special interest in detectors with an analogue gain control.

On the one hand, the first method provides spectrum stabilisation using a mathematical relation between the channel positions and the temperature, even in the absence of known peaks. However, it requires a previous characterization of the detector in the laboratory under controlled temperature conditions. On the other hand, the second method does not require previous measurements in the laboratory but depends on a known peak in all of the spectra, which is not always available or identifiable, especially in the NaI(Tl) detector. For the LaBr<sub>3</sub>(Ce) detector, the internal contaminant of <sup>138</sup>La, together with the better energy resolution of the detector, make it easy to apply this method.

Two real-time water monitors using 2" × 2" NaI(Tl) scintillation detectors were improved by installing a gamma-ray spectrometric module. The monitors were fully calibrated using the previously set methodologies. The efficiency calibration was performed using Monte Carlo simulations. For this, a user code for the EGS5 code system was adapted to include a realistic model of the monitor and counting geometry.

The spectrometric module presented clear advantages in comparison with the old system. For example, it enabled the identification of the involved isotopes in radiological increments and made it possible to discard a possible artificial cause. The capabilities of the new monitor were evaluated with some MDAC calculations. In comparison to other monitors that measure directly in water, the obtained MDAC values were lower, and thus, a faster identification can be performed. In addition, the quantification of the activity can be more precise because the counting geometry is always the same and no assumptions about the source term geometry must be done.

A Real-time Airborne Radioactivity Monitor using gamma-ray spectrometry on a particulate Filter (RARM-F) was developed. Two RARM-Fs, one using a NaI(Tl) detector and

## 6.1. MAIN CONCLUSIONS

63

the other using a LaBr<sub>3</sub>(Ce) detector, were fully calibrated using the formerly developed methodology. This encompasses the energy, resolution and efficiency calibrations. The detection efficiencies were computed by means of Monte Carlo simulations using a model of the monitors, which accounted for the real shapes, dimensions and materials of the elements involved in the radiation detection.

The performance of the different RARM-Fs with different crystals was evaluated with some values of the MDACs for <sup>137</sup>Cs. The results show better performance for these monitors in comparison with other measuring directly in the environment. In particular, the better RARM-F is achieved using a LaBr<sub>3</sub>(Ce) detector.

A Real-time Airborne Radioactivity Monitor using Direct gamma-ray spectrometry with two scintillation detectors (RARM-D2) was developed. The geometrical disposition of the detectors together with the Pb shielding permit the discrimination between the isotopes contained in a radioactive cloud from those deposited or emerging from the ground.

The RARM-D2 was fully calibrated using experimental data except for the efficiency curve, which was set using Monte Carlo simulations with the EGS5 code system that reproduced the responses of the NaI(Tl) and LaBr<sub>3</sub>(Ce) detectors. Prior to setting the efficiency curve, the effect of the radioactive source term size on the efficiency calculations was studied for the gamma-rays from <sup>137</sup>Cs, either for the up-detectors or for the down detectors. This approach made it possible to set a reasonable infinite homogeneous source, which was used to set the entire efficiency curve up to 3000 keV for all studied detectors.

Using the calculated efficiency curves, the capabilities of the RARM-D2 were evaluated with some MDAC calculations over average spectra and for different integration times. This evaluation was performed for all configurations (up and down) of NaI(Tl) and LaBr<sub>3</sub>(Ce) measuring <sup>131</sup>I and <sup>137</sup>Cs.

Finally, after the contributions of this thesis, the automatic real-time environmental radiation surveillance network of Catalonia provides new and better radiological information. This was achieved thanks to the development and calibration of three types of radioactivity monitors using gamma-ray spectrometry, which permit the real-time identification and quantification of radioactive isotope content in water and in air. Thus, the new radiological information enable a comparison of the obtained data with the legal limits established for the activity concentrations, thereby allowing one to establish alarm levels for early warning.

## 6.2 Future work

The CSN (Spanish Nuclear Safety Council) has planned the renewal of the radioactivity monitoring systems of its REA (automatic stations network). For this, a working group was constituted and formed by members of the CSN, members of Spanish regional governments and scientists. The working group discussed different aspects of the project, such as possible types of detectors for the new network, data transmission systems, data analysis methods or establishment of alarm levels. As a part of this working group, we presented the developments that have been carried out in the context of this thesis, with special emphasis in the airborne radioactivity detectors.

The developments were considered by the working group as possible candidates for the renewal of the REA. For this, we are carrying out a R&D project, which is financed by the CSN, related to the analysis of the data obtained with the monitors. The project started at late 2012 and finishes on November 2015. Other R&D projects involving other prototypes are being developed in parallel by other researching groups. After this, the CSN will evaluate all the results and will make a decision.

Regardless of the decision of the CSN, the monitors are working in the Catalan network, and therefore, there is still work to do with them. In particular, the efforts need to be focused not only on improving the monitors but also on data analysis, with special emphasis in methodologies that make it possible to obtain information in real-time. This methodologies should include not only the conventional methods of peak analysis, which cannot provide reliable results in short integration times, but also alternative methods that make it possible to provide a quicker response. This would allow an early generation of automatic alerts in the spectrometric systems, enabling a better and a faster response in case of a possible accident scenario.

Besides, future work should include the evaluation of the performance of LaBr<sub>3</sub>(Ce) detectors in the water monitors and the calibration of the RARM-D2 to obtain the ambient dose equivalent  $H^*(10)$ , which would provide more reliable  $H^*(10)$  measurements to the network than those obtained with Geiger monitors.

Finally, the establishment of calibration methodologies among the development from scratch of different types of monitor will permit us to adapt and use all the developed tools for other applications, such as mobile radioactivity measurements in air or water, which would be of interest either during nuclear emergencies or for routine measurements.

## Chapter 7

# Bibliography

- [1] A. Janssens. *Environmental radiation protection: phylosophy, monitoring and standards*. Journal of Environmental Radioactivity 72 (2004) 65-73.
- [2] 2000/473/Euratom - Commission Recommendation of 8 June 2000. Official Journal of the European Commission, no. 191, 27 July 2000. Available at: [http://ec.europa.eu/energy/nuclear/radioprotection/doc/legislation/00473\\_en.pdf](http://ec.europa.eu/energy/nuclear/radioprotection/doc/legislation/00473_en.pdf)
- [3] A. Janssens, C. Necheva, V. Tanner, I. Turai. *The new Basic Safety Standards Directive and its implications for environmental monitoring*. Journal of Environmental Radioactivity 125 (2013) 99-104.
- [4] *Programas de vigilancia radiológica ambiental. Resultados 2011*. Colección de Informes Técnicos 35.2012. Consejo de Seguridad Nuclear, 2013. Available at: [http://www.csn.es/images/stories/publicaciones/unitarias/informes\\_tecnicos/pvra2011interiores\\_web.pdf](http://www.csn.es/images/stories/publicaciones/unitarias/informes_tecnicos/pvra2011interiores_web.pdf)
- [5] *Red de estaciones automáticas de vigilancia radiológica ambiental (REA) del CSN. Operación y resultados años 2010 y 2011*. Colección de Informes Técnicos 39.2013. Consejo de Seguridad Nuclear, 2013. Available at: [http://www.csn.es/images/stories/publicaciones/unitarias/informes\\_tecnicos/rea\\_2010-11.pdf](http://www.csn.es/images/stories/publicaciones/unitarias/informes_tecnicos/rea_2010-11.pdf)
- [6] Consejo de Seguridad Nuclear (CSN). Informe sobre notificación de sucesos en centrales nucleares, 2008. Available (in Spanish): <http://www.csn.es/descarga/INFSUCiersem08.pdf>
- [7] International Atomic Energy Agency (IAEA). INES The International Nuclear and Radiological Event Scale User's manual, 2008 Edition. Emended version, March 2013. Available at: [http://www-pub.iaea.org/MTCD/publications/PDF/INES2009\\_web.pdf](http://www-pub.iaea.org/MTCD/publications/PDF/INES2009_web.pdf)
- [8] G. Gilmore. Practical Gamma-Ray Spectrometry, 2nd Edition, John Wiley & Sons, England, 2008.

- [9] G.F. Knoll. *Radiation Detection and Measurement*, 3rd Edition, John Wiley & Sons, New York, 2000.
- [10] M. Moszyński. *Inorganic scintillation detectors in  $\gamma$ -ray spectrometry*. Nuclear Instruments and Methods in Physics Research A 505 (2003) 101-110.
- [11] M.J. Weber. *Inorganic scintillators: today and tomorrow*. Journal of Luminescence 100 (2002) 35-45.
- [12] BrilLanCeTM Scintillators Performance Summary (Revision: January, 2009). Saint-Gobain Crystals, Scintillation Products. Available at: [http://www.detectors.saint-gobain.com/uploadedFiles/SGdetectors/Documents/Technical\\_Information\\_Notes/BrilLanCe-Scintillators-Performance-Summary.pdf](http://www.detectors.saint-gobain.com/uploadedFiles/SGdetectors/Documents/Technical_Information_Notes/BrilLanCe-Scintillators-Performance-Summary.pdf)
- [13] W. Westmeier, K. Siemon. *New trends in nuclear spectrometry*. Journal of Environmental Radioactivity 117 (2013) 25-30.
- [14] C. Tsabarlis, C. Bagatelas, Th. Dakladas, C.T. Papadopoulos, R. Vlastou, G.T. Chronis. *An autonomous in situ detection system for radioactivity measurements in the marine environment*. Applied Radiation and Isotopes 66 (2008) 1419-1426.
- [15] A. Mattila, H. Toivonen, K. Vesterbacka, M. Leppänen, S. Salmelin, A. Pelikan. *Radiation monitoring network with spectrometric capabilities: implementation of LaBr<sub>3</sub> spectrometers to the Finnish network*. Proceedings of the 3rd European IRPA Congress (2010) 1958-1966, Helsinki, Finland. Available at: <http://www.irpa2010europe.com/pdfs/proceedings/S12-P12.pdf>

## Appendix A

# Patent applications

### A.1 Estación de identificación y medida en tiempo real de la radiactividad ambiental gamma mediante espectrometría sobre filtro de papel

#### A.1.1 Summary (in Spanish)

Estación de medida de la radiactividad ambiental gamma con un detector con capacidad de realizar espectrometría gamma, enfrentado a un filtro de papel continuo. Gracias a la descarga de un determinado volumen de aire sobre el filtro mediante una bomba de aspiración es posible aumentar la concentración de isótopos radiactivos cerca del detector, de manera que la identificación de los isótopos gamma y cuantificación de su concentración de actividad se hace más precisa, reduciéndose la actividad mínima detectable.

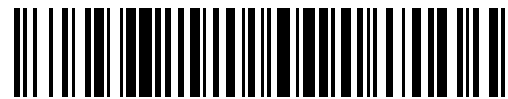
#### A.1.2 Summary (in English)

Measurement station of environmental gamma radioactivity using a gamma-ray spectrometry detector, which is faced toward a continuous particulate filter. The discharge of a given volume of air across the filter using a suction pump makes it possible to increase the radioactive isotope activity concentration near the detector, so that the identification of gamma isotopes and the quantification of its activity concentration becomes more accurate, reducing the minimum detectable activity.



OFICINA ESPAÑOLA DE  
PATENTES Y MARCAS

ESPAÑA



(11) Número de publicación: **2 425 801**

(21) Número de solicitud: 201230408

(51) Int. Cl.:

**G01T 1/202** (2006.01)

(12)

SOLICITUD DE PATENTE

A1

(22) Fecha de presentación:  
**16.03.2012**

(43) Fecha de publicación de la solicitud:  
**17.10.2013**

(56) Se remite a la solicitud internacional:  
**PCT/ES2013/070171**

(71) Solicitantes:

**UNIVERSITAT ROVIRA I VIRGILI (75.0%)  
C/ Escorxador s/n  
43003 Tarragona ES y  
UNIVERSITAT POLITECNICA DE CATALUNYA  
(25.0%)**

(72) Inventor/es:

**LOPEZ TORTOSA, Miguel;  
SALVADÓ ARTELLS, Marçal;  
CASANOVAS ALEGRE, Ramon;  
TAPIA FERNÁNDEZ, Carlos y  
DE BLAS DEL HOYO, Alfredo**

(74) Agente/Representante:

**CARPINTERO LÓPEZ, Mario**

(54) Título: **ESTACIÓN DE IDENTIFICACIÓN Y MEDIDA EN TIEMPO REAL DE LA RADIACTIVIDAD AMBIENTAL GAMMA MEDIANTE ESPECTROMETRÍA SOBRE FILTRO DE PAPEL**

(57) Resumen:

Estación de medida de la radiactividad ambiental gamma con un detector (5) con capacidad de realizar espectrometría gamma, enfrentado a un filtro de papel continuo (2). Gracias a la descarga de un determinado volumen de aire sobre el filtro mediante una bomba de aspiración es posible aumentar la concentración de isótopos radiactivos cerca del detector (4), de manera que la identificación de los isótopos gamma y cuantificación de su concentración de actividad se hace más precisa, reduciéndose la actividad mínima detectable.

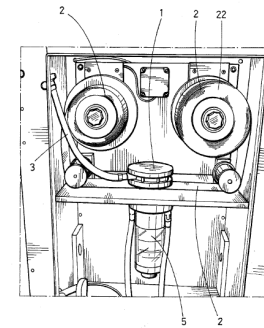


FIG.3

## A.1. PATENT APPLICATION 1

69

ES 2 425 801 A1

### DESCRIPCIÓN

Estación de identificación y medida en tiempo real de la radiactividad ambiental gamma mediante espectrometría sobre filtro de papel

#### 5 CAMPO DE LA INVENCIÓN

La presente invención se refiere a un dispositivo para identificar isótopos radiactivos emisores gamma y medir su concentración de actividad en aire. En particular, el dispositivo comprende un detector de centelleo inorgánico capaz de realizar espectrometría gamma y de proporcionar información acerca del espectro energético de los isótopos emisores gamma depositados en un filtro de papel.

#### ANTECEDENTES DE LA INVENCIÓN

Son conocidos en el estado de la técnica numerosos dispositivos para la detección de radiactividad mediante cristales de centelleo inorgánicos. Ejemplos de los mismos se pueden ver en las solicitudes de patente CN201662623 y US 3781562 B1. En el primero se describe una sonda de LaBr<sub>3</sub> que se usa para medir la radiación ambiente. En el segundo, un cristal de NaI es utilizado para medir radiación producida por efecto Mössbauer. El uso de detectores de centelleo tiene la ventaja de que gracias a ellos se puede realizar un análisis espectrométrico de las señales recibidas. Sin embargo, no existe hasta la fecha un aparato capaz de medir la radiación ambiental en tiempo real, proporcionando una identificación de los posibles isótopos radiactivos gamma y una cuantificación precisa de su concentración de actividad.

#### OBJETO DE LA INVENCIÓN

25 La invención tiene por objeto proporcionar una estación de medida de la radiactividad ambiental en tiempo real que permita una mayor precisión en la identificación de los isótopos emisores de partículas gamma, en la cuantificación de su concentración de actividad y de sus límites de detección. Para ello, la estación está provista de un detector (5) para la realización de espectrometría gamma (que comprende un cristal de centelleo inorgánico y un fotomultiplicador), un filtro de papel continuo (2) y una bomba de aspiración. Gracias al caudal de aire 30 generado por una bomba de aspiración, que circula a través del filtro de papel, se puede aumentar la concentración de isótopos frente al detector y así mejorar la precisión de la medida. El cristal es preferentemente de NaI o LaBr<sub>3</sub>, u otros de funcionalidad equivalente. El filtro de papel se hace circular preferentemente mediante rodillos giratorios motorizados (22). El funcionamiento de la bomba de aspiración se regula a partir de los medios 35 de control incorporados para cuantificar y ajustar el caudal de aire aspirado. De preferencia se incorpora además un circuito neumático para desplazar el cabezal (1) en una dirección vertical y facilitar, cuando sea necesario, el desplazamiento del filtro de papel. La electrónica incluye un analizador de impulsos de tipo multicanal. El dispositivo puede incorporar además sistemas para el envío de las medidas obtenidas en la estación, así como el envío de avisos y almacenamiento/envío de informes acerca de su funcionamiento y un módulo de acceso y control remoto a través de dirección IP para controlar, encender, apagar y reiniciar remotamente el sistema. 40 Opcionalmente se pueden incorporar detectores Geiger (o contadores proporcionales) adicionales para realizar mediciones de tasa de dosis o tasa de dosis equivalente ambiental.

#### BREVE DESCRIPCIÓN DE LAS FIGURAS

45 Con objeto de ayudar a una mejor comprensión de las características de la invención de acuerdo con un ejemplo preferente de realización práctica de la misma, se acompaña la siguiente descripción de unos dibujos en donde con carácter ilustrativo se ha representado lo siguiente:

Figura 1: es una representación esquemática del principio de funcionamiento de la invención (alzado).

Figura 2: corresponde a la vista superior de la figura 1.

Figura 3: es una representación esquemática de la invención sin el blindaje de plomo.

50 Figura 4: es una representación esquemática de la invención con el blindaje de plomo incorporado.

Figura 5: muestra el blindaje de plomo.

#### DESCRIPCIÓN DETALLADA DE LA INVENCIÓN

55 El equipo de medición en tiempo real de la invención (figura 3) capta mediante una bomba de aspiración un volumen de aire predeterminado por el usuario. En el cabezal (1), el aire es descargado sobre el filtro de papel (2) y después es expulsado hacia el exterior a través de los conductos de entrada/salida de aire (3). Se forma así una concentración de isótopos (4) sobre el filtro próximo al detector (5) (figuras 1, 2). El cabezal (1) es una pieza metálica cilíndrica conectada a un actuador neumático que posibilita su movimiento vertical para fijar o liberar el filtro de papel. El cabezal cumple varias funciones simultáneamente; permite la sujeción firme el papel continuo

ES 2 425 801 A1

cerca de la parte superior del detector (5) (zona activa en la medida), contiene el conducto de entrada de aire (proveniente de la bomba de aspiración), crea un volumen con un alto grado de hermeticidad en el volumen del interior del cabezal ocupado por la parte superior del detector y el filtro de papel y, finalmente, homogeneiza el caudal de aire con la finalidad de obtener una concentración de isótopos uniforme en el filtro de papel expuesto (4). El filtro pasa por el interior (a través) del cabezal mediante unas aperturas laterales en el cabezal. De esta manera el aire se introduce (mediante la bomba de aspiración) en el cabezal y es forzado a circula a través del filtro que se mantiene siempre próximo al detector. La bomba de aspiración que genera el flujo de aire (no representada en los esquemas para una mayor claridad) está conectada a un variador de frecuencia que determina las características de velocidad y revoluciones por minuto. Todos estos parámetros se pueden determinar mediante medios de programa de control. Mediante un actuador neumático lineal se puede acercar o alejar el cabezal (1) al papel (2) verticalmente, como se puede apreciar en la figura 3, de manera que el papel es liberado y se puede desplazar para realizar una nueva medida sobre otro segmento limpio. Mediante la bomba de aspiración se hace circular a través del filtro de papel un caudal de aire constante y controlado; aumentando así la concentración de isótopos radiactivos en el mencionado filtro de papel (zona 4 en las figuras 1 y 2, que se encuentra en el interior del cabezal (1) en la figura 3). La parte activa del detector es un cristal de centelleo (NaI, LaBr<sub>3</sub>, u otros de funcionalidad equivalente), rodeado de un blindaje de plomo (6) (figuras 4 y 5), diseñado y construido para la estación, para aislarlo de la radiación exterior (el blindaje de plomo no ha sido representado en las figuras 1, 2 y 3 para una mayor claridad). La parte activa del detector se encara al filtro de papel para medir, en tiempo real, el espectro de los isótopos gamma retenidos en el mismo. El sistema de adquisición de datos multicanal selecciona las energías de las partículas para obtener espectros energéticos a partir de los cuales se puede identificar los isótopos gamma presentes y medir su concentración de actividad. Esta información se obtiene a partir del procesamiento de las señales amplificadas mediante un convertidor analógico-digital. Mediante medios de programa se puede además contabilizar el número de repeticiones de impulsos a una determinada amplitud para realizar histogramas o espectros energéticos con el número total de partículas con una determinada energía. Los dispositivos mecánicos están provistos de sensores para detectar anomalías en el papel o el flujo de aire.

Unos rodillos giratorios motorizados (22) (figuras 3 y 4), permiten el desplazamiento controlado el filtro de papel. El tiempo de integración (tiempo de medida) y el de avance del papel pueden ser determinados libremente. También se puede seleccionar libremente la cantidad de aire (caudal) que atraviesa cada muestra del filtro de papel. El aire aspirado (varios m<sup>3</sup>/h) en una pequeña sección de filtro de papel (4) (algunos cm<sup>2</sup>) conlleva un aumento de concentración isotópica que permite su identificación y cuantificación de su concentración de actividad, ya que la parte activa del detector (5) está situada cerca de la zona del filtro de papel expuesta (4). Cuanto más tiempo circule el aire por la misma muestra de filtro de papel, la concentración isotópica será mayor y por lo tanto mayor también la precisión de la medida, reduciéndose así la actividad mínima detectable.

Preferentemente, el equipo puede estar provisto de medios de programa que aportan un sistema configurable para activar distintos tipos de avisos y alarmas al sobrepasarse cierto umbral de radiación predefinido para cada isótopo analizado o región del espectro previamente definida. La sonda se encuentra rodeada de un blindaje de plomo en las zonas que no están enfrentadas al papel para reducir el fondo radiológico y reducir los límites de detección.

Se incorporan además medios de programa que facilitan el control local o remoto de la estación y la identificación y cuantificación de la actividad radiológica. Medios de programa permiten la estabilización de los espectros (a partir de los valores de una sonda de temperatura en contacto con el cristal u otros sistemas de estabilización), que influye en la estimación de la energía de las partículas incidentes y en la cuantificación de la concentración de actividad asociada a cada isótopo. Se puede incorporar además un sistema de comunicaciones para el envío de las medidas obtenidas en la estación, así como para el envío de avisos y almacenamiento/envío de informes acerca de su funcionamiento y un módulo de acceso y control remoto a través de dirección IP para controlar, encender, apagar y reiniciar remotamente el sistema.

A.1. PATENT APPLICATION 1

71

ES 2 425 801 A1

**REIVINDICACIONES**

- 5 1.- Estación de identificación y medida de radiactividad ambiental gamma en tiempo real, provista de un detector (5) para la realización de espectrometría gamma, que comprende un cristal de centelleo inorgánico y un fotomultiplicador, enfrentado a un filtro de papel continuo (2), caracterizada porque además está provista de un cabezal (1) asociado a una bomba de aspiración que permiten la circulación homogénea de un caudal de aire a través del filtro de papel continuo (2).
- 10 2.- Estación de medida según la reivindicación 1 caracterizada porque el detector de centelleo (5), que comprende un cristal de NaI o LaBr<sub>3</sub>, adaptado para realizar espectrometría gamma.
- 15 3.- Estación de medida según la reivindicación 2 caracterizada porque comprende blindajes de plomo (6) rodeando el cabezal (1) y el cristal (5) en las zonas que no están enfrentadas al papel (2) y por encima del papel.
- 20 4.- Estación de medida según cualquiera de las reivindicaciones anteriores caracterizada porque comprende rodillos giratorios motorizados (22) que permiten el desplazamiento controlado el filtro de papel (2).
- 25 5.- Estación de medida según la reivindicación 4 caracterizada porque está provista de un circuito neumático que permite el desplazamiento del cabezal (1), y que los rodillos giratorios motorizados (22) desplacen el papel (2), de manera que sucesivas medidas puedan ser realizadas en un nuevo segmento de papel.
- 30 6.- Estación de medida según cualquiera de las reivindicaciones anteriores caracterizada porque comprende un analizador de impulsos de tipo multicanal, adaptado para seleccionar las energías de las partículas gamma detectadas para obtener el espectro energético.
- 35 7.- Estación de medida según cualquiera de las reivindicaciones anteriores caracterizada porque está provista de un sistema de comunicaciones para el envío de las medidas obtenidas en la estación, así como para el envío de avisos y almacenamiento/envío de informes.
- 40 8.- Estación de medida según cualquiera de las reivindicaciones anteriores caracterizada porque está provista de detectores Geiger o contadores proporcionales adicionales para realizar mediciones de la tasa de dosis o tasa de dosis equivalente ambiental.
- 9.- Estación de medida según cualquiera de las reivindicaciones anteriores caracterizada porque está provista de sensores capaces de detectar la ausencia o rotura del filtro papel, la velocidad de avance del filtro de papel y cuantificar y regular el flujo de aire que circula a través del filtro de papel.
- 10.- Estación de medida según cualquiera de las reivindicaciones anteriores caracterizada porque comprende además sondas de temperatura asociadas al detector.
- 11.- Estación de medida según cualquiera de las reivindicaciones anteriores caracterizada porque comprende una estación meteorológica.

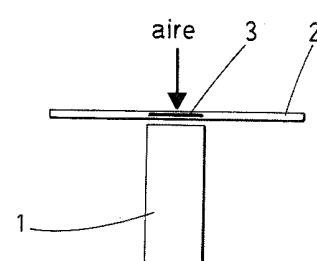


**FIG.1**

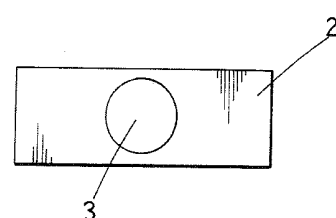


**FIG.2**

A.1. PATENT APPLICATION 1

73

ES 2 425 801 A1

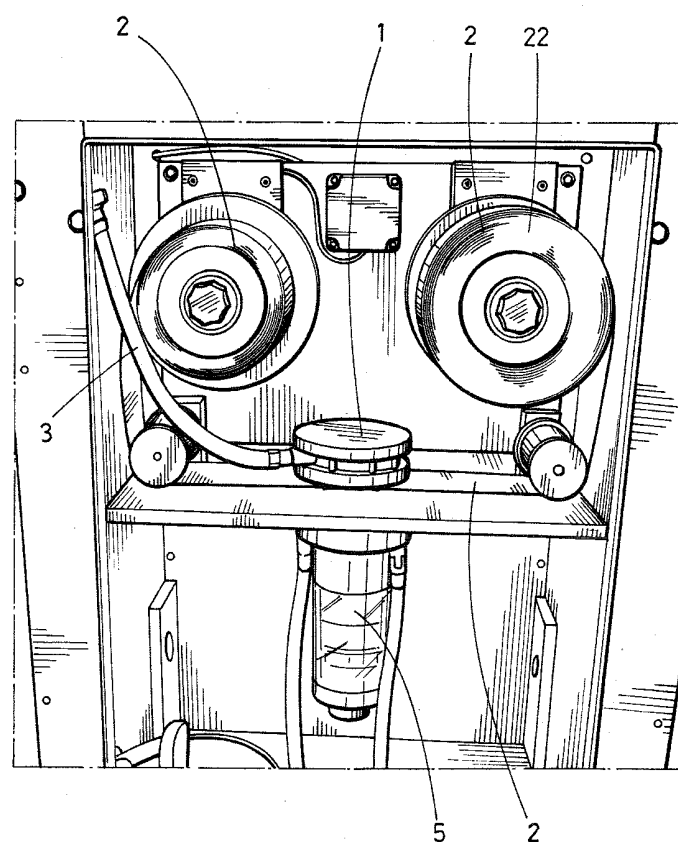


**FIG.3**

ES 2 425 801 A1

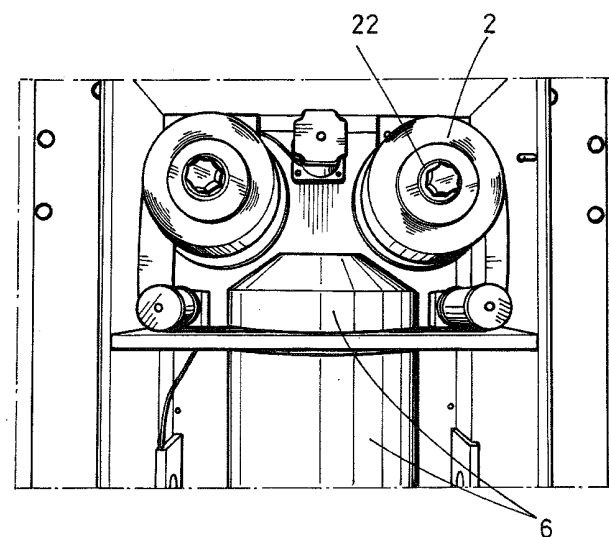


**FIG.4**

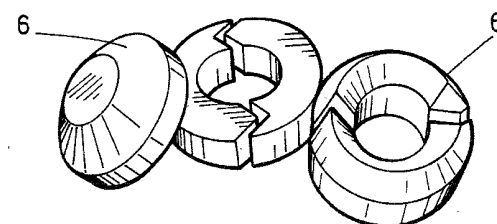


**FIG.5**

## **A.2 Estación de identificación y medida en tiempo real de la radiactividad ambiental gamma, mediante espectrometría con dos cristales de centelleo**

### **A.2.1 Summary (in Spanish)**

Estación de medida de radiactividad con dos detectores de espectrometría gamma aplanallada con plomo que permite identificar isótopos radioactivos gamma en el ambiente y cuantificar en tiempo real la concentración de actividad gamma para isótopos individuales. Un primer cristal está cubierto por un apantallamiento de plomo en su parte superior y lateral y un segundo cristal está cubierto por otro apantallamiento de plomo en la parte inferior y lateral. La doble sonda con apantallamiento hace posible distinguir entre la radiación de origen superior o inferior y evitar interferencias en la medida.

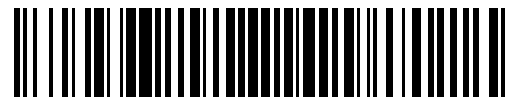
### **A.2.2 Summary (in English)**

Radioactivity measurement station using two gamma-ray spectrometry detectors, which are shielded with lead, that permits the identification of environmental radioactive gamma isotopes and the quantification in real-time of their activity concentration. The first detector (which is pointing down) is shielded with lead in its upper and side part and the second detector (which is pointing up) is shielded in the bottom and side part. The double shielded probe makes it possible to distinguish between the upper or bottom radiation and to avoid interferences in the measurements.



OFICINA ESPAÑOLA DE  
PATENTES Y MARCAS

ESPAÑA



(11) Número de publicación: **2 423 236**

(21) Número de solicitud: 201230236

(51) Int. Cl.:

**G01T 1/202** (2006.01)  
**G01T 1/36** (2006.01)

(12)

SOLICITUD DE PATENTE

A1

(22) Fecha de presentación:  
**15.02.2012**

(71) Solicitantes:

**UNIVERSITAT ROVIRA I VIRGILI (100.0%)**  
C/ Escorxador s/n  
43003 Tarragona ES

(43) Fecha de publicación de la solicitud:  
**18.09.2013**

(72) Inventor/es:

**SALVADÓ ARTELLS, Marçal;**  
**LOPEZ TORTOSA, Miguel;**  
**CASANOVAS ALEGRE, Ramon;**  
**SANCHEZ VIÑES, Javier y**  
**TORAL PLAZA, Juan**

(56) Se remite a la solicitud internacional:  
**PCT/ES2013/070093**

(74) Agente/Representante:

**CARPINTERO LÓPEZ, Mario**

(54) Título: **ESTACIÓN DE IDENTIFICACIÓN Y MEDIDA EN TIEMPO REAL DE LA RADIACTIVIDAD AMBIENTAL GAMMA, MEDIANTE ESPECTROMETRÍA CON DOS CRISTALES DE CENTELLEO**

(57) Resumen:

Estación de identificación y medida en tiempo real de la radiactividad ambiental gamma, mediante espectrometría con dos cristales de centelleo. Estación de medida de radiactividad con dos detectores de espe

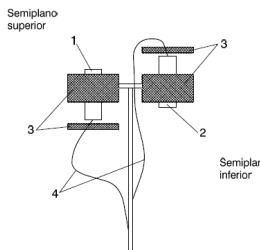


FIG. 1

A.2. PATENT APPLICATION 2

77

ES 2 423 236 A1

**DESCRIPCIÓN**

5 Estación de identificación y medida en tiempo real de la radiactividad ambiental gamma, mediante espectrometría con dos cristales de centelleo

**Campo de la invención**

La presente invención se refiere a un dispositivo para identificar isótopos radioactivos en el ambiente y estimar su concentración de actividad. En particular, el dispositivo es una estación compuesta de diversos subsistemas y que incorpora detectores de centelleo inorgánicos para la realización de espectrometría gamma.

**Antecedentes de la invención**

Son conocidos en el estado de la técnica numerosos dispositivos para la detección de radiactividad mediante cristales de centelleo inorgánicos. Ejemplos de los mismos se pueden ver en las solicitudes de patente CN201662623 y US 3781562. En el primero se describe una sonda de LaBr<sub>3</sub> que se usa para medir la radiación ambiental. En el segundo, un cristal de NaI es utilizado para medir radiación producida por efecto Mössbauer. El uso de detectores de centelleo, junto con una tarjeta multicanal, tiene la ventaja de que gracias a ellos se puede realizar un análisis espectral de las radiaciones recibidas. Sin embargo, no existe hasta la fecha un aparato capaz de medir la radiación ambiental en tiempo real, discriminando la radiación procedente del suelo de la debida a partículas en suspensión y, por tanto, capaz de proporcionar información acerca del origen de dicha radiación (i.e. suelo o aire), lo que es muy necesario en la vigilancia radiológica ambiental alrededor de instalaciones nucleares.

**Objeto de la invención**

La invención tiene por objeto paliar los problemas técnicos citados en el apartado anterior. Para ello, propone una estación de identificación y medida de la radioactividad gamma ambiental mediante espectrometría con dos sondas que comprenden cristales de centelleo orientados en direcciones opuestas. Así, un primer cristal está cubierto por un apantallamiento de plomo en su parte superior (y lateral) y un segundo cristal está cubierto por otro apantallamiento de plomo en la parte inferior (y lateral). La estación está provista además de un analizador de impulsos de tipo multicanal, adaptado para seleccionar las energías de las partículas gamma detectadas para obtener el espectro energético.

35 Los cristales son preferentemente de NaI o LaBr<sub>3</sub>, pero podrían ser fácilmente intercambiables con otros tipos de cristales de centelleo. Preferentemente, la estación puede estar provista de un sistema de comunicaciones para el envío de los datos obtenidos. También comprende preferentemente un sistema de generación de avisos y almacenamiento/envío de informes, una estación meteorológica asociada y sondas de temperatura asociadas a cada cristal.

**Breve descripción de las figuras**

Con objeto de ayudar a una mejor comprensión de las características de la invención de acuerdo con un ejemplo preferente de realización práctica de la misma, se acompaña la siguiente descripción de un juego de dibujos donde con carácter ilustrativo se ha representado lo siguiente:

45 Figura 1.- es una representación esquemática de la estación de la invención.

Figura 2.- muestra un detalle de los apantallamientos superior/inferior y lateral de plomo.

**Descripción detallada de la invención**

50 El equipo de medición de radiactividad con dos sondas de espectrometría gamma apantallada con plomo permite identificar los isótopos radioactivos emisores gamma presentes (ya sea en el aire o depositados en el suelo) y cuantificar la concentración de actividad gamma (con una previa estimación del término fuente) en tiempo real para los distintos isótopos individuales previamente identificados. La combinación de dos detectores con apantallamiento a 180° según se puede apreciar en la figura 1 hace posible distinguir entre la radiación de origen superior o inferior y evitar interferencias en la medida. El uso de las sondas gamma espetrométricas (NaI, LaBr<sub>3</sub> u otras de funcionalidad equivalente) proporciona además gran cantidad de información acerca del origen de dicha radiación. En general, en el semiplano superior de detección se encuentran los aerosoles volátiles, mientras que en la zona inferior de detección se encuentran las deposiciones radiativas y la emanación de radón.

60 En referencia a la figura 1, las sondas 1 y 2 están colocadas a cada lado del eje del dispositivo y apantalladas una en su parte superior y lateral y otra en su parte inferior y lateral por sendas placas de plomo 3. Las sondas están conectadas mediante las conexiones 4 y pueden estar rodeadas de algún material aislante, como porexpan. El conjunto se coloca preferentemente en una carcasa o cubierta plástica para protegerlo de

fenómenos meteorológicos adversos. El dispositivo puede estar colocado a distintas alturas (preferentemente de 1 a 3 m) para captar la radiación proveniente del suelo de un área significativa. El dispositivo puede estar provisto además de una estación meteorológica para correlacionar en tiempo real los datos espectrométricos obtenidos con las condiciones meteorológicas en las que se obtiene la medida (pluviometría, temperatura, 5 humedad, presión, radiación solar velocidad y dirección del viento). Así, el hecho de disponer simultáneamente de los datos meteorológicos con los espectrométricos permite estimar el efecto de los mismos sobre dicha medida. Por ejemplo: los incrementos radiológicos por el efecto de la lluvia, los desplazamientos del espectro con la temperatura, la evolución del término fuente de radiación (nube radiactiva o emanaciones de radón) con el viento, la lluvia, la presión atmosférica, etc.

10 Medios de programa facilitan el control local o remoto de la invención y la identificación de los isótopos presentes y la cuantificación de su actividad radiológica. Medios de programa conocidos facilitan la estabilización de los espectros (a partir de los valores de las sondas de temperatura en contacto con cada cristal u otros sistemas de estabilización). Se puede incorporar un sistema de comunicaciones para el envío de las medidas obtenidas en la estación, así como para el envío de avisos y almacenamiento/envío de informes acerca de su funcionamiento y 15 un módulo de acceso y control remoto a través de dirección IP para controlar, encender, apagar y reiniciar remotamente el sistema.

20 Los diferentes subsistemas que componen el dispositivo (sistema de medida espectrométrica, electrónica global del equipo, sondas de temperatura, etc.) son controlados por un sistema informático de forma local o remota. Ese sistema informático también se encarga de realizar funciones de almacenaje de datos y transmisión de la información derivada de los mismos y realizar representaciones gráficas y cálculos asociados a las medidas radiológicas obtenidas por la estación. El sistema analizador de impulsos es de tipo multicanal, y su función principal es seleccionar las energías de las partículas gamma detectadas para obtener el espectro energético. 25 Esta información se obtiene a través del procesamiento de los impulsos eléctricos suministrados por un amplificador mediante un convertidor analógico-digital. La distribución de las amplitudes de los impulsos permite la discriminación energética de la radiación incidente. El sistema contabiliza el número de repeticiones en la obtención de impulsos de una determinada amplitud, permitiendo así la elaboración de un histograma o espectro energético. Este histograma proporciona información básica que permite calcular el número total de partículas 30 gamma con una determinada energía detectadas durante el tiempo en el que se ha efectuado la medida. En la electrónica de control del sistema se dispone de dos tarjetas multicanal, una para cada cristal.

El dispositivo puede cuantificar (con una adecuada estimación de la geometría del término fuente) la concentración de actividad ( $Bq/m^3$ ) para cada uno de los isótopos identificados.

35

A.2. PATENT APPLICATION 2

79

ES 2 423 236 A1

**REIVINDICACIONES**

- 1.- Estación de identificación y medida de radioactividad caracterizada porque comprende dos sondas de cristal de centelleo gamma espectrométrico, donde un primer cristal (1) está cubierto por un apantallamiento de plomo (3) en su parte superior y lateral y un segundo cristal (2) está cubierto por otro apantallamiento de plomo (3) en la parte inferior y lateral y un analizador de impulsos de tipo multicanal, adaptado para seleccionar las energías de las partículas gamma detectadas para obtener el espectro energético.
- 5 2.- Estación de medida según la reivindicación 1 caracterizada porque el cristal es de NaI o LaBr<sub>3</sub>.
- 10 3.- Estación de medida según cualquiera de las reivindicaciones anteriores caracterizada porque comprende además una sonda de temperatura asociada a cada cristal.
- 15 4.- Estación de medida según cualquiera de las reivindicaciones anteriores caracterizada porque comprende una estación meteorológica asociada.
- 20 5.- Estación de medida según cualquiera de las reivindicaciones anteriores caracterizada porque está provista de un sistema de comunicaciones adaptado para realizar el envío de las medidas obtenidas en la estación, así como para el envío de avisos y almacenamiento/envío de informes.

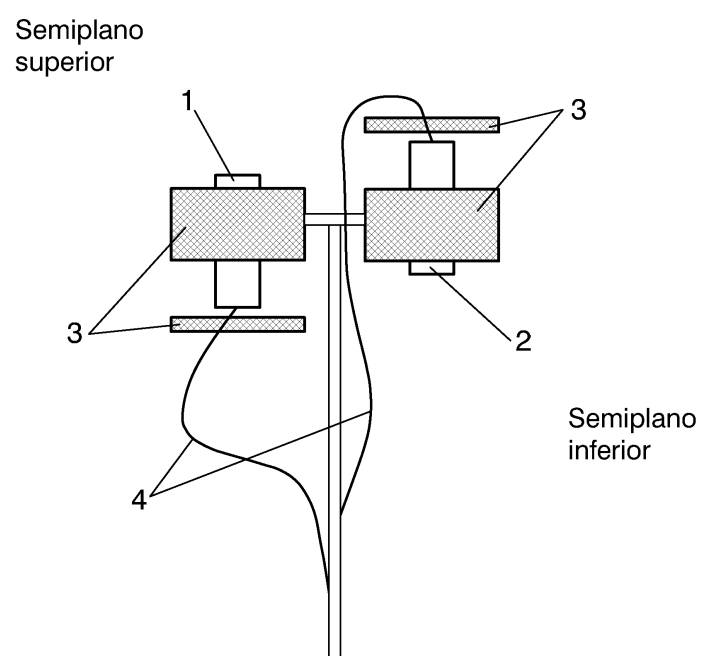


**FIG. 1**

A.2. PATENT APPLICATION 2

81

ES 2 423 236 A1

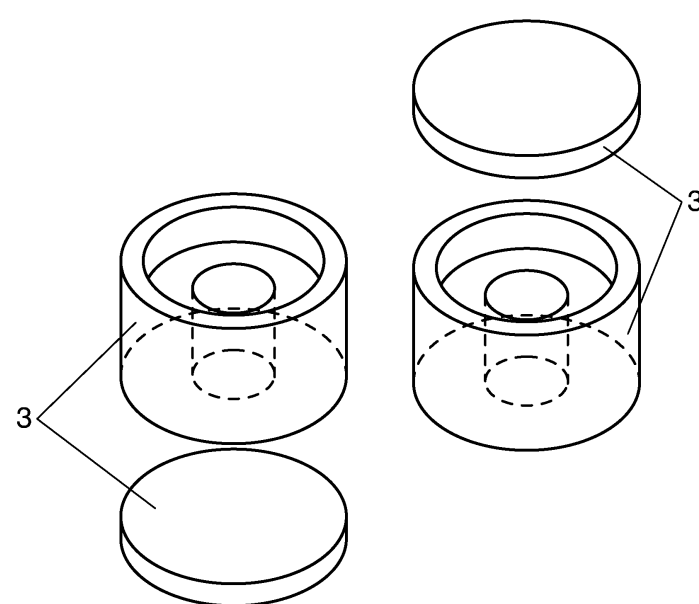


**FIG. 2**





## Development and calibration of automatic real-time environmental radioactivity monitors using gamma-ray spectrometry

This doctoral thesis presents a collection of six scientific papers, which have been published in peer-reviewed scientific journals, in the field of real-time environmental radioactivity detection. After the contributions of this thesis, the automatic real-time environmental radiation surveillance network of Catalonia provides new and better radiological information. This was achieved thanks to the development and calibration of three types of radioactivity monitors using gamma-ray spectrometry, either with NaI(Tl) or LaBr<sub>3</sub>(Ce) detectors, which permit the real-time identification and quantification of radioactive isotope content in water and in air. In the thesis, details on general calibration methodologies can be found. The mentioned developments as well as their specific calibrations are also discussed. For each monitor, an evaluation of their measurement capabilities is also performed.

Ramon Casanovas Alegre

